DUDLEY KNOX LIBRARY
NAVAL POSTGRADUATE SCHOOL
MONTEREY CALIFORNIA 93943-5002

Unclassified

SECURITY CLASSIFICATION OF THIS PAGE

REPORT DOCUMENTATION PAGE

1a. REPORT SECURITY CLASSIFICATION Unclassified	1b. RESTRICTIVE MARKINGS
2a. SECURITY CLASSIFICATION AUTHORITY	3. DISTRIBUTION/AVAILABILITY OF REPORT Approved for public release; distribution is unlimited.
2b. DECLASSIFICATION/DOWNGRADING SCHEDULE	
4. PERFORMING ORGANIZATION REPORT NUMBER(S)	5. MONITORING ORGANIZATION REPORT NUMBER(S)
6a. NAME OF PERFORMING ORGANIZATION Naval Postgraduate School 6b. OFFICE SYMBOL (*If applicable*) 55	7a. NAME OF MONITORING ORGANIZATION Naval Postgraduate School
6c. ADDRESS (*City, State, and ZIP Code*) Monterey, CA 93943-5000	7b. ADDRESS (*City, State, and ZIP Code*) Monterey, CA 93943-5000
8a. NAME OF FUNDING/SPONSORING ORGANIZATION 8b. OFFICE SYMBOL (*If applicable*)	9. PROCUREMENT INSTRUMENT IDENTIFICATION NUMBER
8c. ADDRESS (*City, State, and ZIP Code*)	10. SOURCE OF FUNDING NUMBERS Program Element No. / Project No. / Task No. / Work Unit Accession Number

11. TITLE (*Include Security Classification*)
Upper-Tropospheric Forcing of the Intensification Rates of Tropical Cyclones Flo and Ed Based on TCM-90 Observations

12. PERSONAL AUTHOR(S) Rucker, Jeff H.

13a. TYPE OF REPORT	13b. TIME COVERED	14. DATE OF REPORT (*year, month, day*)	15. PAGE COUNT
Master's Thesis	From To	June 1992	201

16. SUPPLEMENTARY NOTATION
The views expressed in this thesis are those of the author and do not reflect the official policy or position of the Department of Defense or the U.S. Government.

17. COSATI CODES			18. SUBJECT TERMS (*continue on reverse if necessary and identify by block number*)
FIELD	GROUP	SUBGROUP	Environmental forcing of tropical cyclone intensity , Supertyphoon Flo, Typhoon Ed, TCM-90

19. ABSTRACT (*continue on reverse if necessary and identify by block number*)

A case study of the upper-tropospheric forcing of the intensification rates of typhoons Flo and Ed has been accomplished. High-resolution, hand-drawn streamline analyses of the 150, 200, 250, and 300 mb winds from the final observational data set of the Tropical Cyclone Motion (TCM-90) field experiment were constructed for 00, 06, 12, and 18 UTC during the period 00 UTC 12 September through 00 UTC 19 September. Three basic interaction mechanisms that appeared to have major roles in upper-level forcing on Flo and Ed were defined. Outflow layer changes were quantified through calculation of the mass divergence and eddy flux convergence of relative angular momentum using a radial-band averaging technique at 200 mb. A nearly 1:1 qualitative relationship was found to exist between the development of one or more of the these mass/heat export mechanisms and corresponding changes in the intensification rates. These calculations from the best-ever typhoon region data set strongly suggest that upper-level forcing leads the intensification process by 12-24 h.

T258503

20. DISTRIBUTION/AVAILABILITY OF ABSTRACT	21. ABSTRACT SECURITY CLASSIFICATION	
☒ UNCLASSIFIED/UNLIMITED ☐ SAME AS REPORT ☐ DTIC USERS	Unclassified	
22a. NAME OF RESPONSIBLE INDIVIDUAL Elsberry, Russell L.	22b. TELEPHONE (*Include Area code*) (408) 646-2373	22c. OFFICE SYMBOL MR/ES

DD FORM 1473, 84 MAR

83 APR edition may be used until exhausted
All other editions are obsolete

SECURITY CLASSIFICATION OF THIS PAGE
Unclassified

Approved for public release; distribution is unlimited.

Upper-Tropospheric Forcing of the Intensification Rates of Tropical Cyclones Flo and Ed based on TCM-90 Observations

by

Jeff H. Rucker
Lieutenant, United States Navy
B.S., United States Naval Academy, 1986

Submitted in partial fulfillment
of the requirements for the degree of

MASTER OF SCIENCE IN Meteorology and Physical Oceanography

from the

NAVAL POSTGRADUATE SCHOOL
June 1992

ABSTRACT

A case study of the upper-tropospheric forcing of the intensification rates of typhoons Flo and Ed has been accomplished. High-resolution, hand-drawn streamline analyses of the 150, 200, 250, and 300 mb winds from the final observational data set of the Tropical Cyclone Motion (TCM-90) field experiment were constructed for 00, 06, 12, and 18 UTC during the period 00 UTC 12 September through 00 UTC 19 September 1990. Three basic interaction mechanisms that appeared to have major roles in upper-level forcing on Flo and Ed were defined. Outflow layer changes were quantified through calculation of the mass divergence and eddy flux convergence of relative angular momentum using a radial-band averaging technique at 200 mb. A nearly 1:1 qualitative relationship was found to exist between the development of one or more of these mass/heat export mechanisms and corresponding changes in the intensification rates. These calculations from the best-ever typhoon region data set strongly suggest that upper-level forcing leads the intensification process by 12-24 h.

N 9222
C.1

TABLE OF CONTENTS

I. INTRODUCTION 1

A. BACKGROUND 1

B. GOALS 6

II. APPROACH 8

A. DATA SET 8

B. ANALYSIS STRATEGY 11

1. Streamline analyses 11

2. Correlation of upper-level forcing with intensification rates 16

3. Tools for examining the vertical structure of cold lows 25

a. Temperature cross-sections in space . . 28

b. Time series of rawinsondes 34

C. LIMITATIONS / QUALIFICATIONS 36

III. SUPERTYPHOON FLO 39

A. ORGANIZATION AND DEVELOPMENT TO TROPICAL STORM 39

1. Initial Development 39

2. The TUTT cell reservoir function 43

B. INTENSIFICATION TO TYPHOON 47

1. Reservoir function effects 47

DUDLEY KNOX LIBRARY
NAVAL POSTGRADUATE SCHOOL
MONTEREY, CALIFORNIA 93943-5002

2. Upper-level anticyclone influences 55
3. The TUTT cell flywheel export mechanism . . 60
C. INTENSIFICATION TO SUPERTYPHOON 69
1. Initial interaction with the subtropical ridge 70
2. The vacuum export mechanism 72
3. Effects of multiple interaction channels . 77
D. INTENSIFICATION TO MAXIMUM STRENGTH 83
1. Complex interaction with C1 and the subtropical ridge 83
2. TUTT cell interaction effects 92
3. Emergence of vacuum effect as dominant export mechanism 93
E. INITIAL WEAKENING 100
1. Loss of the flywheel mechanism 100
2. Resurgence of the reservoir function . . . 110

IV. TYPHOON ED 119
A. DEVELOPMENT TO TYPHOON 119
1. Slow evolution period 120
2. Intensification period 131
3. Mature stage 136
B. INTENSIFICATION TO MAXIMUM STRENGTH 141
C. INITIAL WEAKENING 147
1. Approach of landfall 147

2. Resurgence of a dual outflow channel pattern 147

V. SUMMARY AND CONCLUSIONS 150

A. GOALS AND METHOD 150

B. SUMMARY OF INTERACTION MECHANISMS 156

1. The TUTT cell reservoir function 157

2. The TUTT cell flywheel mechanism 158

3. The vacuum export mechanism 161

C. SUMMARY OF THE INTENSIFICATION PROCESSES . . . 163

1. Supertyphoon Flo 163

2. Typhoon Ed 167

D. CONCLUSIONS 170

VI. RECOMMENDATIONS 176

LIST OF REFERENCES 180

INITIAL DISTRIBUTION LIST 183

LIST OF FIGURES

Fig. 1. Positions of upper-level cold lows C1, C2, C3, C4 (solid lines) each 6 h based on hand analyses of streamlines. Best tracks of tropical cyclones Flo and Ed (ATCR 1990) are indicated by dashed lines. Map times are indicated in the form DAY/UTC. 15

Fig. 2. Best track information for Supertyphoon Flo from ATCR (1990). 18

Fig. 3a. Average mass flux across 6° lat. radius (kt) at 200 mb for Supertyphoon Flo. Bold smoothed line is subjective best-fit to the mass flux calculations indicated at each map time by the dot. Intensity estimates are from ATCR 1990 (solid thin line) and the intensity change (dashed) is over each 6 h period. 21

Fig. 3b. As in (a), except for Typhoon Ed. 22

Fig. 4a. Eddy flux convergence (EFC) of relative angular momentum (kt^2) across 6° lat. radius at 200 mb for Supertyphoon Flo. Bold smoothed line is subjective best-fit to the EFC calculations indicated at each map time by the dot. Intensity and intensity change are as in Fig. 3. 23

Fig. 4b. As in (a), except for Typhoon Ed. 24

Fig. 5a. Bulk vertical wind shear (kt) between mean 200 mb wind speed at 6° lat. radius and storm speed for

Supertyphoon Flo. Bold smoothed line is subjective best fit to the bulk vertical shear calculations indicated at each map time by the dot. Intensity and intensity change are as in Fig. 3 26

Fig. 5b. As in (a), except for Typhoon Ed. 27

Fig. 6. Statistics of layer-mean virtual temperature difference (°C) between (a) clear satellite temperature retrievals and degraded rawinsondes, and (b) cloudy and partly cloudy satellite temperature retrievals and degraded rawinsondes. Colocation threshold is ±100 km and ±6 h. Dashed line is bias and solid line is RMS difference (°C) 31

Fig. 7. (a) Cross-section of satellite temperature deviations from standard atmospheric values through western portion of upper-level cold low C1 at 06 UTC 14 September. Abscissa is retrieval position number and ordinate is pressure level in mb. Cold low C1 is indicated by the region of minimum temperature deviation (C1). (b) Orientation of cross-section (bold solid line) in (a). Positions of Flo and Ed are marked by the tropical cyclone symbols 33

Fig. 8. Time series of upper-air winds (kt; full barb equals 10 kt) at Marcus Island (WMO station number 47991; 24.0°N, 154°E) from 00 UTC 13 September through 12 UTC 18 September. Dashed line marks the signature of cold low C1 as it passed south of the station on a

westward track. Cold low C1 was at closest point of approach (CPA) to the station at 12 UTC 15 September 35

Fig. 9. 200 mb streamline analysis for 00 UTC 12 September. Observation symbols are as follows: ■, rawinsonde; □, dropwinsonde; ●, conventional aircraft (AIREP); *, NASA DC8 research aircraft; x, operational cloud-track wind; ⊠, reprocessed cloud-drift wind. Dashed lines are isotachs of tropical cyclone outflow jets and synoptic-scale jets in 20 kt increments beginning at 40 kt. Tropical cyclone positions are marked by the storm symbol and upper-level cold lows are labeled C1, C2, C3 etc 40

Fig. 10. As in Fig. 9., except for 12 UTC 12 September. 41

Fig. 11. Schematic of the TUTT cell reservoir function. (a) 200 mb flow pattern indicating convergence of outflow from tropical cyclone into cold lows labeled C. (b) Topography of 200 mb surface oriented North (left) - South (right) with outflow into weak TUTT cell to the north and strong outflow to the south. (c) Topography of 200 mb surface oriented West (left) - East (right) with enhanced outflow from tropical cyclone into strong TUTT cell to the east 44

Fig. 12. As in Fig. 9, except for 00 UTC 13 September. 46

Fig. 13. Infrared satellite imagery for 2332 UTC 12 September. Upper-level cold lows are labeled C1, C2, C3 etc. 48
Fig. 14. As in Fig. 9, except for 00 UTC 14 September. 50
Fig. 15. As in Fig. 13, except for 2333 UTC 13 September. 51
Fig. 16. (a) Rawinsonde temperature deviations (°C) from standard atmosphere values and winds (kt) along cross-section through southern portion of upper-level cold low C2 at 18 UTC 13 September. Ship designator at positions of upper-air soundings are indicated. Cold low C2 is in the region of minimum temperature deviation labeled C2. (b) Ship positions for upper-air soundings used in (a) 54
Fig. 17. As in Fig. 9, except for 12 UTC 14 September. 56
Fig. 18. As in Fig. 9, except at 250 mb for 12 UTC 14 September. 58
Fig. 19. Schematic of the TUTT cell flywheel mechanism. (a) 200 mb flow pattern indicating large region of upper-level diffluence on southeastern periphery of TUTT cell (C). (b) 200 mb surface oriented West (left) - East (right) with enhanced outflow into and around TUTT cell to the east of the tropical cyclone . . . 61
Fig. 20. As in Fig. 13, except for 1233 UTC 14 September. 62

Fig. 21. Visible channel satellite imagery for 2332 UTC 14 September. Upper-level cold lows are labeled C1, C2 etc. 64
Fig. 22. As in Fig. 9, except for 00 UTC 15 September. 67
Fig. 23. As in Fig. 9, except for 12 UTC 15 September. 71
Fig. 24. As in Fig. 9, except for 18 UTC 15 September. 73
Fig. 25. Schematic of the vacuum export mechanism. (a) 200 mb flow pattern depicting development of strong tropical cyclone outflow jet across a weakness in the subtropical ridge and into the subtropical jet. (b) Topography of 200 mb surface oriented North (left) - South (right) depicting enhanced outflow due to steeper north-south pressure gradient on northern side of subtropical ridge. (c) Topography of 200 mb surface oriented North (left) - South (right) depicting enhanced outflow across a break in the subtropical ridge 74
Fig. 26. As in Fig. 13, except for 2032 UTC 15 September. 78
Fig. 27. As in Fig. 9, except for 00 UTC 16 September. 80
Fig. 28. (a) As in Fig. 7a, except for cold low C1 at 00 UTC 16 September. (b) As in Fig. 7b, except for cross-section in (a). 82
Fig. 29. As in Fig. 8, except for ship EREH (20.0°N, 126°E) from 00 UTC 13 September through 06 UTC 18

September. Cold low C2 tracked westward and passed over the ship around 12 UTC 15 September. 84
Fig. 30. As in Fig. 9, except for 06 UTC 16 September. 86
Fig. 31. As in Fig. 9, except for 12 UTC 16 September. 87
Fig. 32. As in Fig. 9, except for 00 UTC 17 September. 90
Fig. 33. As in Fig. 13, except for 2332 UTC 16 September. 91
Fig. 34. As in Fig. 9, except for 06 UTC 17 September. 95
Fig. 35. As in Fig. 13, except for 0533 UTC 17 September. 96
Fig. 36. (a) As in Fig. 7a, except for 06 UTC 17 September. (b) As in Fig. 7b, except for cross-section in (a). 98
Fig. 37. As in Fig. 9, except for 12 UTC 17 September. 99
Fig. 38. As in Fig. 13, except for 1232 UTC 17 September. 101
Fig. 39. (a) As in Fig. 7a, except for 18 UTC 17 September. (b) As in Fig. 7b, except for cross-section in (a). 103
Fig. 40. As in Fig. 9, except for 18 UTC 17 September. 104
Fig. 41. As in Fig. 13, except for 2132 UTC 17 September. 106
Fig. 42. As in Fig. 9, except for 00 UTC 18 September. 108
Fig. 43. As in Fig. 13, except for 2332 UTC 17 September. 109
Fig. 44. As in Fig. 9, except for 06 UTC 18 September. 111

Fig. 45. As in Fig. 8, except for Chi Chi Jima (27.0°N, 142.0°E; WMO station number 47971) from 00 UTC 16 September through 12 UTC 18 September. Cold low C1 passed south and west of the station on an increasingly west to northwesterly track. 113
Fig. 46. As in Fig. 9, except for 12 UTC 18 September. 114
Fig. 47. As in Fig. 9, except for 18 UTC 18 September. 116
Fig. 48. (a) As in Fig. 7a, except for 12 UTC 18 September. (b) As in Fig. 7b, except for cross-section in (a). 117
Fig. 49. As in Fig. 13, except for 1832 UTC 18 September. 118
Fig. 50. Best track information for Typhoon Ed from ATCR (1990). 121
Fig. 51. As in Fig. 9, except for 06 UTC 13 September. 123
Fig. 52. As in Fig. 13, except for 0633 UTC 13 September. 125
Fig. 53. As in Fig. 9, except for 12 UTC 13 September. 128
Fig. 54. As in Fig. 9, except for 150 mb at 00 UTC 14 September. 129
Fig. 55. As in Fig. 9, except for 150 mb at 06 UTC 14 September. 130
Fig. 56. As in Fig. 9, except for 150 mb at 12 UTC 13 September. 132
Fig. 57. As in Fig. 13, except for 1234 UTC 13 September. 134

Fig. 58. As in Fig. 9, except for 18 UTC 14 September. 139
Fig. 59. As in Fig. 13, except for 1932 UTC 14 September. 140
Fig. 60. As in Fig. 9, except for 250 mb at 18 UTC 15 September. 144
Fig. 61. Timeline of the intensification of Supertyphoon Flo. "+" ("-") within the timeline indicates times when the intensification rate increased (decreased), and "TS", "TY", "STY" indicate the times at which Flo attained tropical storm, typhoon, and supertyphoon intensity respectively. Lines below the timeline depict when each of the three interaction mechanisms was operating, with the thickness indicating the relative strength of the mechanism 152
Fig. 62. As in Fig. 61, except for Typhoon Ed. 153

ACKNOWLEDGEMENTS

I would like to thank Mr. Pat Harr for his gracious help throughout the course of this thesis. He provided the charts on which all of the analyses were made and was always willing to answer my questions with a fresh perspective. I would also like to thank LCDR Dave Titley for his help with the computer programming requirements of the study and for graciously taking the time to review portions of the text. Special thanks go to my second reader, LCDR George Dunnavan, who was exceedingly helpful from the very beginning - from answering my numerous questions to reviewing the text while it was in progress.

Finally, I would especially like to thank my advisor, Prof. Russell Elsberry, for providing me with his insight, motivation, and patience that started me off and kept me going. Without his help this study would not have been possible.

I. INTRODUCTION

A. BACKGROUND

Tropical cyclone intensification at the most fundamental level is a result of convective instability processes driven by the energy sources of oceanic heat and moisture fluxes and the latent heat of condensation. Studies (e.g., Miller 1958; Emanuel 1988) suggest that sea-surface temperature (SST) establishes a maximum potential intensity that the tropical cyclones may attain, which tends to support the view that internal and local processes such as moist convection and air/sea interaction dominate the intensification process. Numerical modeling studies (Ooyama 1982; Emanuel 1986), which have historically treated the intensifying storm as existing in an inert environment, have further shown that an intense tropical cyclone can be maintained only through the addition of heat by ocean surface fluxes. Clearly, the processes of moist convection and air/sea interaction lay the foundation for the intensification process.

Interactions between the tropical cyclone and the environment have also been shown to play a significant role in the intensification process. Motivation for many of these studies has been the desire to explain why only a few tropical cyclones attain their maximum potential intensity. Merrill

(1988) addressed this issue directly and argued that since the maximum intensity is rarely reached, the environment generally must exert a negative influence that contributes to a weakening of the storm. Conversely, other studies (Riehl 1950; Miller 1958; Sadler 1976, 1978) have shown that environmental interactions can contribute to intensification of the tropical cyclone. One basic idea is that the subsidence associated with the upper-level outflow must not occur in the immediate environment of the storm (Riehl 1950). Subsidence in the near-storm environment would weaken and eventually destroy the horizontal temperature gradient needed to intensify the storm. Holland and Merrill (1984) speculated that as the tropical cyclone intensifies, the anticyclonic asymmetric outflow at the upper levels must increase and become less inertially stable. As described by Holland (1987), decreasing inertial stability in the outflow layer results in less resistance to environmental forcing. Thus, the upper troposphere is considered to be the favored layer for interactions between the tropical cyclone and the environment to influence intensification.

The observational studies of Miller (1958) and Sadler (1978) are consistent with the ideas of Riehl (1950) and Holland and Merrill (1984) since they relate the intensification to interactions with the upper-tropospheric environment. Using analyses of 200 mb geopotential heights compositied from five mature tropical cyclones, Miller (1958)

found that the storms deepened as an upper-level trough shifted inward toward the center of the outflow regime. The interaction mechanism is similar to that described by Holland (1987), in which a strong outflow channel to the midlatitude westerlies develops concurrently with the approach of an upper-level trough from the west. Sadler (1978) found a similar result, and argued that the large-scale circulation of the upper troposphere and the existence of multiple outflow channels play a major role in tropical cyclone intensification. He described the intensification of four typhoons in the western North Pacific that developed a strong outflow channel to the north into the Tropical Upper-Tropospheric Trough (TUTT) along with an outflow channel into the upper-level equatorial easterlies to the south. Rapid intensification occurred when an especially vigorous outflow channel to the north developed in conjunction with the proper positioning of the storm relative to intense, cyclonic cells within the TUTT. Consistent with the ideas of Riehl (1950), Sadler (1978) reasoned that the existence of these strong outflow channels permitted the efficient removal of mass and heat away from the central convective region of the storm such that intensification was likely to occur. Moreover, the decay of the efficient outflow channel and the corresponding loss of the dual outflow pattern resulted in the weakening of an intense tropical cyclone.

Significant evidence exists therefore that interactions between the environment and the tropical cyclone, especially those that occur within the upper-tropospheric outflow layer where the inertial stability is favorably low, can play a major role in determining the rate of intensification. As described by Molinari and Vollaro (1989), the role of environmental forcing may be best considered as one of modulating the ultimate intensity of the storm. Whereas lack of upper-level interaction may result in conditions unfavorable for intensification, significant upper-level interaction may produce much more rapid intensification than would normally occur in isolation (Sadler 1978). Such upper-level forcing cannot produce an intensity beyond the upper bound set by the SST, because in such a case the ocean fluxes could not support the storm. Since tropical cyclones seldom develop to their maximum potential intensity, forecasting the ultimate intensity of a deepening storm may well depend more on the ability to forecast the upper-level forcing than on the knowledge of the SST within a presumably near-uniform warm oceanic region. Forecasting such upper-level forcing requires an understanding and quantification of the physical mechanisms that have been described in observational studies such as Miller (1958) and Sadler (1978).

Pfeffer (1958) proposed that the role of environmental interactions in tropical cyclone intensification could be quantified by the calculation of the horizontal transport of

angular momentum by azimuthal eddies in the cyclone-environment system. Subsequent compositing and modeling studies (McBride and Zehr 1981; Pfeffer and Challa 1981) have shown that the outflow layers of developing storms are characterized by large inward eddy fluxes of cyclonic angular momentum, while such fluxes were weaker in the non-developing storms. As described by Holland (1987), fluxes of eddy cyclonic angular momentum provide a potential mechanism for intensification by enhancing the outflow of the storm. This idea was verified by the case study of Hurricane Elena (1985) in which Molinari and Vollaro (1989) found that outflow-layer eddy angular momentum fluxes were correlated with the changes in intensity. On the other hand, Merrill (1988) found no significant relationship between such fluxes and corresponding intensity changes in a 5 - year composite of Atlantic hurricanes. More recently, DeMaria et al. (1991) calculated the eddy flux convergence (EFC) of relative angular momentum at 200 mb for the named storms during two Atlantic hurricane seasons. They found only a small (but statistically significant) positive correlation between EFC and intensity changes. They suggested that other environmental factors such as the influences of SST and vertical shear not accounted for in their study may have also played a role.

Studies of eddy momentum forcing have therefore added significantly to the understanding and quantification of the physical mechanisms that have been hypothesized to relate

environmental forcing to tropical cyclone intensification. Nevertheless, a precise understanding of the interaction between the convective scale of the tropical cyclone and the synoptic-scale forcing remains unclear. Such an understanding is hampered by the scarcity of detailed observations of the three-dimensional structure of the tropical cyclone outflow layer.

B. GOALS

The Tropical Cyclone Motion (TCM-90) field experiment conducted in the western North Pacific from August to September 1990 provides a high density of observations from various data sources (Elsberry 1990; Elsberry et al. 1990; Harr et al. 1991). To better understand the interactions between the tropical cyclone and its environment, particular emphasis was placed on obtaining observations of the outflow layers of the six target tropical cyclones during the experiment. Prior data sets and the routine operational data have historically lacked the spatial and temporal resolution necessary to fully describe the upper-level interactions that may play a role in the intensification process.

Of particular interest during TCM-90 was the near-simultaneous, yet considerably different, developments of two tropical cyclones over the same region of favorably warm ocean. Tropical cyclone Ed, which was the first to develop, achieved only slightly more than minimum typhoon intensity

(65 kt), while Flo intensified rapidly and achieved supertyphoon intensity (≥ 130 kt). The TCM-90 data set (Harr et al. 1991; see description in next section) provides an outstanding opportunity to determine what role upper-level forcing may have played in the development of these two storms.

The hypothesis of this study is that the post-processed TCM-90 data set provides sufficient spatial and temporal resolution to depict upper-tropospheric forcing on tropical cyclones Flo and Ed, and that such forcing can be related to changes in the intensification rates of these storms. The goal of the study is to use this best-ever typhoon region data set to: (i) identify specific interactions between the upper-level environment and the tropical cyclones; and (ii) correlate changes in these interactions with observed changes in the intensities of Flo and Ed.

II. APPROACH

A. DATA SET

The final TCM-90 data base is described in detail by Harr et al. (1991) and is comprised of two categories: (i) real-time data; and (ii) delayed data. Real-time data were collected and processed during the field phases of the experiment in conjunction with the Navy Operational Global Atmospheric Prediction System (NOGAPS) at the Fleet Numerical Oceanography Center (FNOC), Monterey CA. Real-time data include: 90 % of the rawinsonde observations; all of the pilot balloons; most of the surface data (land, ship and buoy); aircraft observations (mostly conventional aircraft reports); satellite temperature soundings retrieved by the National Environmental Satellite, Data and Information Service (NESDIS); and satellite cloud-tracked winds (from the Japanese Meteorological Agency). Extensive quality control procedures that were applied to the real-time data are described in Baker (1991).

Delayed data were collected after the field phase and consist of both observations that were not received in real-time and observations that were reprocessed prior to being added to the data base. Delayed data include: radar wind profiler data; surface synoptic reports (from the USSR ships

and Japanese islands); some of the drifting buoy data; flight-level data and dropwinsondes from the NASA DC8 research aircraft; reprocessed satellite cloud-drift winds (manually processed by the University of Wisconsin); and the remaining 10 % of rawinsonde soundings received later. While some of the delayed data were subjected to some type of quality control at the source, none of these data underwent the vertical consistency checks associated with the NOGAPS quality control process.

Gradient-level and upper-level (200 mb) streamlines were analyzed operationally at 00 and 12 UTC by the Joint Typhoon Warning Center (JTWC), Guam staff based on real-time wind observations received at JTWC. Real-time satellite imagery and working best tracks from the Automated Tropical Cyclone Forecast (ATCF) system were also used in the preparation of the operational analyses.

Summaries of the Intensive Observing Periods (IOPs) by the TCM-90 research team are provided in Elsberry et al. (1990). Subjective interpretations of the operational analyses, synoptic discussions, hypotheses and research aspects, and notes on the data coverage are included in these IOP summaries. Summaries for IOPs 5, 6 and 7 (00 UTC 13 September - 12 UTC 14 September, 00 UTC 15 September - 12 UTC 16 September, and 00 UTC 17 September - 00 UTC 19 September respectively) describe tropical cyclones Ed and Flo and suggest that upper-level interaction may have played a role in

the intensification of these two storms. Flo developed to supertyphoon intensity, while Ed reached only slightly more than minimum typhoon strength, despite the nearly simultaneous development of the two storms within the same region. Of specific interest was the apparent interaction between Flo and an adjacent large TUTT cell, whereas no strong forcing of Ed was evident.

A review of the operational JTWC streamline analyses and accompanying hard-copy satellite imagery for IOPs 5, 6 and 7 was accomplished as a first step. The goal was to determine whether the additional real-time data provided by the TCM-90 experiment were sufficient to characterize the upper-level interactions that induced intensity changes in the tropical cyclones. While evidence of synoptic-scale interactions was found, the spatial and temporal (12 h) resolution afforded by the real-time observations was insufficient to fully describe the upper-level forcing. Tracks of upper-level anticyclones and cold lows were often erratic due to a lack of time continuity. As a result of the sporadic development and decay of these features as depicted on the operational charts, possible interactions between these features and the tropical cyclones were difficult to analyze. In particular, correlations between changes in the upper-level circulation pattern and corresponding changes in the intensities of Flo and Ed were inconclusive. This preliminary analysis indicated that a detailed examination of upper-level forcing on the

intensification rates of the two storms would require the additional spatial and temporal resolution afforded by the delayed data in the final TCM-90 data base.

B. ANALYSIS STRATEGY

1. Streamline analyses

High-resolution, hand-drawn streamline analyses of the 150, 200, 250 and 300 mb winds from the final TCM-90 observational data set were constructed at 00, 06, 12 and 18 UTC for the period 00 UTC 12 September through 00 UTC 19 September. Isotachs also were analyzed in limited regions of the tropical cyclone outflow and synoptic-scale jets. Consistent with generally accepted guidelines, the hierarchy of reports used in constructing the streamlines was (in order of decreasing significance): (i) real-time upper-air station soundings, including pilot balloon reports from the U.S. Pacific Islands; (ii) delayed upper-air station soundings; (iii) NASA DC8 flight-level winds; (iv) dropwindsondes; (v) reprocessed satellite cloud-drift winds; (vi) real-time conventional aircraft reports; and (vii) operational cloud-track winds. Real-time upper-air soundings were considered to be more representative of the atmospheric state than were the delayed rawinsondes because the real-time data were subjected to NOGAPS quality control procedures. The reprocessed cloud-drift winds were considered to be more accurate than operational cloud-drift winds because the height assignment of

the operational winds is known to be suspect (Harr et al. 1991). By contrast, a careful height assignment could be done at the University of Wisconsin after the field experiment by using the additional upper-air observations from TCM-90 and the other international experiments.

Four levels were analyzed to achieve vertical consistency and to increase the horizontal resolution at adjacent levels in data-sparse regions. The existence of reprocessed cloud-drift winds at all four pressure levels was of particular significance. Since these observations require clouds as tracers, and since the strong tropical cyclone outflow jets are typically marked by cirrus streamers, changes in the maximum outflow layer may be represented by changes in the level of maximum density of cloud-drift wind observations. These observations were critical to assess the vertical structure of the outflow layer. The objective of this multi-layer analysis approach was to describe the vertical structure, or topography, of the upper-level flow pattern. For example, the vertical structure of adjacent synoptic-scale features such as cold lows may play a role in upper-level forcing of the tropical cyclone and thus must be considered.

Hard-copies of the satellite imagery were used extensively during the construction of these analyses. This imagery provides a means of independently verifying the observations in regions where the circulation was revealed in the cloud patterns, and as a means of identifying and locating

circulation centers of features such as cold lows. Imagery was particularly useful in describing the orientation of the upper-level anticyclones that were revealed by the clear regions that had upper-level convergence and subsidence versus regions with high clouds (upper-level divergence and deep convection) that marked the outdraft circulations.

In general, the wind observations near the center of the tropical cyclone are a reflection of both the horizontal motion of the air parcels and of previous vertical motion. For example, if the observations nearest the tropical cyclone at 250 mb are located 100 km from the storm center and suggest anticyclonic outflow, then the air parcels may have originated as an outflow from a higher level (e.g., between 200 - 100 mb) within the storm. Thus, outflow at a certain level cannot necessarily be inferred based solely upon observations that are located more than 100 km from the storm center. This concept of the outflow regime was invoked only in the subjective interpretation of the analyses, because there was no way in which to represent vertical motion with the horizontal streamlines. Adhering to generally accepted guidelines, the streamline analyses were constructed by "drawing to the observations," and thus care must be taken when evaluating outflow at a certain level based on a literal interpretation of the streamline direction relative to a circle about the storm center.

Since the motion of significant upper-level circulation features relative to the tropical cyclones was required to assess possible interactions, considerable emphasis was placed on defining the locations of the features at each map time. Working best tracks of the upper-level cold lows and anticyclones were constructed simultaneously with the construction of the streamlines. Initial positions of the various circulation features were estimated from the first set of streamlines that mainly consisted of a comparison of the wind observations and the satellite imagery. Spatial and temporal continuity concepts were then applied in an iterative fashion to adjust the feature centers on the analyses. This iterative streamline analysis technique was utilized in both the horizontal and vertical directions, as observations at adjacent levels could often be used to better locate a circulation feature. After several iterations using all of the available data, best tracks were constructed for each of the upper-level cold lows (Fig. 1). Best tracks for the upper-level anticyclones were not constructed because of the small displacements of these features during the period of study.

In summary, the streamline and isotach hand analyses produced here offered many improvements over the operational charts and enabled the study of upper-level forcing on Flo and Ed. While the increased number of observations was certainly significant, the spatial resolution was most improved by the four layer, subjective iteration analysis technique. Temporal

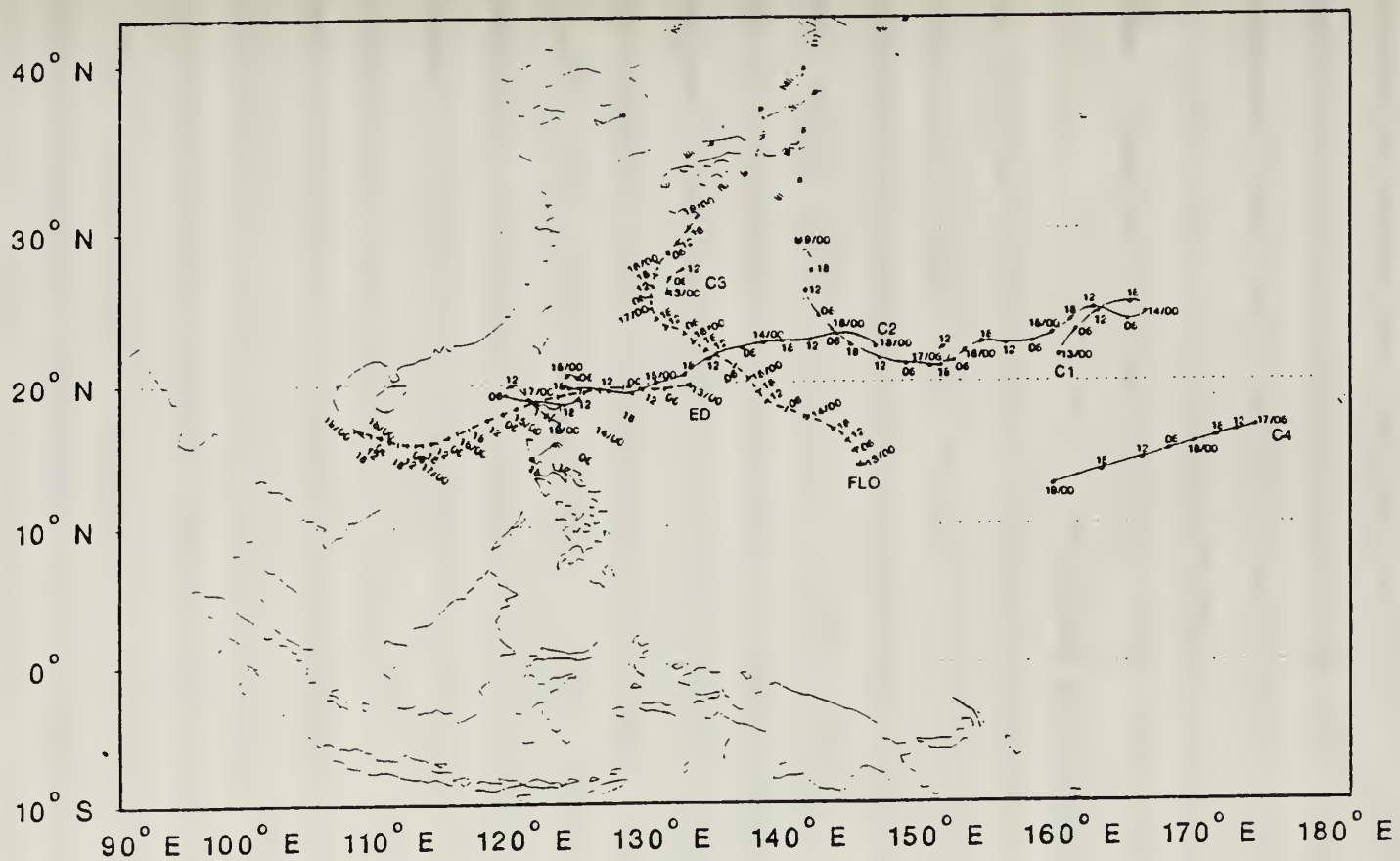

Fig. 1. Positions of upper-level cold lows C1, C2, C3, C4 (solid lines) each 6 h based on hand analyses of streamlines. Best tracks of tropical cyclones Flo and Ed (ATCR 1990) are indicated by dashed lines. Map times are indicated in the form DAY/UTC.

resolution was similarly improved through the construction of analyses each 6 h. With improved continuity in both time and space, the development, motion and decay of the upper-level circulation features could be described with more confidence. Most importantly, the resolution was improved to the degree that upper-level interactions could be identified, tracked, and correlated with intensity changes.

2. Correlation of upper-level forcing with intensification rates

The final set of streamline and isotach analyses and the corresponding satellite imagery were carefully studied, and a detailed, subjective meteorological summary was compiled for both Flo and Ed. Several aspects of the upper-level circulation pattern were examined: (i) changes in the orientation and level of maximum outflow of the tropical cyclone outflow jets; (ii) changes in the strength and position of the subtropical ridge and subtropical jet; (iii) changes in the orientation and apparent strength of the upper-level long-wave trough; (iv) changes in the horizontal extent and motion of the TUTT cells; (v) development and decay of both indraft and outdraft anticyclones; (vi) changes in the synoptic-scale, background flow pattern; and (vii) indications of any direct interaction between the two tropical cyclones. Each of these aspects was compared independently and in combination to changes in the observed intensities of the

tropical cyclones as determined by JTWC (e.g., Fig. 2). Of specific interest was the degree to which changes in the upper-level flow pattern could account for the development of Flo to supertyphoon intensity while Ed achieved only slightly more than minimal typhoon strength. As a result of the careful study, three basic interactions between the tropical cyclones and the upper-tropospheric environment were identified and subjectively correlated with changes in the intensification rates. These are described in detail in Chapter III.

The intensification rates used here are based on the post-storm interpretations by JTWC in the Annual Tropical Cyclone Report (ATCR). JTWC uses the Dvorak pattern recognition technique and available observations to estimate the minimum pressure and maximum sustained surface winds (ATCR 1990). Only in a few special cases, such as penetration of the eyewall by the NASA DC8 research aircraft, are direct intensity measurements available in the western North Pacific. Estimates of intensity are provided each 6 h (Fig. 2). As described by Frank (1987), the accuracy of these intensity estimates is difficult to assess without direct observations, and thus the ability to accurately define the intensity change over a 6 h period is somewhat questionable. For this reason, the study is primarily concerned with trends in the intensification rates. An intensity error of ±5 kt was assumed in correlating changes in the upper-level forcing to changes in the intensification rates.

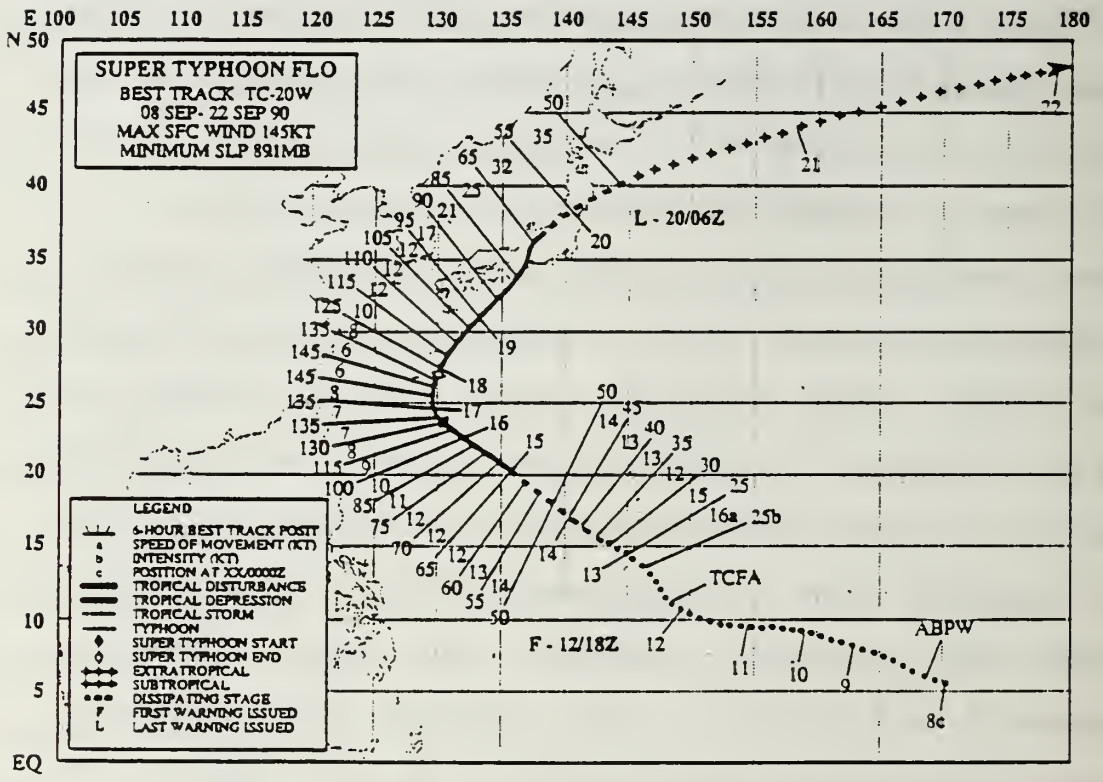

Fig. 2. Best track information for Supertyphoon Flo from ATCR (1990).

A quantitative measure of the upper-level forcing was determined through the use of a radial-band averaging technique similar to that described by Chan and Gray (1982). A circle of radius 6 deg. lat. was divided into 16 radial sectors and was geographically oriented (versus a storm-following orientation) on the best track positions of both storms. The speed and direction of the average wind crossing this circle were estimated for each of the radial sectors at each map time based on the final set of 200 mb streamline and isotach analyses. Radial and tangential wind components relative to the storm center were then calculated using the average wind for each sector at each map time. The 16 average winds and radial and tangential wind components were then used to calculate the direction and speed of the mean wind crossing the circle and the mean radial and tangential wind component for each map time.

As described by Holland (1987), a radial distance of 6 deg. lat. from the storm center is well within the anticyclonic outflow regime that is characterized by low inertial stabilty and hence low resistance to radial motion. It is within this regime therefore that interactions between the tropical cyclone and the environment that may produce intensity changes are most likely. For this reason, the magnitude of the average radial wind component at each map time was interpreted as a measure of the mass flux across the circle (mass divergence). Such changes in the mass divergence

were subjectively correlated with both the development of the three interaction mechanisms that were identified and the intensity estimates provided by JTWC (ATCR 1990). Graphs of the mass flux at 200 mb for the outflow regimes of Flo and Ed are shown in Figs. 3a and 3b respectively.

The 16 radial and tangential wind components were also used to calculate the eddy flux convergence (EFC) of relative angular momentum at 200 mb for both Flo and Ed using the relationship

$$EFC = \overline{v_r' \, v_\theta'} = \sum v_r v_\theta - \overline{v_r} \, \overline{v_\theta} \, ,$$

where v_r and v_θ are the radial and tangential wind components respectively. As described by DeMaria et al. (1991), changes in EFC are related to the interactions between the tropical cyclone and the environment. Thus, the changes in EFC at 200 mb for Flo and Ed were subjectively correlated with the development of the three identified interaction mechanisms and the storm intensity estimates. Graphs of the EFC at 200 mb for Flo and Ed are shown in Figs. 4a and 4b respectively.

Finally, the mean 200 mb wind speed and direction crossing the 6 deg. lat. circle at each map time were subtracted from the corresponding best track course and speed of the storm (ATCR 1990). The resulting vector difference was interpreted as a measure of the bulk vertical shear of the outflow layer

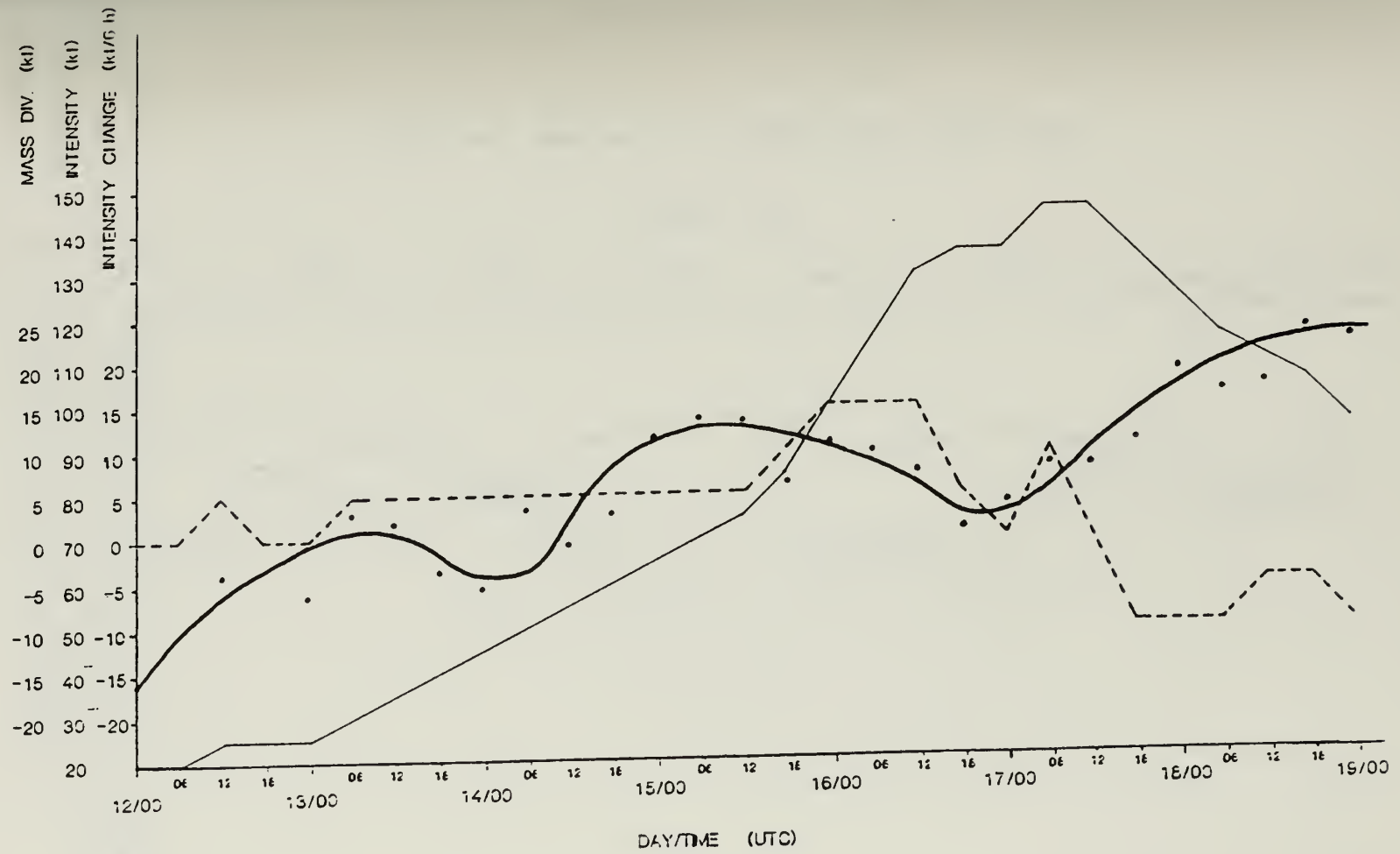

Fig. 3a. Average mass flux across 6° lat. radius (kt) at 200 mb for Supertyphoon Flo. Bold smoothed line is subjective best-fit to the mass flux calculations indicated at each map time by the dot. Intensity estimates are from ATCR 1990 (solid thin line) and the intensity change (dashed) is over each 6 h period.

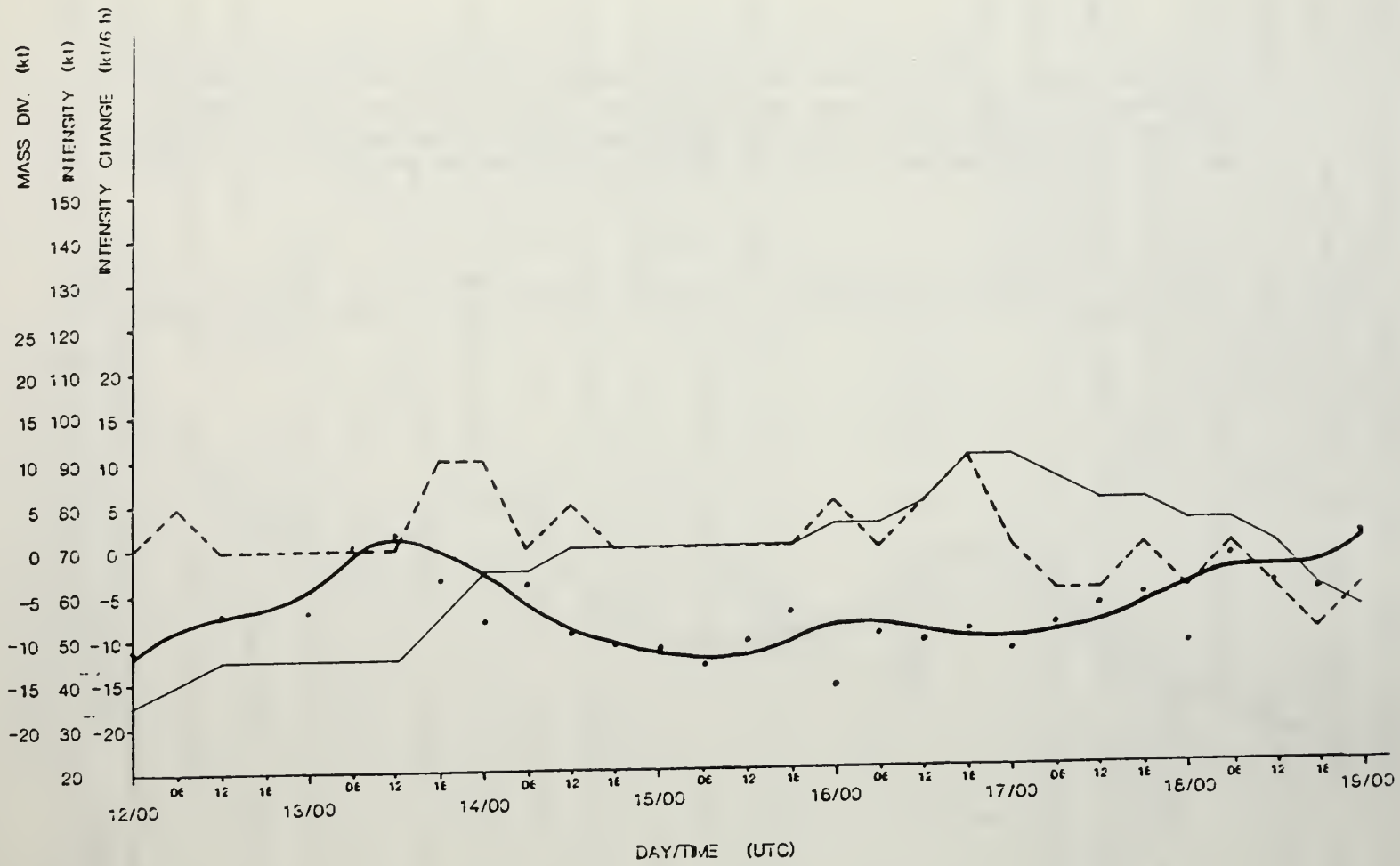

Fig. 3b. As in (a), except for Typhoon Ed.

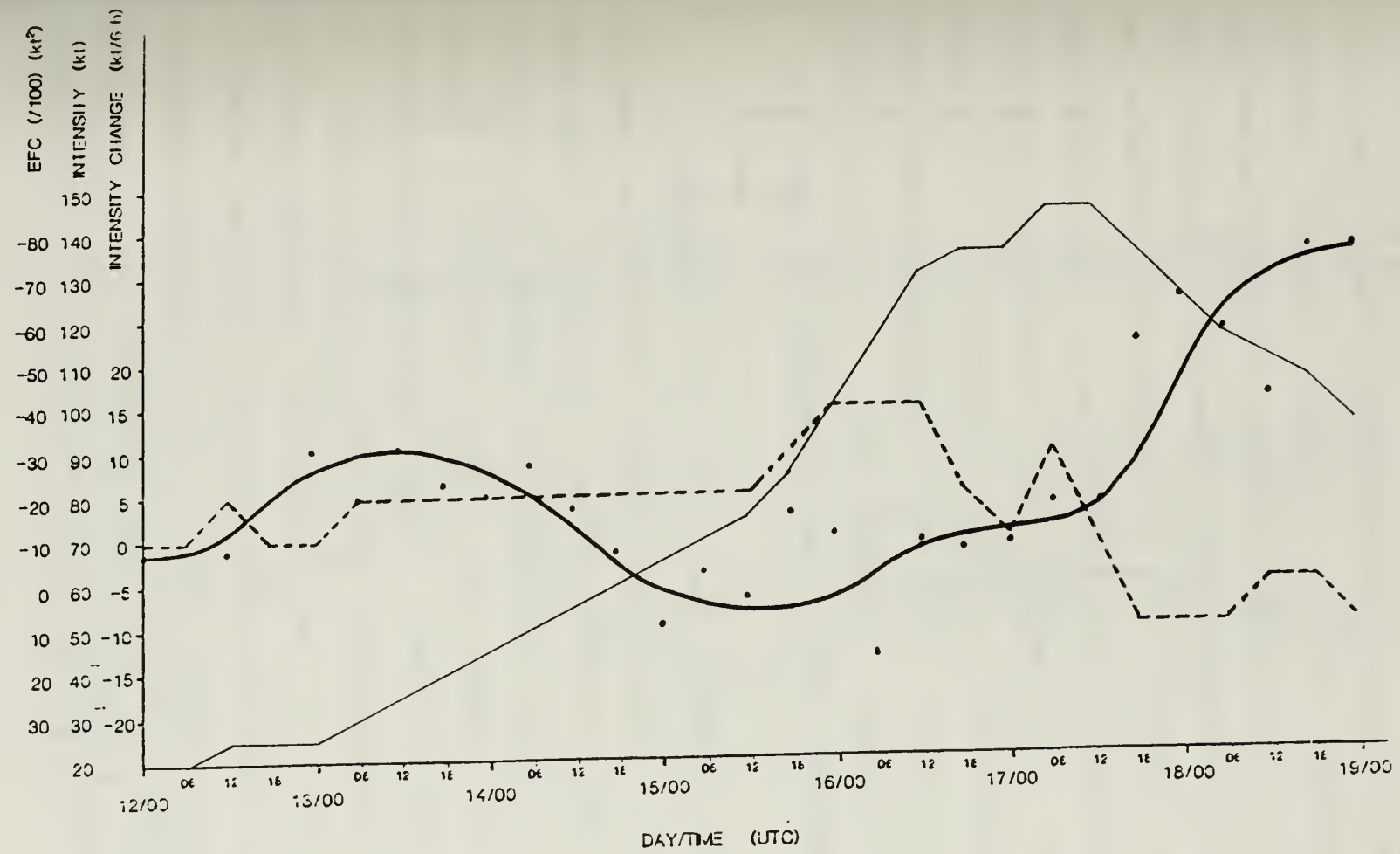

Fig. 4a. Eddy flux convergence (EFC) of relative angular momentum (kt^2) across 6° lat. radius at 200 mb for Supertyphoon Flo. Bold smoothed line is subjective best-fit to the EFC calculations indicated at each map time by the dot. Intensity and intensity change are as in Fig. 3.

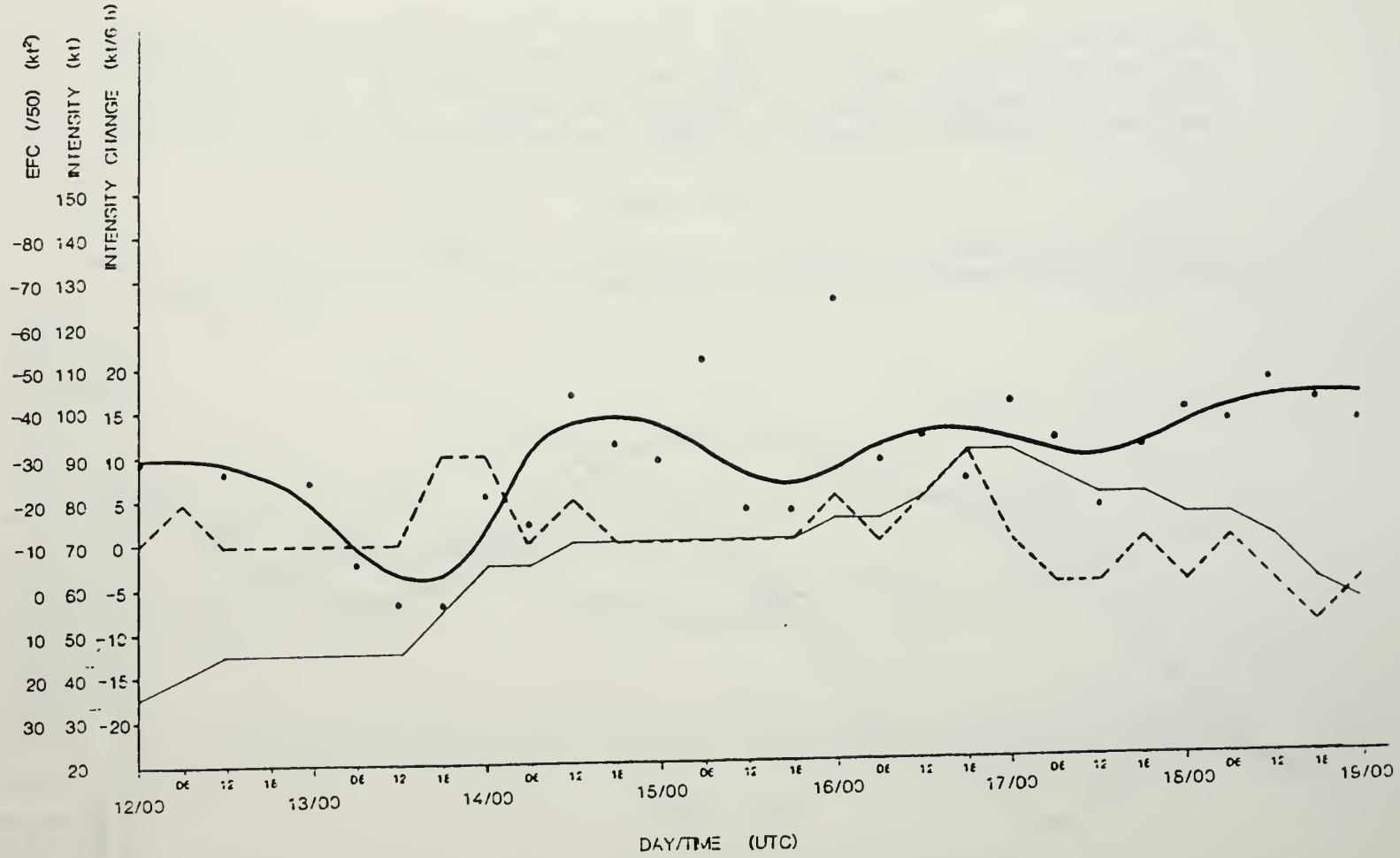

Fig. 4b. As in (a), except for Typhoon Ed.

relative to the lower troposphere winds that are advecting the storm. Large values of the magnitude of this bulk shear vector therefore indicated periods when the storms may have experienced tendencies towards disorganization of the outflow layer, which would represent negative upper-level forcing on the intensification rates. Thus, the magnitude of the bulk shear vector was an additional factor considered in the subjective correlation of the changes in the upper-level forcing with corresponding changes in the intensification rates. Graphs depicting the bulk shear vector at 200 mb for Flo and Ed are shown in Figs. 5a and 5b respectively.

3. Tools for examining the vertical structure of cold lows

Interpretation of the final streamline and isotach analyses suggested that the vertical structure of significant upper-level circulation features such as cold lows was important for gaging the upper-level forcing on tropical cyclone intensification rates. Two methods, or tools, were used to better define the vertical structure of the cold lows: (i) spatial cross-sections from rawinsondes and satellite-derived temperature retrievals; and (ii) time series of selected rawinsondes. The goal was to determine whether these features penetrated down to the middle troposphere. In addition, a more complete description of how the vertical structure of these features changed during the period of study

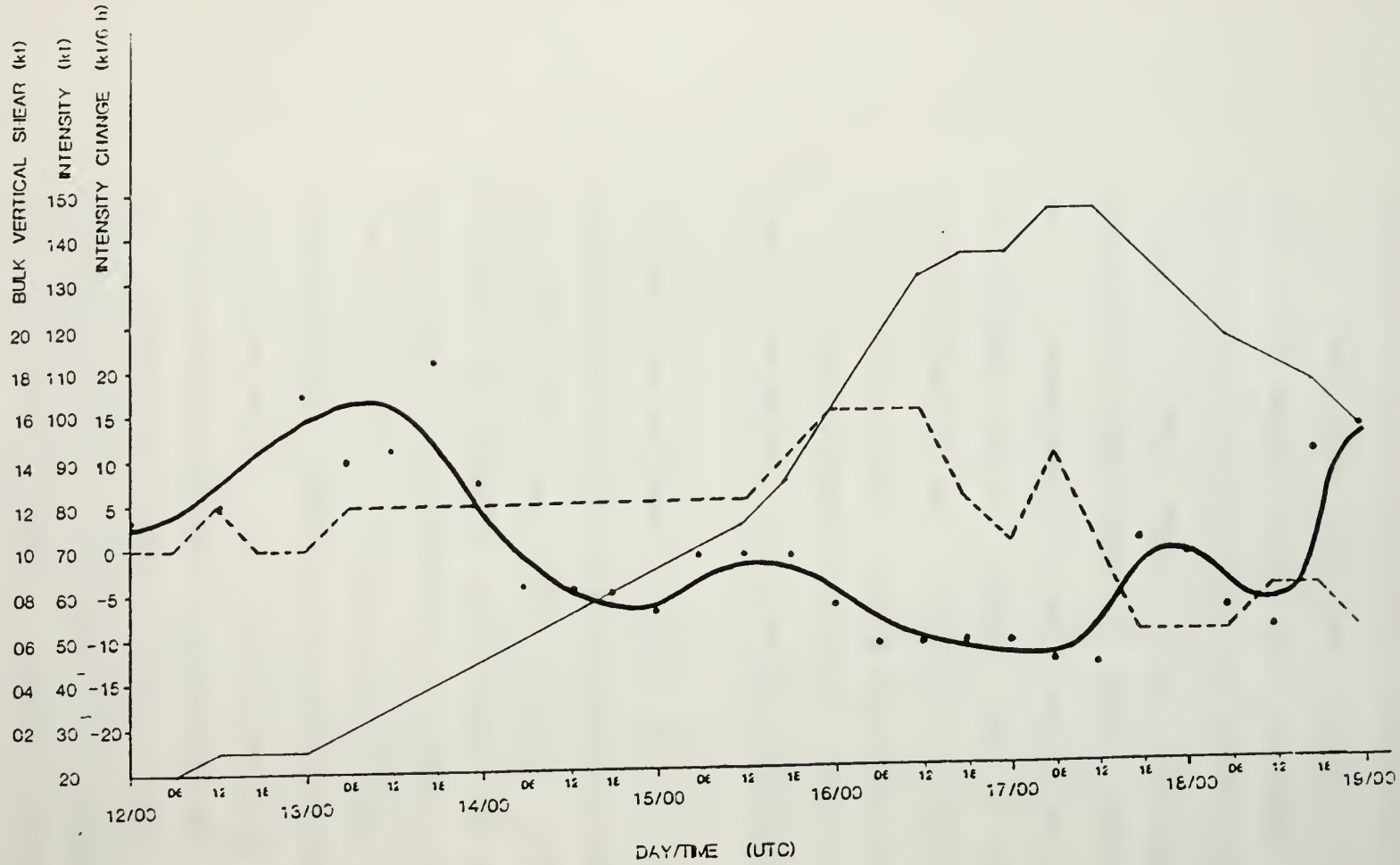

Fig. 5a. Bulk vertical wind shear (kt) between mean 200 mb wind speed at 6° lat. radius and storm speed for Supertyphoon Flo. Bold smoothed line is subjective best-fit to the bulk vertical shear calculations indicated at each map time by the dot. Intensity and intensity change are as in Fig. 3.

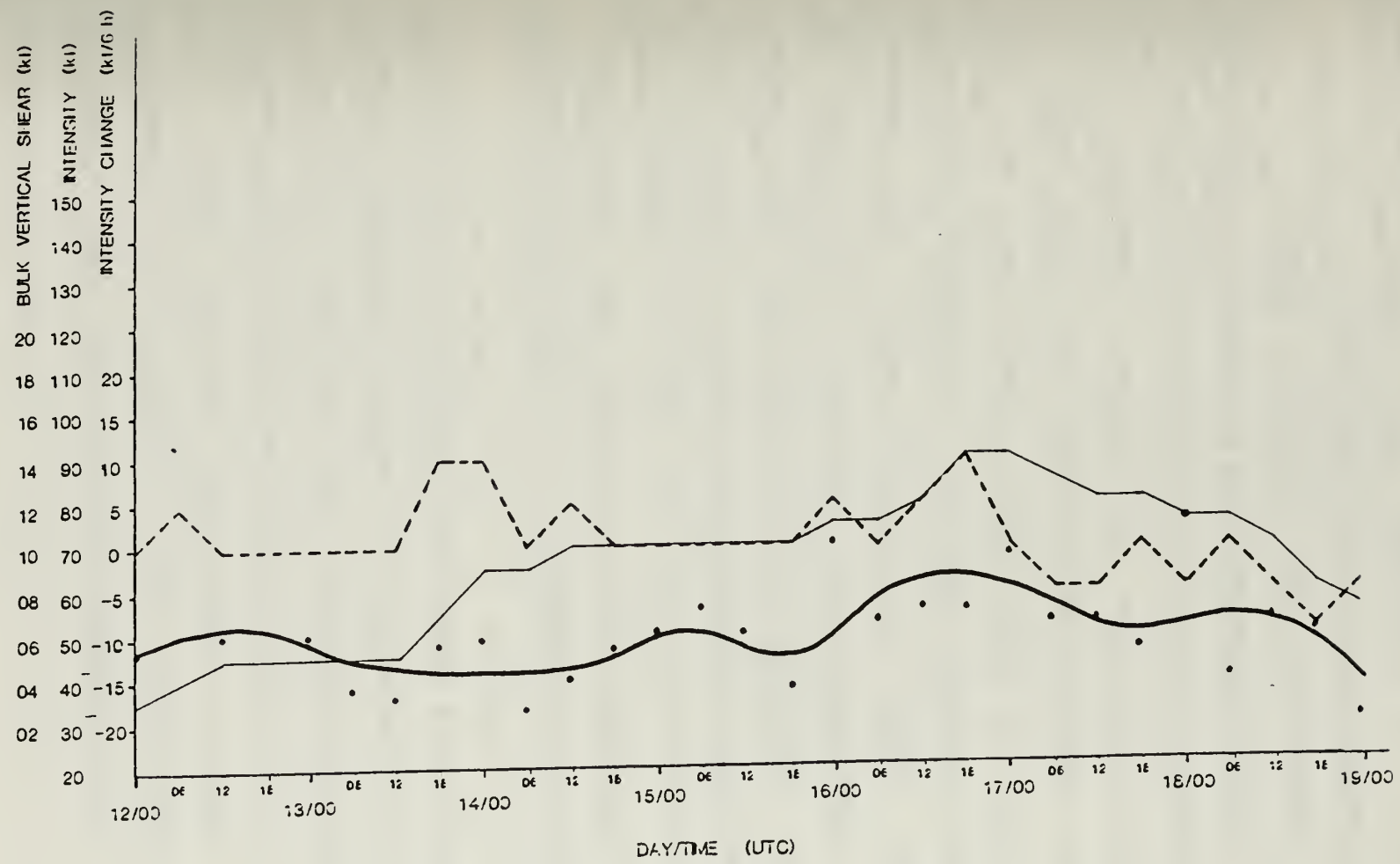

Fig. 5b. As in (a), except for Typhoon Ed.

would enable a better understanding as to what role the cold lows played in the development and/or decay of the three interaction mechanisms that were identified.

a. Temperature cross-sections in space

Spatial cross-sections of temperature provided an independent means of identifying and quantifying the vertical structure of the cold lows. Two sources of temperature data were used to construct the cross-sections. First, upper-air soundings from the final TCM-90 observational data base provided high vertical resolution of observed atmospheric temperatures. Despite the improved spatial and temporal resolution provided by the additional TCM-90 upper-air stations, the rawinsonde soundings were still widely spaced. Thus, the ability to describe the structure of the cold lows depended on fortuitous tracks over upper-air stations. The paucity of stations east of 140°E was particularly debilitating to the construction of cross-sections through cold lows.

An improved data density was provided by the real-time TCM-90 satellite temperature retrievals. These soundings were obtained by the NOAA-TOVS and DMSP-SSM/T instruments. Thicknesses for the standard atmospheric layers were produced by NESDIS using a statistical retrieval method. The hypsometric equation was used to convert the thicknesses to layer-mean virtual temperatures that could then be used to

construct a nine-layer, satellite-derived temperature sounding from which cross-sections were constructed.

Since the goal of constructing the cross-sections was to describe the vertical structure of the TUTT cell, the coarse vertical resolution in these satellite soundings was of some concern. The quality or accuracy of the retrieval thicknesses in the tropics also is unknown. Thus, the satellite soundings first were compared with the TCM-90 rawinsondes, which were degraded to match the layer-mean values of the satellite soundings. The rawinsonde data were degraded by using the height information for the same levels used to define the layer thicknesses in the satellite soundings. The measured thicknesses were then applied to the hypsometric equation to derive a layer-mean virtual temperature for each of the nine pressure levels.

Temperature differences between the layer-mean satellite and degraded rawinsonde virtual temperatures were computed for all colocations between 00 UTC 13 September to 00 UTC 19 September within the region 5° - 30°N, 110° - 160°E. The colocation thresholds were ± 6 h and ± 100 km. Separate statistics were computed for the clear, cloudy and partly cloudy retrievals (Table I). Statistics for an additional category consisting of the partly cloudy and cloudy retrievals (CY/PC) were also computed. Since the differences between the cloudy and partly cloudy statistics were negligible, the CY/PC statistics are shown with those of the clear retrievals in

Table I. Temperature differences (°C) between satellite retrievals and colocated rawinsondes during TCM-90.

	PRESSURE LEVEL (mb)								
RETRIEVAL TYPE	925	775	600	450	350	275	225	175	125
CLEAR									
-Number of samples	73	87	87	87	88	88	87	84	79
-Bias	1.00	0.66	-0.16	-0.37	0.04	-0.33	-0.21	-0.27	0.21
-RMS difference	2.72	1.79	1.16	1.17	1.16	1.47	1.59	1.52	2.18
CLOUDY									
Number of samples	35	35	35	34	35	34	34	34	34
-Bias	1.84	0.57	-0.46	-0.13	-0.14	-0.43	-0.16	-0.21	0.44
-RMS difference	2.87	1.35	1.28	1.93	1.52	1.72	1.36	1.84	2.11
PARTLY CLOUDY									
-Number of samples	15	14	14	13	14	14	14	15	14
-Bias	0.47	-0.41	-0.73	-0.41	-1.15	-0.94	-1.09	-0.40	0.30
-RMS difference	1.33	1.61	1.78	1.43	1.89	1.94	2.00	1.65	2.05
CLOUDY / PARTLY CLOUDY									
-Number of samples	50	49	49	47	49	48	48	49	48
-Bias	1.43	0.29	-0.49	-0.21	-0.35	-0.57	-0.43	-0.27	0.40
-RMS difference	2.51	1.43	1.44	1.81	1.64	1.79	1.58	1.79	2.09

Figs. 6a and 6b respectively.

This limited intercomparison is in excellent agreement with Kelly et al. (1991), who indicated that the satellite temperature bias for all retrieval categories is typically less than 1° C. More importantly, the RMS difference between the satellite soundings and the layer-mean rawinsonde values is typically between 1° - 2° C. Largest differences occurred above 175 mb near the tropical tropopause and between 775 mb and the surface. These results suggested that temperature anomalies of 2° C or more, such as those associated with upper-level cold lows, might be detected by the satellite

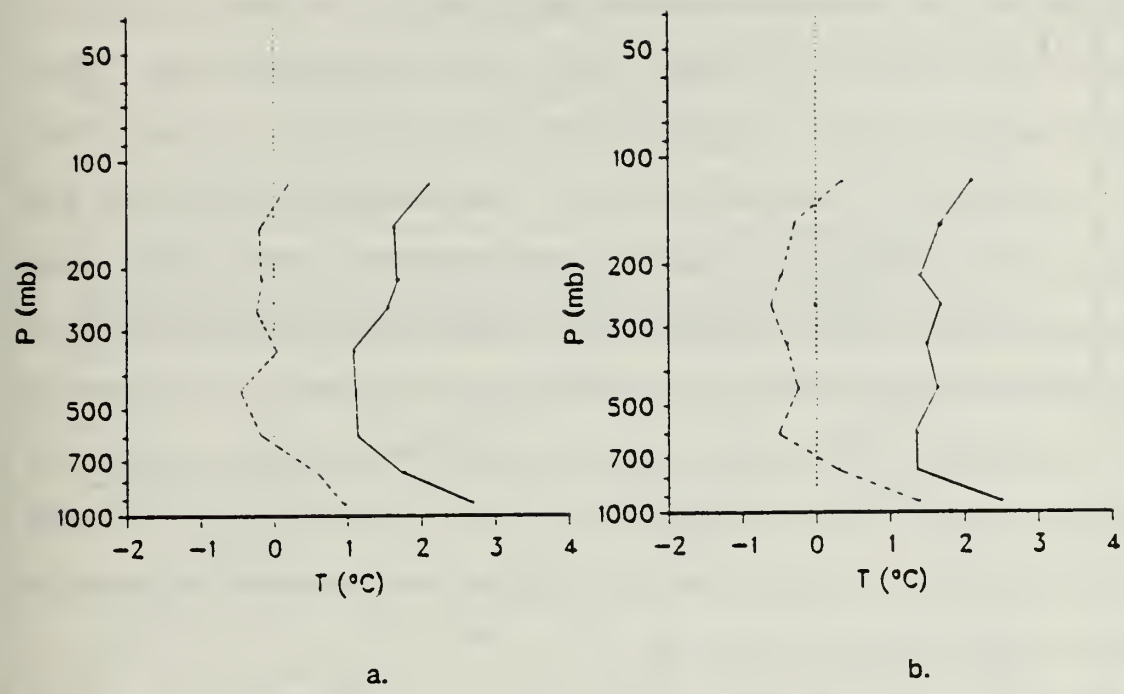

Fig. 6. Statistics of layer-mean virtual temperature difference (°C) between (a) clear satellite temperature retrievals and degraded rawinsondes, and (b) cloudy and partly cloudy satellite temperature retrievals and degraded rawinsondes. Colocation threshold is ±100 km and ±6 h. Dashed line is bias and solid line is RMS difference (°C).

soundings.

Temperature deviation cross-sections were constructed by subtracting from each the corresponding (midlatitude) standard atmospheric temperature for each pressure level. Such deviations facilitate the identification of temperature anomalies on the spatial cross-sections. As shown in Fig. 7a, the tropical temperature deviations are generally positive relative to the standard atmosphere. Negative deviations, or smaller positive deviations, are cold anomalies and hence should mark the cold signature of a TUTT cell. On the other hand, regions of large positive temperature deviation are regions of abnormally warm temperatures, and such warm anomalies match the signature of warm-core systems such as tropical cyclones. The 14°C temperature deviation isopleth in Fig. 7a indicates a cold anomaly centered slightly north of sounding 50447. This matches fairly well the position of TUTT cell C1 as shown in Fig. 7b and suggests a vertical signature down to approximately 500 mb.

Similar temperature deviation cross-sections were constructed from both the rawinsonde and satellite soundings for the upper-level lows shown in Fig. 1 whenever the orientation and density of the observations were favorable. The vertical structure information derived from these cross-sections will be used below in the interpretation of the interaction between the cold lows and the tropical cyclones.

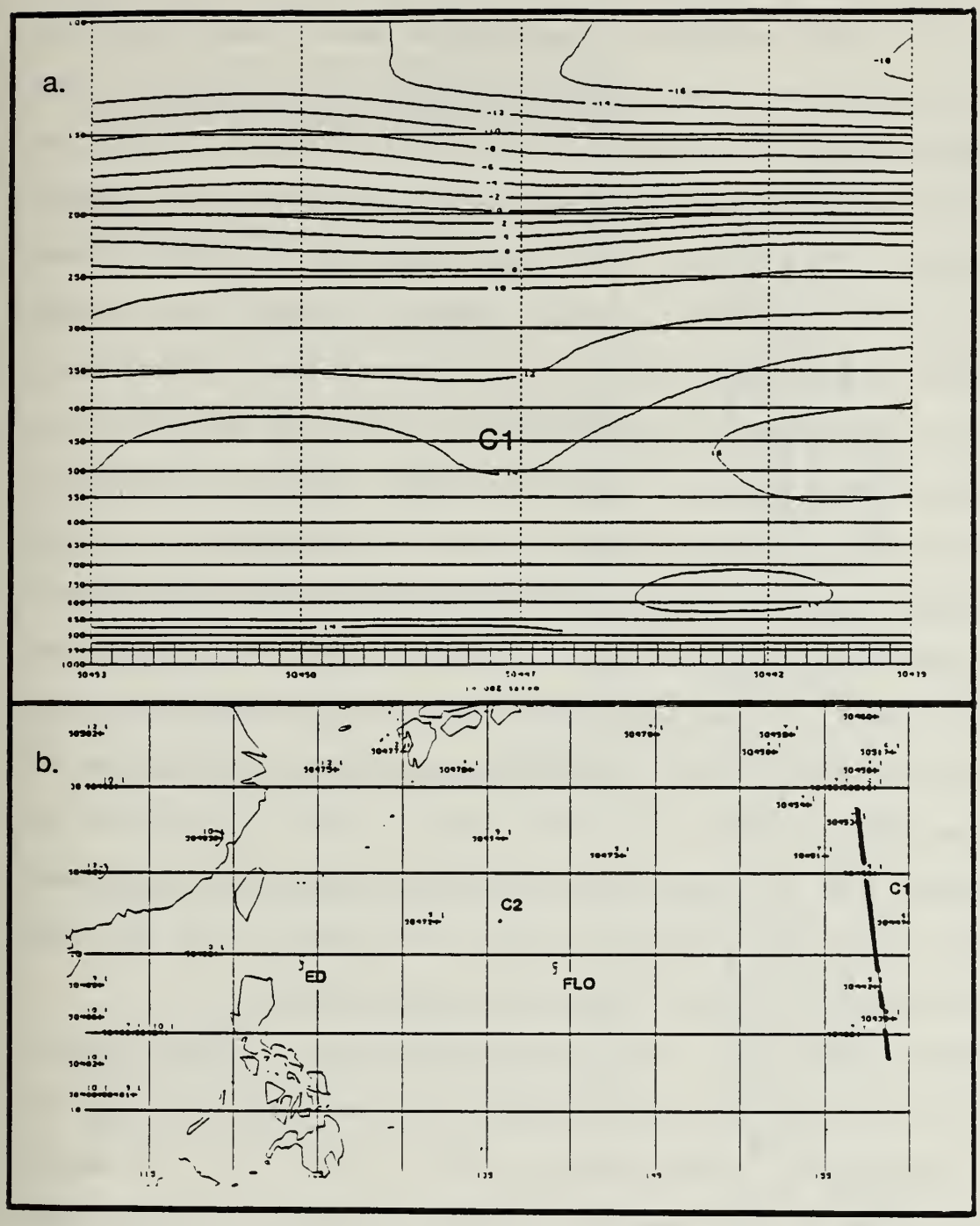

Fig. 7. (a) Cross-section of satellite temperature deviations from standard atmospheric values through western portion of upper-level cold low C1 at 06 UTC 14 September. Abscissa is retrieval position number and ordinate is pressure level in mb. Cold low C1 is indicated by the region of minimum temperature deviation (C1). (b) Orientation of cross-section (bold solid line) in (a). Positions of Flo and Ed are marked by the tropical cyclone symbols.

b. Time series of rawinsondes

Time series of rawinsondes were constructed for upper-air stations when a cold low passed (e.g., Fig. 8). The time series depicts the horizontal and vertical structure as the circulation feature (assumed to be in steady-state) passes the station. In Fig. 8, a TUTT cell labelled C1 in Fig. 1 was south of the upper-air station (Marcus Island) and moving westward. The signature of the cold low was first detected at 12 UTC 14 September by the veering of the winds above 400 mb. At the closest point of approach (CPA), which was directly south of the station at about 12 UTC 15 September, a strong cold-core signature extended down to about 500 mb. The upper-level winds continued to veer through 00 UTC 17 September as the TUTT cell tracked westward. The strong cyclonic flow on the western side of the cold low is denoted by the 55 - 70 kt observations at 200 -300 mb from 06 UTC to 12 UTC 16 September. The cell appeared to have maintained a significant vertical structure through 12 UTC 17 September, and then was not detected as it moved away from the station.

These rawinsonde time series provide a much better depiction of the vertical structure of the cold low than do the temperature cross-sections as in Fig. 7a. A major disadvantage of this method is that it requires a fortuitous passage of a cold low near the upper-air station. Given the paucity of upper-air stations in the tropics, the opportunities to construct a rawinsonde time series of winds

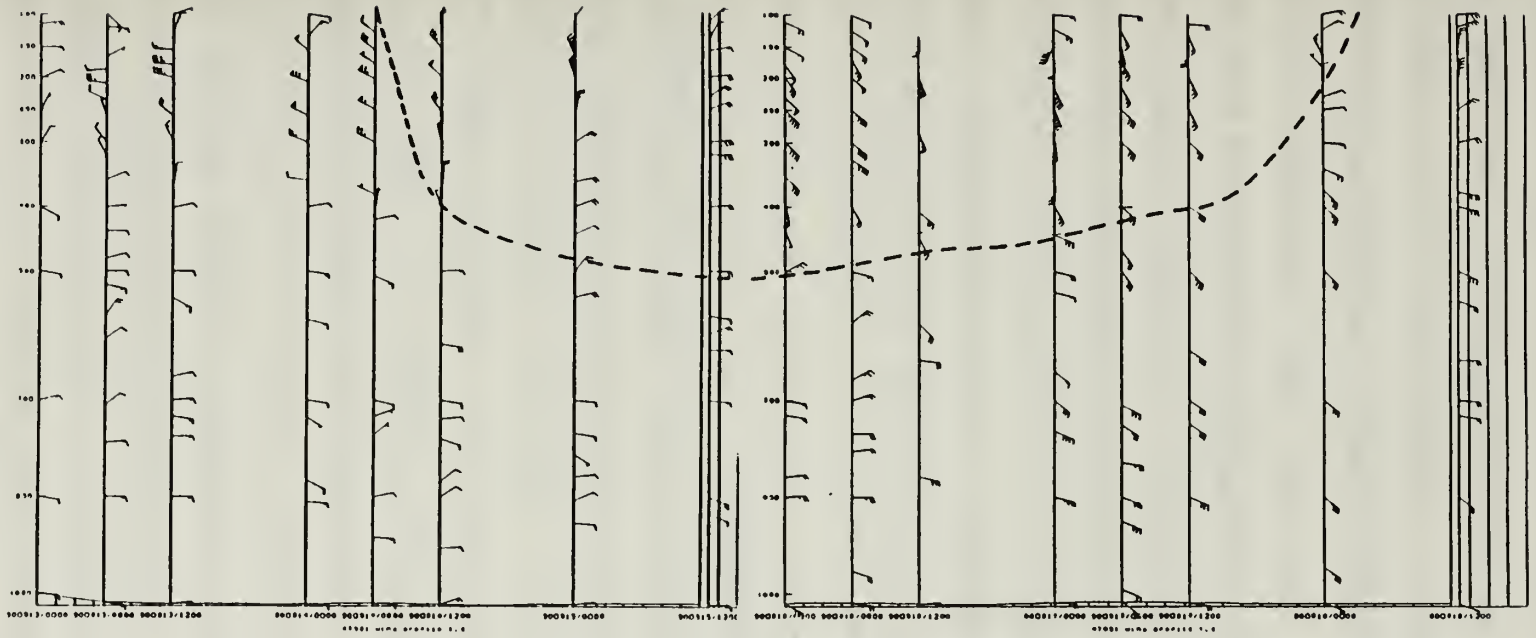

Fig. 8. Time series of upper-air winds (kt; full barb equals 10 kt) at Marcus Island (WMO station number 47991; 24.0°N, 154.0°E) from 00 UTC 13 September through 12 UTC 18 September. Dashed line marks the signature of cold low C1 as it passed south of the station on a westward track. Cold low C1 was at closest point of approach (CPA) to the station at 12 UTC 15 September.

are significantly less than that of being able to construct a temperature cross-section based on the more frequent satellite soundings. This method is not as useful in real-time use because a complete series of profiles must be available to depict the vertical structure. Finally, interpretation of the rawinsonde time series requires some knowledge of the circulations being studied. For example, it might be difficult to associate veering of the winds at the upper levels in Fig. 8 with the passage of a cold low without some knowledge of the position and motion of the cold low relative to the station. While this is not a problem from a research perspective, such requirements would hinder the utility of the method in an operational environment.

C. LIMITATIONS / QUALIFICATIONS

The analysis and interpretations here are primarily a descriptive case study of the upper-level influences on Flo and Ed. The high-resolution, hand-drawn streamline analyses were subjectively interpreted to identify upper-level interactions that may have played a role in the intensification rates of the two storms. The tropical cyclone outflow jets were subjectively analyzed using the outflow regime concepts previously discussed. Although various tools were used to elucidate a more quantitative description of the upper-level features such as cold lows, the significance of the structures were determined primarily by subjective

interpretation of the accompanying charts and imagery. Calculations of the mass divergence and EFC were also used to subjectively correlate changes in the mass outflow with corresponding changes in the intensification rates of the tropical cyclones.

The case study admittedly has a somewhat biased upper-level perspective because it will not be demonstrated that other physical mechanisms or factors at lower levels did not have some role in the intensity changes of the two storms. Only two factors were checked to determine whether low-level forcing also could have contributed to the intensity changes.

First, the September 1990 monthly mean and monthly anomaly SST (the difference between the monthly mean SST and the climatological monthly mean value) data produced by NESDIS (NOAA 1990) were reviewed to determine whether conditions were favorable for tropical cyclone development and intensification throughout the period of study. As described by Holland (1987), the potential intensity of a tropical cyclone increases significantly for ocean temperatures above 27° C. The September 1990 data indicates that the monthly mean SST was greater than 27° C for both Flo and Ed during the entire period. Neither storm traversed a significant SST gradient until Flo became extratropical after 12 UTC 19 September. A cold monthly SST anomaly of between 0.0° - 0.5° C was indicated for most of the region bounded by 5° - 30° N, 110° - 170° E as would be expected due to the significant tropical

cyclone activity that occurred in this region during the month (Elsberry et al. 1990). Therefore, the SST conditions were probably favorable for intensification of both storms. The fact that Ed developed much more slowly and achieved a much lower intensity than did Flo, despite nearly identical SST conditions, suggests that other environmental influences (e.g. upper-level forcing) may have been important.

Second, the operational 850 mb analyses winds were reviewed to determine whether any significant changes in the low-level circulation pattern may have occurred that could have resulted in significant changes in the low-level forcing. Although the strong cross-equatorward inflow into Ed appeared to diminish after 00 UTC 14 September, no significant changes in the lower-level flow pattern were found. Therefore, the significant changes in the intensification rates that occurred during the lifetimes of both Flo and Ed did not appear to have been supported by corresponding changes in these other factors.

III. SUPERTYPHOON FLO

A. ORGANIZATION AND DEVELOPMENT TO TROPICAL STORM

1. Initial Development

The early stages of tropical depression WP2090 (Flo) were characterized by slow organization and vertical development. WP2090 increased in intensity an average of less than 5 kt per day from its initial detection at 00 UTC 8 September (ATCR 1990) to 00 UTC 13 September 1990, when its intensity (maximum sustained surface winds) reached 25 kt (Fig. 2). Environmental variables such as sea-surface temperature (SST) and low-level moisture content provided conditions favorable for further development of this system. A comparison of the 200 mb analyses for 00 and 12 UTC 12 September (Figs. 9 and 10 respectively) suggests that the upper levels of the troposphere only began to provide substantial support for significant storm intensification on 12 UTC 12 September. The key change in Flo's outflow pattern during this period was the beginning of a second eastward outflow channel toward the upper-level low to the northeast, which supplemented the existing channel into the background flow of upper-level northeasterlies.

The hypothesis to be examined in this section is that the position of the storm relative to the upper-level circulations

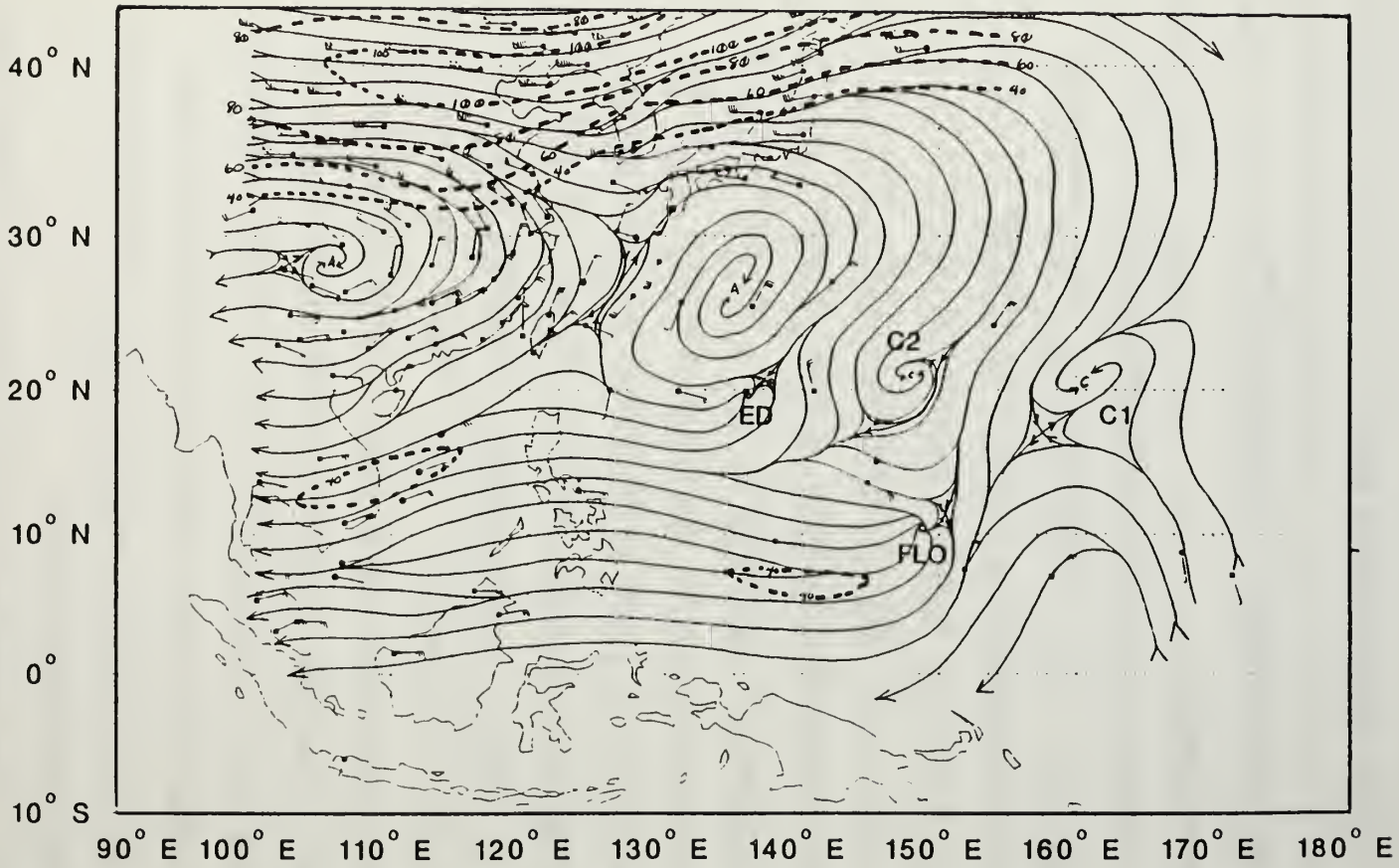

Fig. 9. 200 mb streamline analysis for 00 UTC 12 September. Observation symbols are as follows: ■, rawinsonde; □, dropwinsonde; ●, conventional aircraft (AIREP); *, NASA DC8 research aircraft; x, operational cloud-track wind; ⊠, reprocessed cloud-drift wind. Dashed lines are isotachs of tropical cyclone outflow jets and synoptic-scale jets in 20 kt increments beginning at 40 kt. Tropical cyclone positions are marked by the storm symbol and upper-level cold lows are labeled C1, C2, C3 etc.

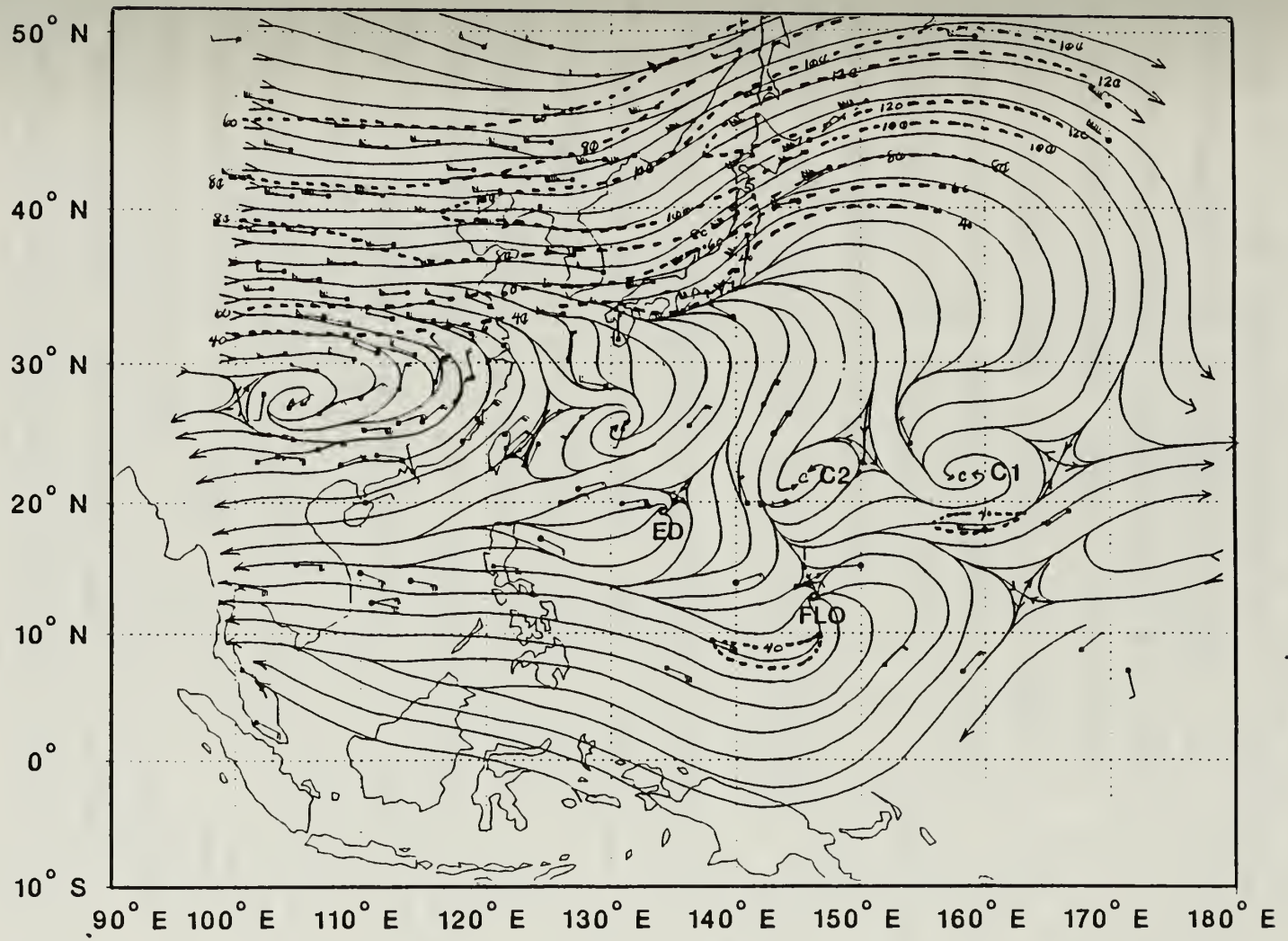

Fig. 10. As in Fig. 9, except for 12 UTC 12 September.

determines when favorable conditions exist such that one or more of three upper-level interaction mechanisms induce or sustain increased intensification rates. The three upper-level interaction mechanisms (to be described below) are: (i) an adjacent TUTT cell that acts as a reservoir for the mass and heat removed by outflow jets of the tropical cyclone; (ii) the juxtaposition of a TUTT cell to create an accelerated flow (flywheel effect) in these outflow jets, which enhances the upper-level mass outflow from the tropical cyclone into the distant environment; and (iii) the creation of a vacuum-type effect as a strong tropical cyclone outflow jet merges into the region of enhanced baroclinity associated with the subtropical jet.

Each of these three interaction mechanisms may contribute to the efficient export of mass and heat from the developing storm such that further intensification can occur. That is, the upper-level outflow from a developing tropical cyclone serves to evacuate mass such that the central pressure can continue to decrease. If the evacuated mass subsides in the immediate surroundings of the storm, the tropical cyclone is likely to develop only slowly, and may not even reach typhoon strength. However, an efficient upper-level export mechanism not only increases the removal of mass and heat from the storm, it also removes this mass and heat far enough away from the storm such that the subsequent subsidence does not impede intensification.

2. The TUTT cell reservoir function

In the case of WP2090, the first upper-level export mechanism to develop was that of a TUTT cell acting as a mass/heat reservoir. As depicted in Fig. 11, a TUTT cell can function as a mass/heat reservoir when a significant fraction of the inflow converges towards the center of the cold-core cell. In the discussion below, this flow pattern will be contrasted with a simple cyclonic rotation around the periphery of a TUTT cell that turns anticyclonically into a region of upper-level divergence. If the TUTT cell is to function as a mass reservoir, large-scale subsidence must occur within the center of the cell. Hence, a TUTT cell functioning in this manner is identified on satellite imagery as a markedly clear region, and is occasionally surrounded on the periphery by elongated cirrus streaks. Isolated cumulonimbus within the center of the cell marking warm, moist low-level conditions and hence increased instability may also indicate the presence of a TUTT cell. This function contrasts with the tropical cyclone - TUTT cell interaction described by Sadler (1978), in which a region of upper-level divergence adjacent to the TUTT cell results in low-level convergence and convective activity. Hence, the function of a TUTT cell as a reservoir implies a relatively weather-free region.

The TUTT cell acting as a reservoir will likely maintain a significant vertical structure for several days as a result of subsidence and mid- to low-level divergence of the upper-

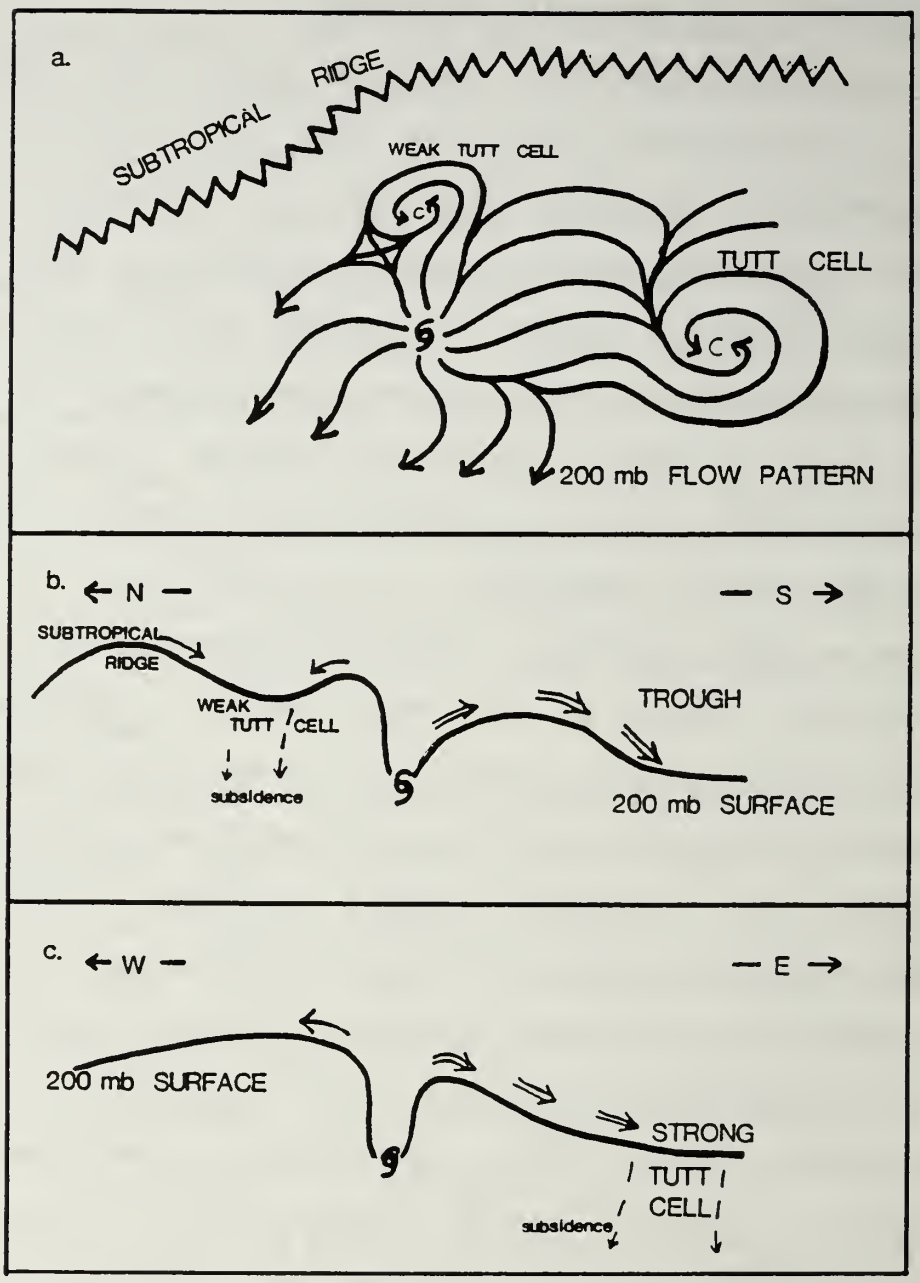

Fig. 11. Schematic of the TUTT cell reservoir function. (a) 200 mb flow pattern indicating convergence of outflow from tropical cyclone into cold lows labeled C. (b) topography of 200 mb surface oriented North (left) - South (right) with outflow into weak TUTT cell to the north and strong outflow to the south. (c) Topography of 200 mb surface oriented West (left) - East (right) with enhanced outflow from tropical cyclone into strong TUTT cell to the east.

level inflow. However, this export mechanism is not likely to result in prolonged, rapid (greater than one Dvorak T-number or 20 kt per day) intensification of a tropical cyclone. As mass continues to subside within the TUTT cell, it gradually weakens and fills, and eventually becomes a benign feature in the upper-level flow pattern. Furthermore, if the TUTT cell is located within approximately 2°-3° lat. of the tropical cyclone, then the subsidence may occur within the storm environment. In this case, the addition of mass and heat to the middle and upper layers of the troposphere will oppose tropical cyclone development. The position of the TUTT cell relative to the incipient tropical cyclone and the strength, or vertical extent, of the TUTT cell are therefore key parameters for determining whether it will be effective as a mass/heat reservoir.

The reservoir function of a TUTT cell (named C1 for convenient reference) appeared to be initiated at 12 UTC 12 September (Fig. 10). At that time, the distance between WP2090 and C1 exceeded 800 nm, and thus a time lag of several hours would be expected before development of the improved outflow channel might be reflected as an increase in Flo's intensification rate. As shown in Fig. 12, both TUTT cells C1 and C2 (new cell just to north of Flo) were properly positioned by 00 UTC 13 September to act as mass/heat reservoirs for the outflow from Flo. As determined by the iterative multilayer analysis, the majority of the inflow to

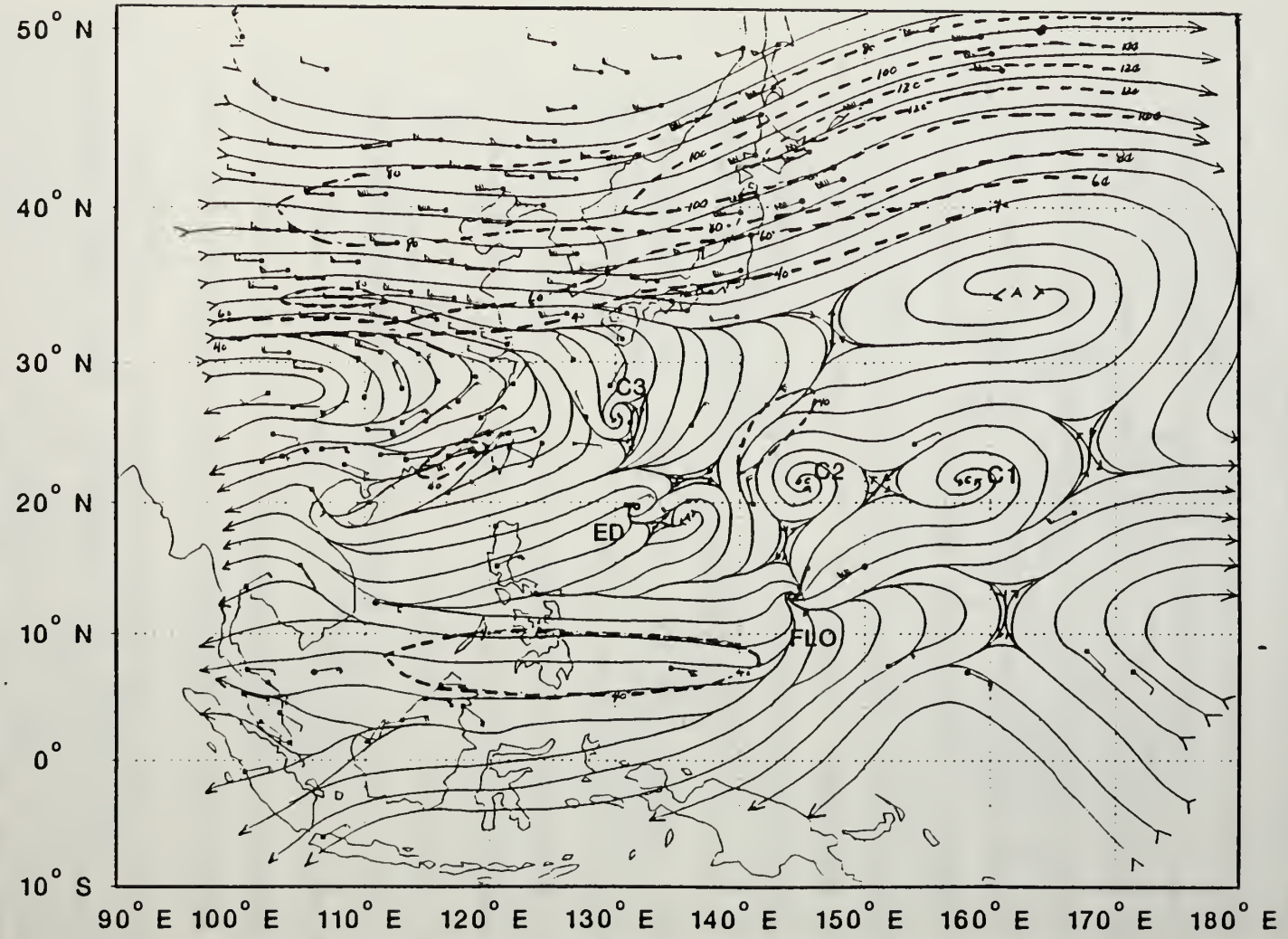

Fig. 12. As in Fig. 9, except for 00 UTC 13 September.

these cells converged towards the cell centers, which remained sufficiently far (approximately 1000 km) from the developing cyclone that the subsidence within the cells did not impede further development of the cyclone. As shown in Fig. 13, both cells were defined by relatively cloud-free regions with minimal peripheral clouds that would imply the presence of a divergence mechanism of Sadler (1978). Furthermore, most of the divergent outflow at this stage appeared to be southward into the equatorward branch (Fig. 11b) associated with the characteristic background environment of upper-level easterlies.

B. INTENSIFICATION TO TYPHOON

1. Reservoir function effects

It is hypothesized that the development of a more efficient upper-level export mechanism in conjunction with the TUTT cells contributed to an increase in the storm intensification rate from less than 5 kt per day prior to 00 UTC 13 September to 5 kt per 6 h after 00 UTC 13 September. The increased mass flux (Fig. 3a) which occurred coincident with the development of the reservoir function at 12 UTC 12 September is consistent with this hypothesis. The fact that the intensification rate apparently did not increase until 06 UTC 13 September lends credence to the supposition that a time lag of perhaps 12 to 18 h separated initial development of the reservoir function from a corresponding increase in intensity.

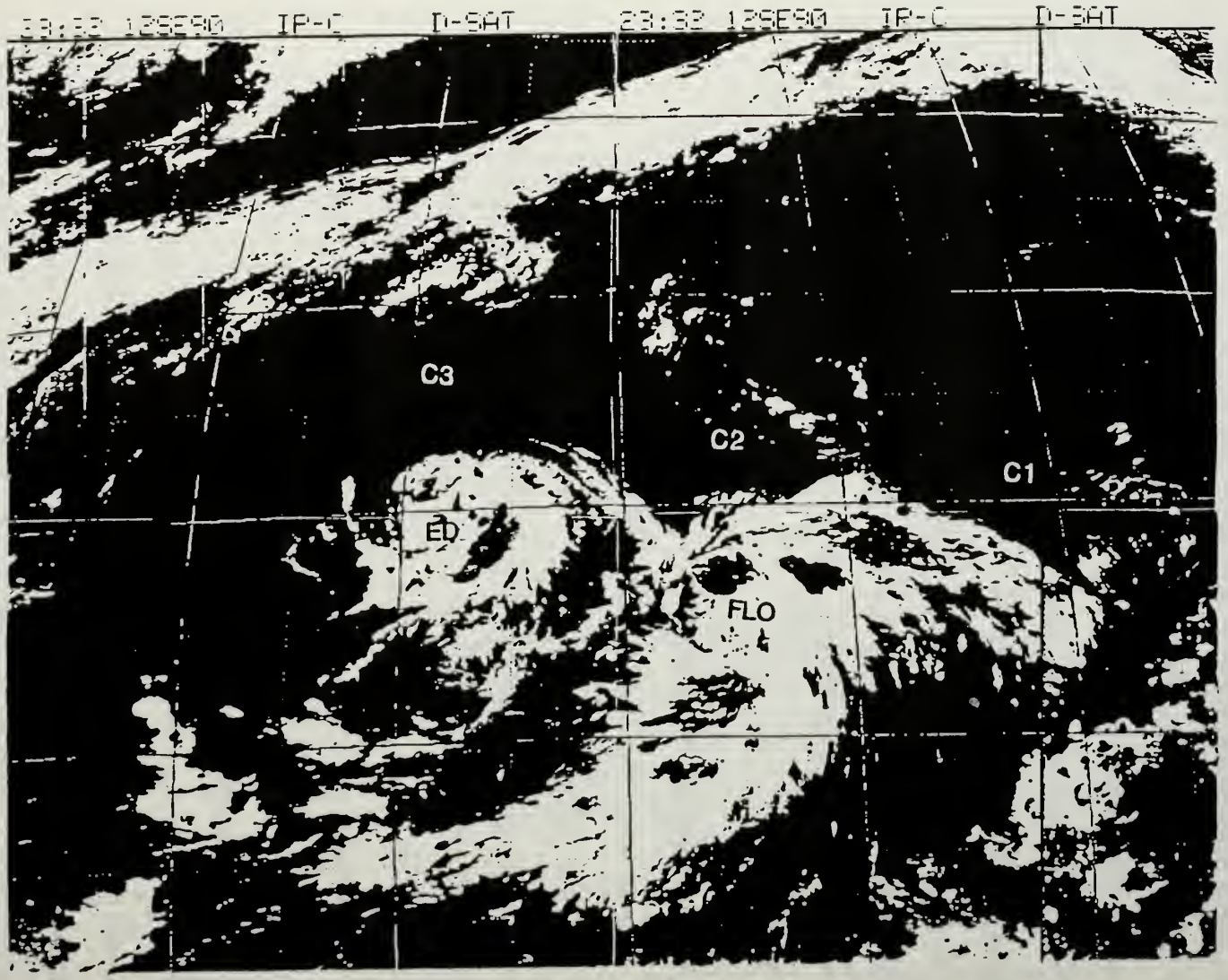

Fig. 13. Infrared satellite imagery for 2332 UTC 12 September. Upper-level cold lows are labeled C1, C2, C3 etc.

As a result of this continued efficient export mechanism, WP2090 steadily intensified and was designated Tropical Storm Flo with maximum sustained winds of 35 kt at 12 UTC 13 September. As depicted in Fig. 2, the motion of C2 relative to Flo during the following 12 h decreased the separation distance between the two features and brought the cold-core cell to a position north-northwest of Flo at 00 UTC 14 September. This was apparently a less favorable tropical cyclone - TUTT cell orientation because the mass flux began to decrease slightly during this period (Fig. 3a). Although C2 continued to function as a mass/heat reservoir (Figs. 14 and 15), the orientation of the cell within the outflow regime suggests that it had become a less effective mass/heat export mechanism.

Disregarding any other changes in the upper-level flow pattern, the decreasing mass flux in the outflow layer (Fig. 3a) might suggest a decrease in the intensification rate. However, the magnitude of the bulk vertical shear in the outflow regime (Fig. 5a) had decreased considerably during the period 00 UTC 14 September through 18 UTC 14 September. As a result, the negative effects of slightly decreased outflow may have been counterbalanced by changes in the upper-level environment that favored organization and hence continued steady intensification of the storm.

Although the relationship is unclear, three significant changes in the upper-level flow pattern occurred during this

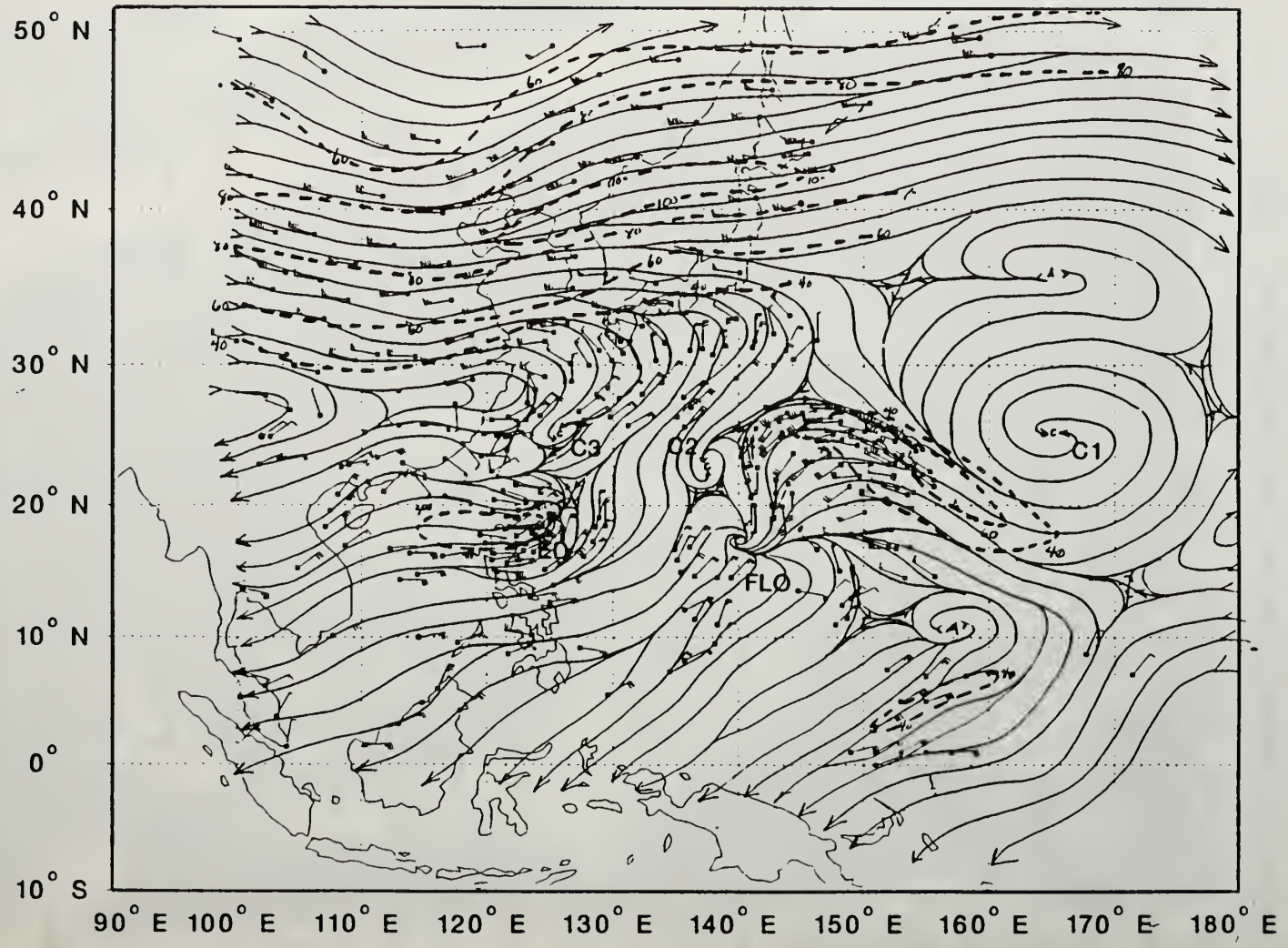

Fig. 14. As in Fig. 9, except for 00 UTC 14 September.

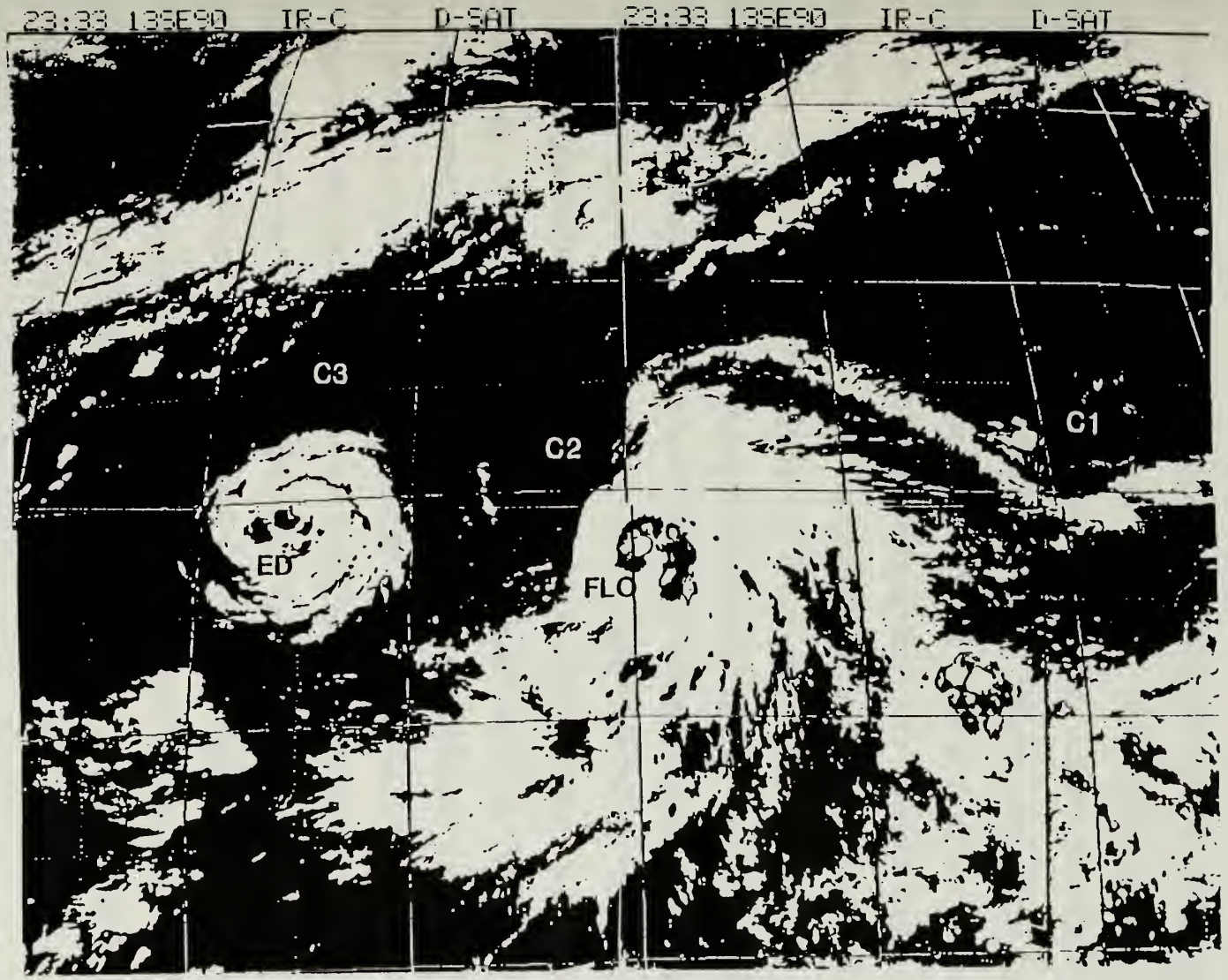

Fig. 15. As in Fig. 13, except for 2333 UTC 13 September.

period of decreased bulk vertical shear. First, it appears from Fig. 14 that the areal extent of C2 had decreased significantly since 00 UTC 13 September (Fig. 12). While it is not clear from this 200 mb analysis whether C2 remained a closed, cyclonic circulation, several factors were considered that support both the analyzed position and orientation of this cold low. Vertical consistency provided by the analysis of four pressure levels, time consistency provided by analysis of these level every 6 h, and use of satellite imagery to locate and orient the various circulation features were all factors that contributed to define TUTT cell C2. The reduced areal extent of this cold-core low suggests that filling of C2 had taken place during this 24-h period, and thus it follows that Flo had considerable influence on at least the horizontal structure of this TUTT cell. Consistent with the hypothesized evolution of the reservoir mechanism, filling of C2 implies a weakening of C2, and hence the role of this TUTT cell in modifying the intensification rate of Flo began to diminish.

Second, although C2 did maintain a weakening reservoir function, a much larger proportion of Flo's outflow was now directed towards the more substantial C1 (Fig. 14). The position of C1 east of 160° E (outside the TCM-90 area of interest) prevented the construction of a rawinsonde cross-section through the center of this cold-core cell. However, the western edge of C1 is apparent from satellite vertical temperature profile retrievals in Fig. 7a, and indicates a

vertical structure extending down to 500 mb. This contrasts with the weaker signature of C2 shown in Fig. 16a. The stronger reservoir function provided by C1 appears to have been more important to the continued development of the storm than was the less favorable position of C2. Reflecting the increasing effectiveness of the reservoir function of TUTT cell C1, the mass flux began to increase during the period 00 UTC - 06 UTC 14 September (Fig. 3a).

Finally, a significant change in the upper-level inflow pattern became apparent at 00 UTC 14 September (not shown). Prior to this time, a majority of the flow toward the storm at 300 mb was from the south, whereas it now became more evenly distributed from both the north and the south. This was a transient feature as the upper-level flow pattern shifted back to a predominantly southern origin following 00 UTC 14 September. It is possible that a significant portion of these changes may be due to the small number of upper-air observations near the storm center. The paucity of near-storm observations could result in an inaccurate representation of the near-storm wind field in the relatively large-scale streamline analyses constructed for this study. However, the changes in the apparent inflow pattern of Flo during this stage in Flo's development appear to be large enough to warrant further study.

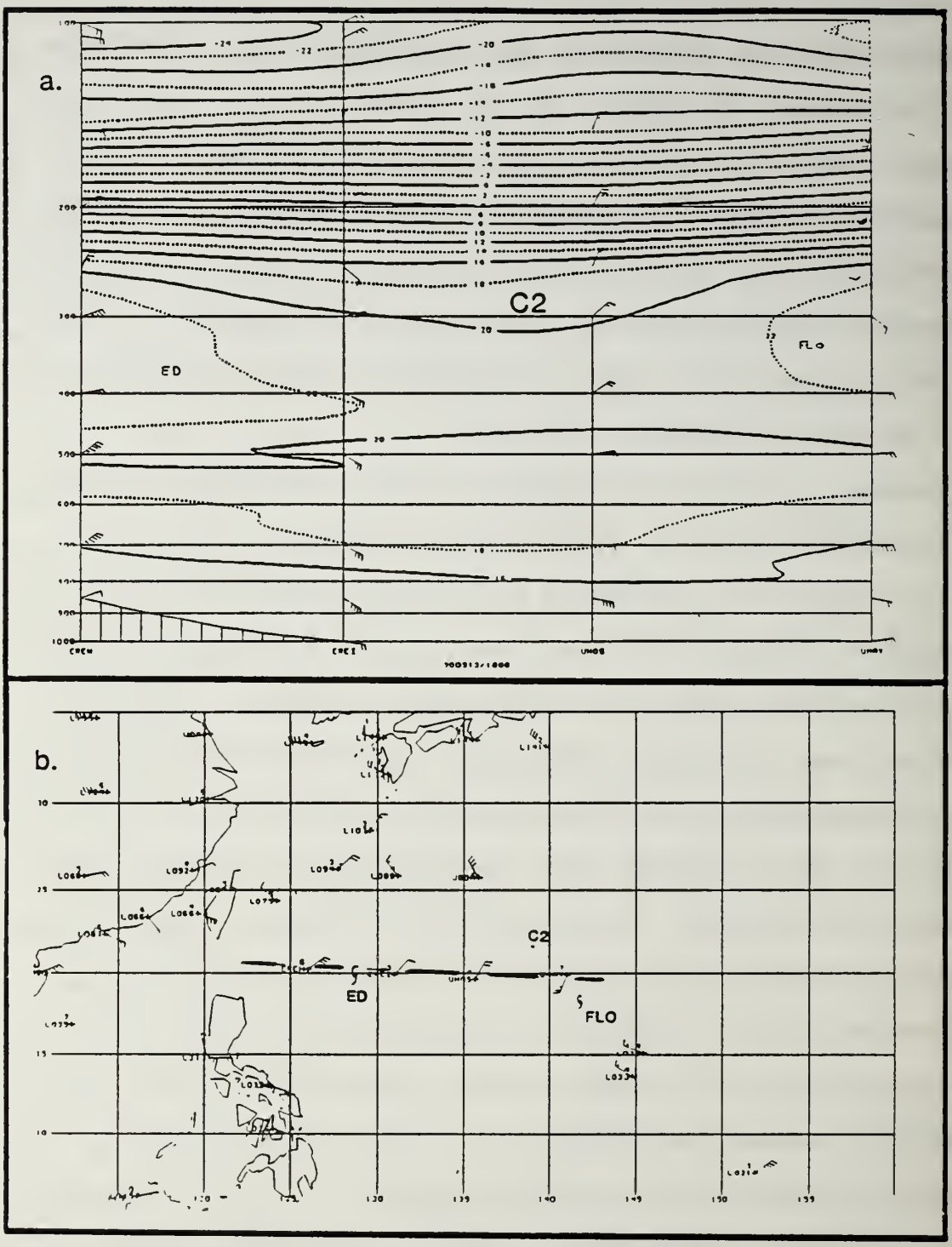

Fig. 16. (a) Rawinsonde temperature deviations (°C) from standard atmosphere values and winds (kt) along cross-section through southern portion of upper-level cold low C2 at 18 UTC 13 September. Ship designator at positions of upper-air soundings are indicated. Cold low C2 is in the region of minimum temperature deviation labeled C2. (b) Ship positions for upper-air soundings used in (a).

2. Upper-level anticyclone influences

Flo's steady intensification at the rate of 5 kt per 6 h continued through 12 UTC 14 September despite the increasingly less favorable position of TUTT cell C2. Another possible contribution to Flo's intensification was the development of an upper-level anticyclone at 10°N, 156°E during this period. This anticyclone was first detected at 200 mb on 00 UTC 14 September (Fig. 14) in conjunction with a region of deep convection (Fig. 15) with outflow primarily towards the south. By 12 UTC 14 September (Fig. 17), all four analyzed levels (300, 250, 200 and 150 mb) depict multiple interactions among two upper-level anticyclones, Flo, and TUTT cells C1 and C2.

Two of these interactions may have contributed to a decrease in Flo's intensification rate. First, the outflow associated with the poleward anticyclone near 18°N, 142°E was superposed with Flo's northeast-directed outflow to increase the mass flow into C1 (Fig. 17). Disregarding any other changes in the orientation or function of this TUTT cell, an increased mass flow into C1 would suggest the possible filling and eventual weakening of the cell. Weakening of C1 in such a case would therefore lead to a diminishing reservoir export mechanism that could indirectly contribute to a decrease in Flo's intensification rate. Satellite temperature cross-sections indicate that such a weakening did not occur, and thus the strong inflow to C1 was apparently balanced by low to

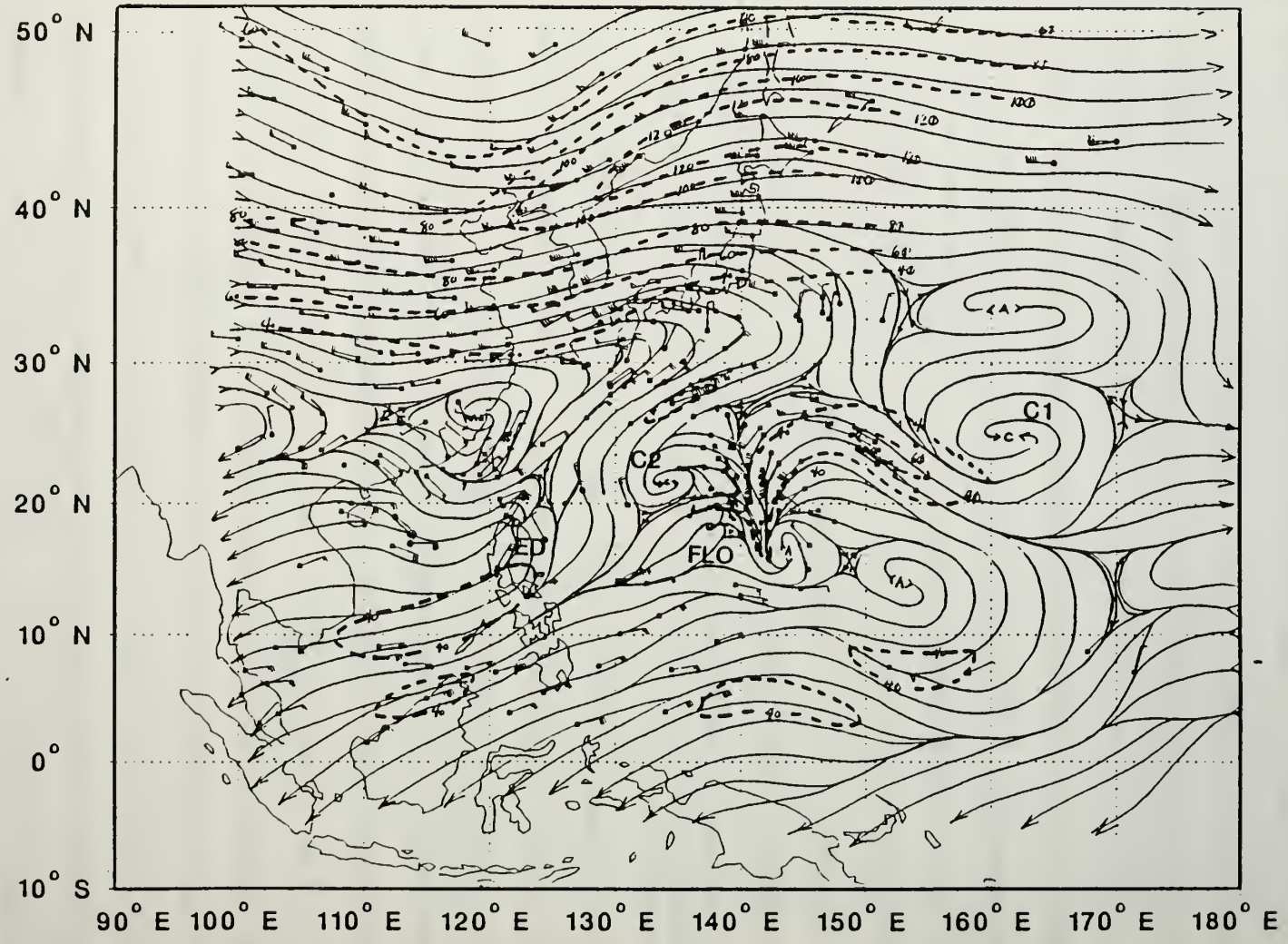

Fig. 17. As in Fig. 9, except for 12 UTC 14 September.

mid-level divergence of the subsiding air within the cell.

Second, a portion of the outflow associated with the anticyclone southeast of Flo (Figs. 17 and 18) was directed into the near-storm environment and suggests the possibility of vertical shear occurring directly over the storm. Such shear at the outflow levels could ventilate the storm and thus cause a disruption in the organization of the central convective region. While such an effect would decrease the intensification rate, the magnitude of the bulk shear vector at 200 mb (Fig. 5a) does not indicate that any significant increase in the bulk shear occurred during the period 06 UTC - 18 UTC 14 September. Thus, the outflow jets from the anticyclone were apparently deflected around the eyewall such that the organization of the storm was not significantly affected. Conversely, a decrease in the eddy flux convergence (EFC) of relative angular momentum (Fig. 4a) did occur concurrent with the development of the anticyclones southeast of Flo. McBride and Zehr (1981) showed that decreased EFC was associated with non- or slowly- developing tropical cyclones, and thus this change in the forcing might suggest a tendency towards a decrease in Flo's intensification rate.

The ridging associated with the two anticyclones results in a third possible interaction between the upper-level circulations of Flo and TUTT cell C1. There appear to be two possible consequences of this ridging. First, the ridging southeast of Flo (Fig. 18) effectively blocked the southern

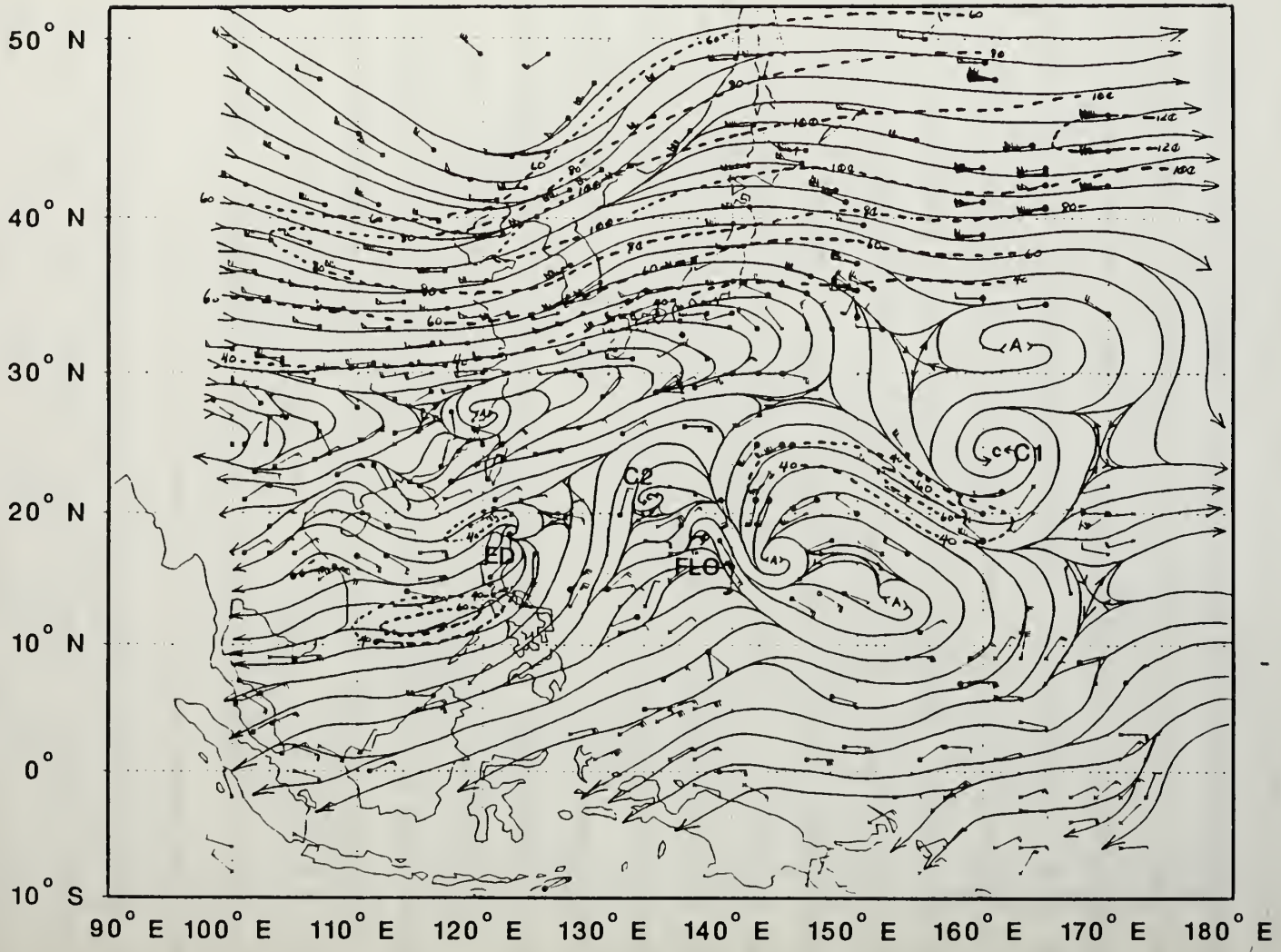

Fig. 18. As in Fig. 9, except at 250 mb for 12 UTC 14 September.

outflow channel by raising the geopotential heights such that the lower heights west and east of Flo appear to be favored. The loss of the southern outflow channel would therefore seem to support a reduction in Flo's intensification rate. However, the second consequence of this ridging was to strengthen the outflow channel into C1 and thereby initiate development of the flywheel mechanism (to be discussed below).

The period 12 UTC 13 September through 12 UTC 14 September was therefore characterized by complex changes in the upper-level flow pattern as the interactions between Flo and TUTT cells C1 and C2 continued to evolve. The combined factors of the loss of the southern outflow channel and the reduced EFC, both associated with the development of the anticyclones south of Flo, suggest that upper-level support for an increase in the intensification rate might have been diminished during the later part of the period. However, the mass flux at 200 mb (Fig. 3a) continued to increase following the initial decrease in outflow associated with the weakening of the C2 reservoir function at 18 UTC 13 September. The negative effects of the upper-level anticyclones were apparently counterbalanced by the increasing outflow associated with the development of a second interaction mechanism, which appears to have played an increasingly important role in Flo's development to typhoon strength at 00 UTC 15 September.

3. The TUTT cell flywheel export mechanism

It is hypothesized that the development of TUTT cell C1 to function as a flywheel for Flo's eastward-directed outflow jets played a significant role in the continued intensification of Flo. A schematic of this mass/heat export mechanism is provided in Fig. 19. Unlike the flow associated with a TUTT cell acting as a reservoir (Fig. 11), a significant proportion of the flow is accelerated around the TUTT cell, which is interpreted here to function similar to a flywheel. This flow does not converge into the cell's center. Instead, the trajectories of these high velocity outflow parcels diverge on the southeastern periphery of the cell in response to the upward sloping pressure surface associated with the subequatorial ridge south of the cell. Associated with this diffluence is the development of a secondary circulation that results in upward motion and deep convection.

The TUTT cell C1's transition from primarily a mass/heat reservoir to its more important role as a flywheel can be detected by comparing Figs. 14 and 18. The most obvious difference in the flow pattern around C1 between these two analyses is the increasingly distinct divergence region that developed on the southeastern periphery of the cell. Since the southeastern quadrant of C1 is in a very data- sparse region at both of these times, the analyses in this region mainly reflect changes in the corresponding satellite imagery (Figs. 15 and 20 respectively). The increased deep convective

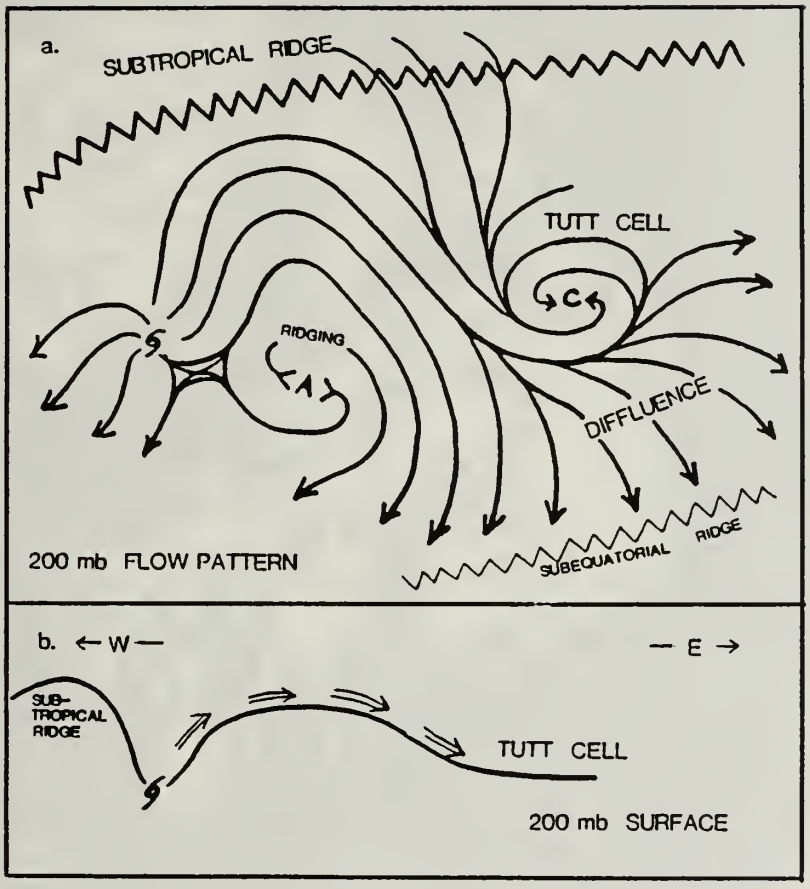

Fig. 19. Schematic of the TUTT cell flywheel mechanism. (a) 200 mb flow pattern indicating large region of upper-level diffluence on southeastern periphery of TUTT cell (C). (b) 200 mb surface oriented West (left) - East (right) with enhanced outflow into and around TUTT cell to the east of the tropical cyclone.

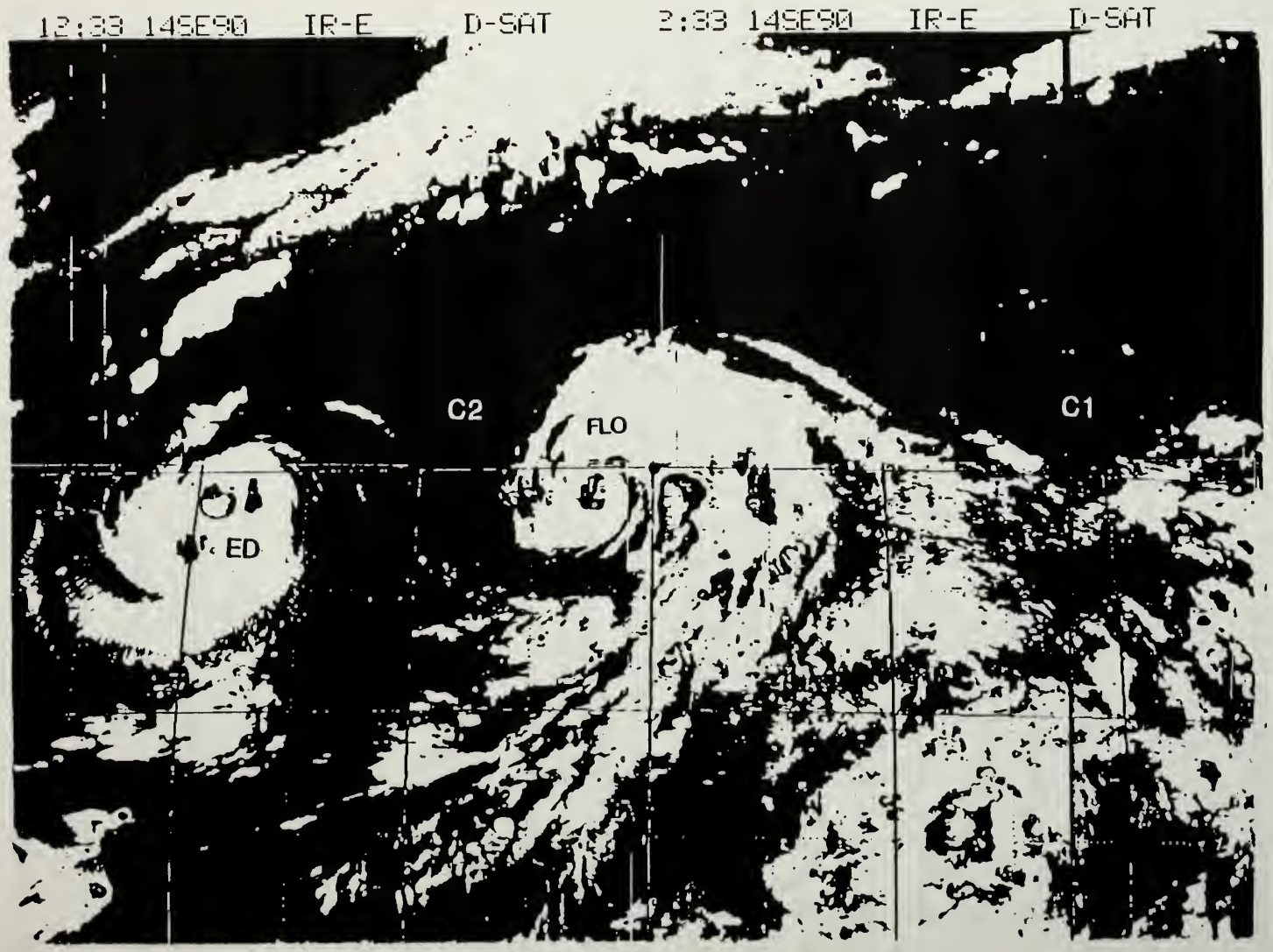

Fig. 20. As in Fig. 13, except for 1233 UTC 14 September.

cloudiness at 12 UTC 14 September marks the region of upper-level divergence. Existence of this divergence region is similar to that in the model of a tropical cyclone - TUTT cell interaction mechanism described by Sadler (1978), in which the intense cyclonic flow around the cold-core cell serves to accelerate the mass associated with the outflow jet away from the storm's environment. However, the divergence region in this case is more of a symptom that a strong outflow jet exists upstream, rather than being the upper-level divergence that triggers or sustains low-level convergence in a developing tropical storm as in the Sadler mechanism.

Satellite imagery, such as in Fig. 21, depicts the flywheel mechanism by a characteristic signature of: (i) elongated cirrus streaks around the periphery of the TUTT cell that change from cyclonic curvature to anticyclonic curvature downstream; and (ii) towering cumulus and cumulonimbus clouds that mark the region of upper-level diffluence and deep convection.

Prior to discussing the means by which the flywheel function can produce an increased intensification rate, it is important to note the conditions under which this mechanism is presumed to develop. It is hypothesized that the development of a flywheel mechanism marks the evolution of the typical interaction between a TUTT cell and a tropical cyclone given the following upper-tropospheric environment: i) a TUTT cell properly positioned relative to the cyclone (to be discussed

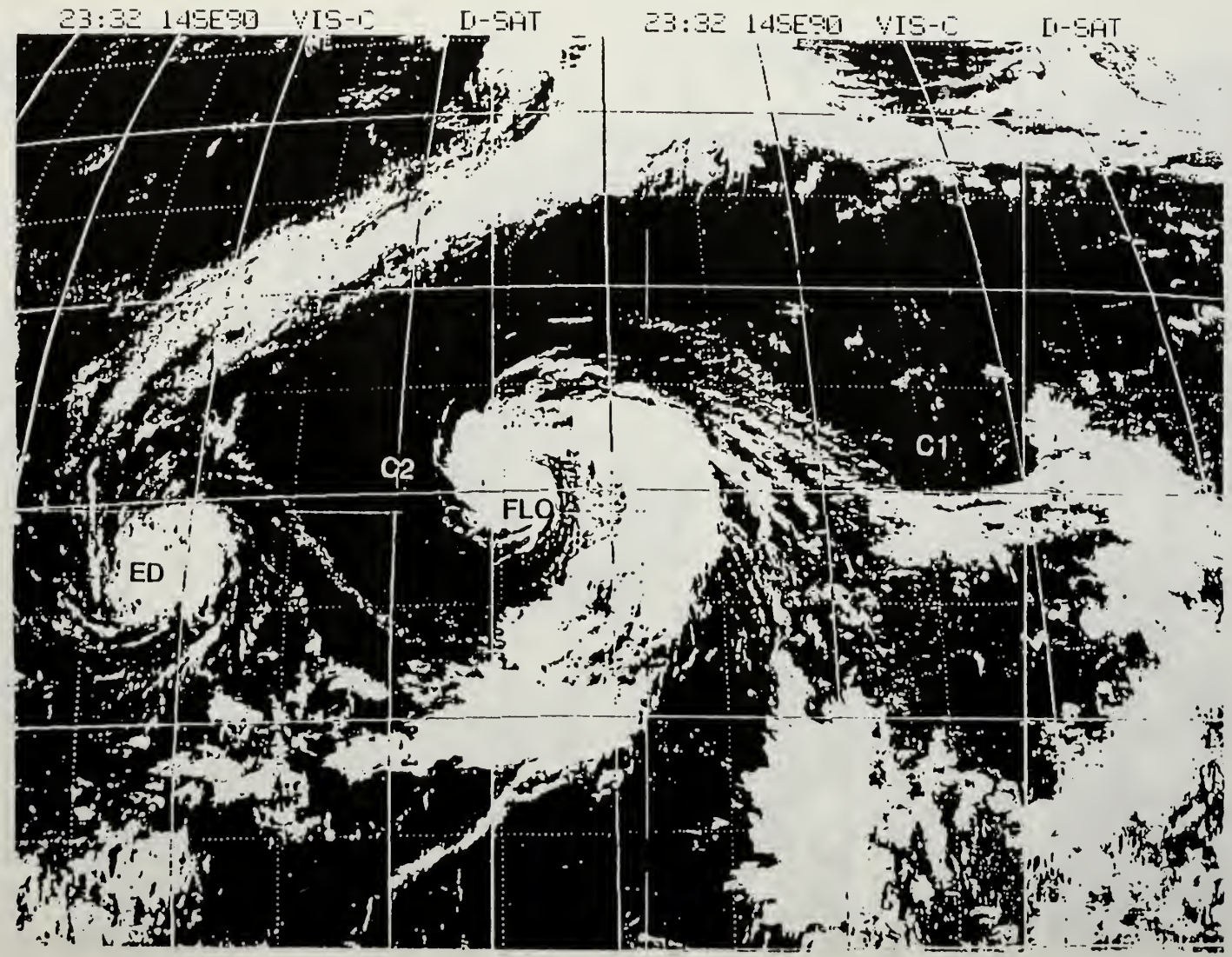

Fig. 21. Visible channel satellite imagery for 2332 UTC 14 September. Upper-level cold lows are labeled C1, C2 etc.

below); and ii) a sufficiently baroclinic flow channel. While several mechanisms may develop and maintain such a baroclinic flow channel, the key idea is that the slope of the pressure surface must be sufficient to provide a path along which the outflow parcels can accelerate to the velocities that will produce a region of diffluence in the southeastern periphery of the cell. Such velocities must be attained for the outflow parcels to develop a centrifugal force that exceeds the pressure gradient force associated with the pressure surface slope(s) in the TUTT cell.

C1 was well positioned to maintain its reservoir function while simultaneously developing a very efficient flywheel mechanism. This cell was approximately 20° east of Flo at 12 UTC 14 September (Fig. 17) and therefore satisfies the position requirement by enabling the development of a sufficiently distinct and elongated flow channel. The requirement that the flow channel be of a sufficiently baroclinic nature appears to have been satisfied beginning 12 UTC 14 September (Fig. 17) in association with three upper-tropospheric circulations. First, ridging associated with the anticyclones southeast of Flo raised the geopotential heights on the southwestern side of the flow channel. As discussed previously, the orientation of these heights, combined with the relatively warm outflow from the anticyclones, helped to increase the baroclinity of the flow channel. Second, the baroclinity was further enhanced by the indirect secondary

circulation associated with the exit region of the jet streak located in the channel. Finally, the north-south flow across a break in the subtropical ridge at approximately 30°N, 150°E superposed with both outflow from Flo and outflow from the anticyclones to produce a broad jet streak between Flo and C1. The high cirrus clouds marking Flo's northern outflow jets and the southern periphery of C1, plus the cold, towering cumulus on the southeastern periphery of C1 (Fig. 21), indicate the initial development of an effective flywheel function. Consistent with a hypothesized 12 to 18 h time lag, the maximum velocity of this outflow reached 80 kt at 00 UTC 15 September (Fig. 22), which was a 15 kt increase over the maximum velocity 12 h earlier.

As shown in Fig. 3a, development of the flywheel mechanism at 12 UTC 14 September was consistent with initiation of significant outward mass flux that continued through 06 UTC 16 September. It is hypothesized that this outward mass flux contributed to a marked increase in Flo's intensification rate beginning at 18 UTC 15 September. The time lag here is consistent with the large separation distance between the flywheel interaction channel and the storm. The generally small values of bulk vertical shear that occurred during this period (Fig. 5a) may have also contributed to the upper-level support for intensification. Because Flo continued to intensify during this period despite the negative influences reduced EFC (Fig. 4a), the two factors of increased

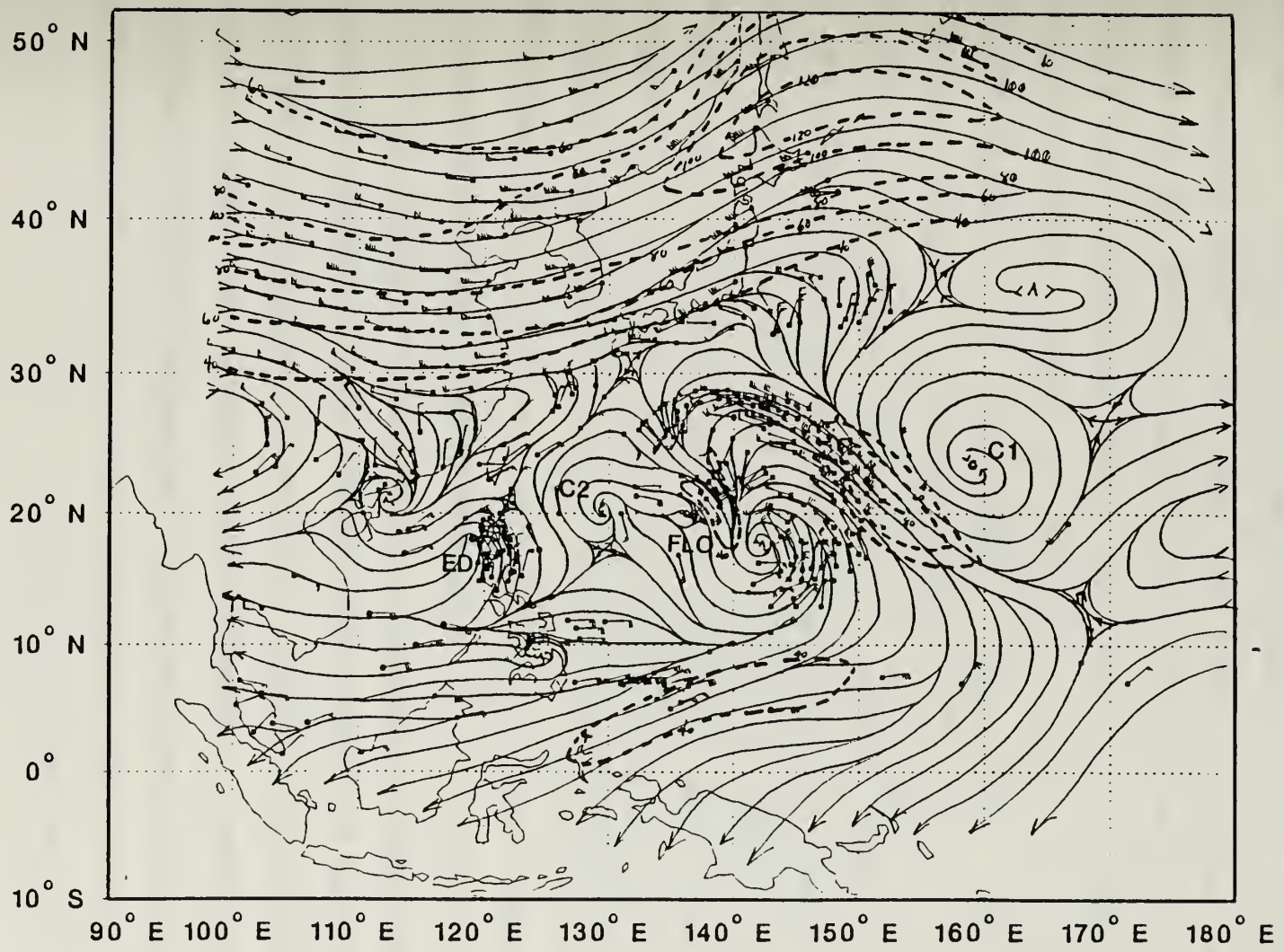

Fig. 22. As in Fig. 9, except for 00 UTC 15 September.

mass outflow and low bulk vertical shear apparently dominated the upper-level forcing.

The flywheel function supports a rapid intensification rate and/or a high intensity storm by contributing to a more efficient export of mass and heat. The large separation between the TUTT cell and the tropical cyclone implies that the subsidence within the cell occurs sufficiently far from the storm's environment such that it does not hamper further development. Furthermore, a TUTT cell that develops and maintains a significant flywheel function is less likely to fill and weaken because a smaller proportion of the mass entering the cell's periphery converges towards the center of the cell. Since a large proportion of this inflow is accelerated around the cell, less subsidence, and hence less filling, occurs within the cell. Thus, the TUTT cell that maintains a significant flywheel function is expected to decay at a slower rate than a TUTT cell that maintains mostly a reservoir function. A slow decay rate implies that the efficient export mechanism provided by the flywheel function can continue to support development of the tropical cyclone for a longer time. Thus, a TUTT cell that fills and weakens only very slowly can continue to provide the deep vertical structure that contributes to the sloping pressure surface needed to accelerate the mass around the cell and create the region of upper-level diffluence.

The importance of the position of the TUTT cell relative to the tropical cyclone is further illustrated by a description of why C2 fails to develop the flywheel function. Unlike the reservoir function, the flywheel mechanism cannot develop if the TUTT cell is located very near the tropical cyclone. In the case of C2, the baroclinic flow channel was not of sufficient length to allow the outflow parcels to accelerate to the velocities necessary to create the strong diffluent region on the southeastern periphery of the cell. As shown on the satellite imagery and 200 mb analysis for 00 UTC 15 September (Figs. 21 and 22 respectively), C2 continued to serve mainly as a reservoir and is clearly identified on the imagery as a marked cloud-free indentation on the western periphery of Flo. The distance between Flo and C2 is simply so minimal that development of a baroclinic interaction channel does not occur.

C. INTENSIFICATION TO SUPERTYPHOON

Flo continued to intensify at the constant rate of 5 kt per 6 h and reached typhoon strength at 00 UTC 15 September. By 12 UTC 15 September, significant changes in Flo's outflow pattern began to occur that eventually resulted in enhancements of the mass/heat export mechanisms, and thus provided support for an increased intensification rate.

1. Initial interaction with the subtropical ridge

A noticeable change at 12 UTC 15 September was the development of a transient upper-level cold low northeast of Flo and slightly north of the strong, eastward directed outflow jets that comprised a significant portion of C1's flywheel function (Fig. 23). This transient eddy may have formed as a result of significant horizontal shear in the upper-level circulation pattern. Although weak and short-lived, this cell provided a new mass/heat reservoir for Flo's northward-directed outflow jets. More importantly, development of this cell appeared to combine with the slow approach of a long-wave trough from the west to lower geopotential heights north of Flo and thus to initiate a clear break in the subtropical ridge. This break occurred well before Flo reached the subtropical ridge and will be shown below to have been a primary factor in Flo's future development.

These two effects resulted in the initial development of a flow channel across the subtropical ridge and into the midlatitude westerlies that appears to have been comprised of the outflow parcels possessing the largest northward velocity component. However, the pre-existing northeast channel still constituted the bulk of the mass flow and is attributed to the flywheel function of C1. The additional (weak) reservoir function provided by the small cold-core cell to the north and the weak but steady reservoir function provided by TUTT cell C2 that had now rotated to a position west of Flo also

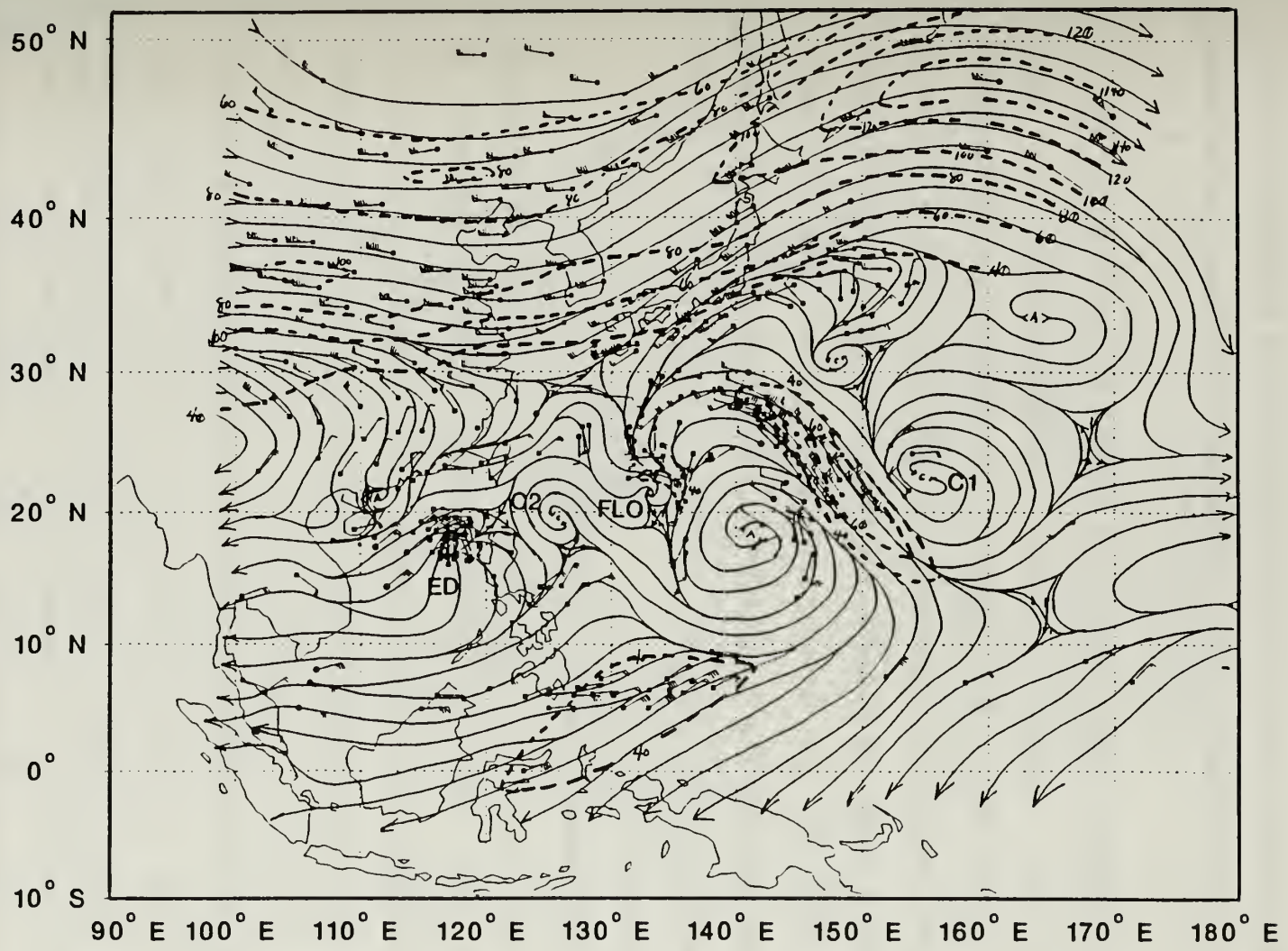

Fig. 23. As in Fig. 9, except for 12 UTC 15 September.

provided support for intensification. A combination of these favorable factors is consistent with an increase in Flo's maximum sustained winds to 85 kt at 18 UTC 15 September, which reflected a doubling of the intensification rate to 10 kt per 6 h.

The transient upper-level low ceased to exist at 18 UTC 15 September, as it quickly filled and merged with the more substantial C1 (Fig. 24). However, the subsequent development of the northward and northeastward-directed outflow channels as discussed above is clearly evident on this 200 mb analysis. More importantly, the upper-level flow pattern now included a third type of efficient mass/heat export mechanism that may have contributed to a further increase in Flo's intensification rate.

2. The vacuum export mechanism

The third type of upper-level outflow interaction mechanism (Fig. 25a) is hypothesized to form as a result of the development of an efficient flow channel across the subtropical ridge and into the subtropical jet. The key idea here is that the outflow from the tropical cyclone can be increased by the introduction of an increased pressure surface slope on the northern side of the subtropical ridge (Fig. 25b). Such an increase in the pressure surface slope could have been produced, for example, by the approach of a long-wave trough from the west (Fig. 25c). The effective slope of

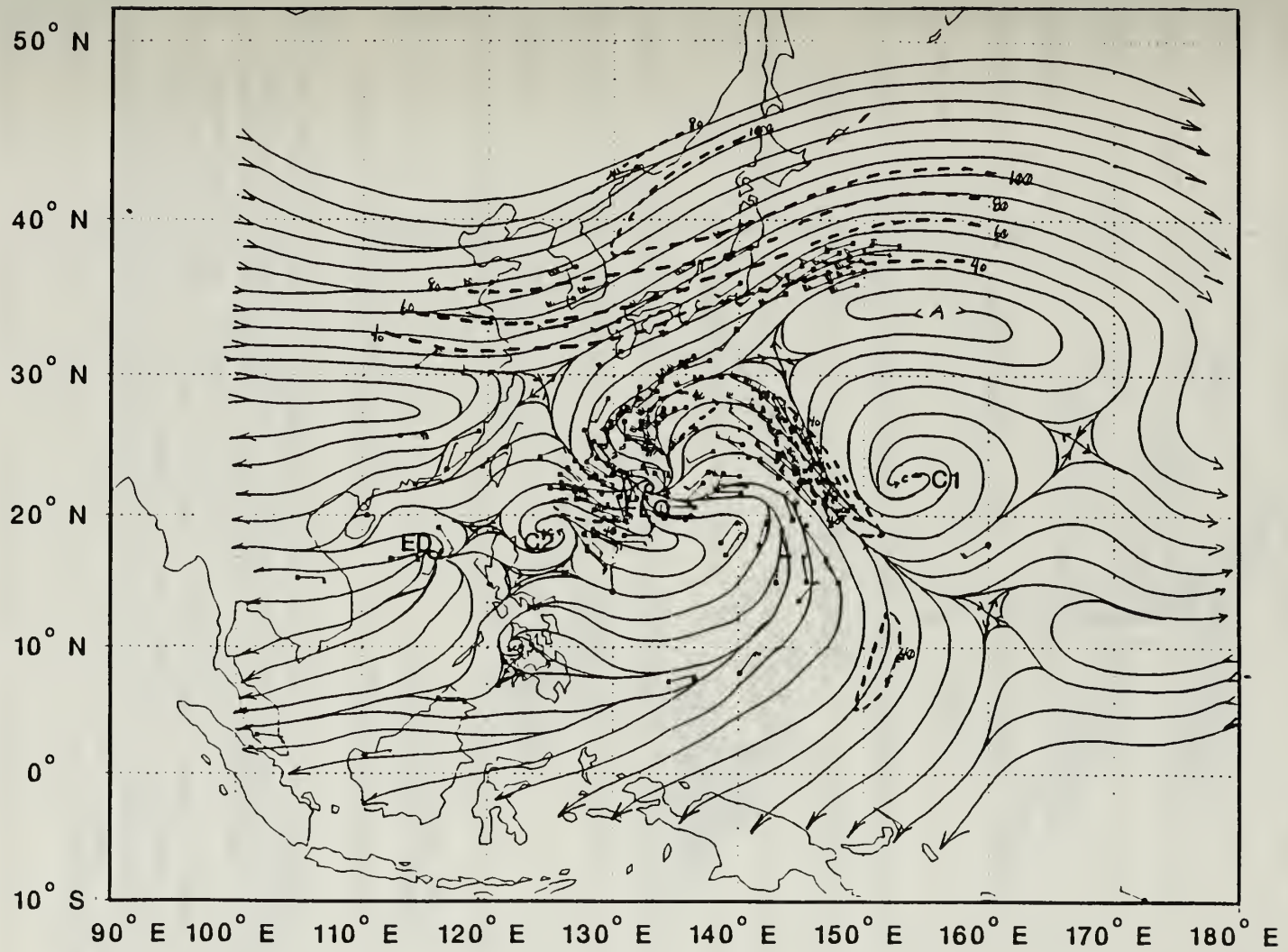

Fig. 24. As in Fig. 9, except for 18 UTC 15 September.

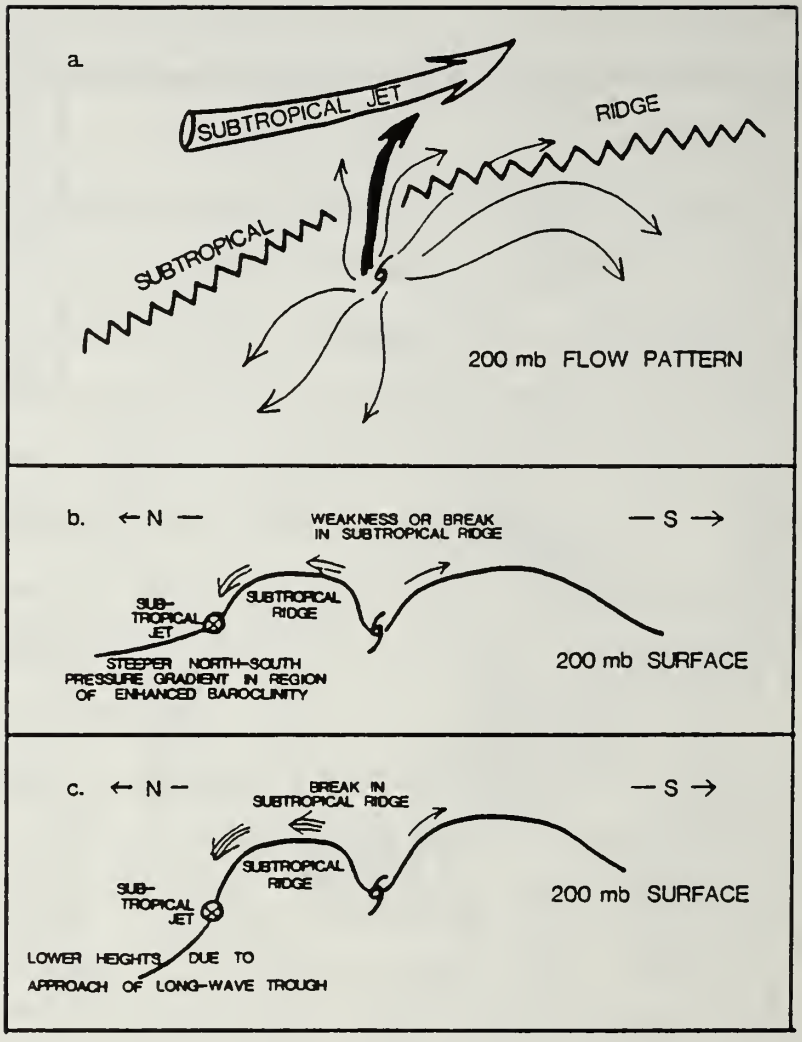

Fig. 25. Schematic of the vacuum export mechanism. (a) 200 mb flow pattern depicting development of strong tropical cyclone outflow jet across a weakness in the subtropical ridge and into the subtropical jet. (b) Topography of 200 mb surface oriented North (left) - South (right) depicting enhanced outflow due to steeper north-south pressure gradient on northern side of subtropical ridge. (c) Topography of 200 mb surface oriented North (left) - South (right) depicting enhanced outflow across a break in the subtropical ridge.

the pressure surface increased, and thus the subtropical jet was intensified as the base of the trough moved into the region and lowered heights northwest of Flo. The subtropical jet is therefore useful as a means of identifying a steeper north-south slope. A steeper pressure surface slope implies that the kinetic energy (velocity squared) of the outflow parcels from the tropical cyclone is increased as they are merged into the subtropical jet. This is hypothesized to have created a Bernoulli or "vacuum-type" effect that resulted in a highly efficient mass/heat export mechanism.

Similar to the flywheel mechanism, the vacuum mechanism removes mass and heat from the tropical cyclone environment such that the subsidence occurs at distances sufficiently remote to have negligible impact on future storm development. Moreover, the longevity of the vacuum mechanism appears to depend to a large degree upon the position of the tropical cyclone relative to the subtropical jet, and not upon the subsidence, as is the case with the reservoir function.

Based upon this case study, it is hypothesized that two major controlling factors determine whether a tropical cyclone is properly positioned such that the vacuum mechanism is likely to develop. First, the outflow jet must be provided a favorable path into the synoptic-scale jet. Prior to the time when Flo achieved typhoon strength, the vacuum mechanism was not present because the circulations of adjacent upper-level features (TUTT cells and the upper-level anticyclones)

combined to provide a more favorable pressure surface slope, i.e., a more efficient "path of least resistance." For example, Flo's outflow pattern at 12 UTC 14 September (Fig. 17) appeared to have been principally controlled by the positions of TUTT cells C1 and C2 superposed on the equatorward background flow, which effectively deflected the outflow jets away from the higher heights associated with the subtropical ridge. Even when Flo moved closer to the subtropical jet at 00 UTC 15 September (Fig. 22), the strong ridging northeast of Flo continued to prevent the development of the vacuum mechanism by deflecting the outflow trajectories anticyclonically into the C1 channel. It was not until 12 UTC 15 September (Fig. 23) that the northern channel began to become effective as the result of a break in the ridge coincident with the development of the transient upper-level low described previously.

The second important factor related to the development of the vacuum mechanism is the distance between the tropical cyclone and the subtropical jet. If this distance is so large that the turning associated with the Coriolis forcing becomes dominant, the outflow jet will undergo the characteristic anticyclonic turning associated with the normal outflow regime and will only slowly descend the pressure surface on the northern side of the subtropical ridge. Slow descent implies less rapid increases in kinetic energy at the expense of potential energy, and hence only a marginally efficient

outflow channel can develop. Conversely, if the distance between the tropical cyclone and the synoptic-scale jet becomes too small, a large vertical wind shear will develop within the storm environment that will result in ventilation and impede further development or even weaken the storm.

As shown in Fig. 3a, the trend in the mass flux at 200 mb that began at 12 UTC 15 September appears to contradict the expected increase in the outflow associated with the vacuum mechanism. It is hypothesized that the loss of the southern outflow channel into the background flow of upper-level easterlies resulted in a decrease in the total outflow. The blocking action of the flow pattern associated with the adjacent upper-level anticyclone is evident in Fig. 26. This effect appeared to continue until 00 UTC 17 September, at which time a change in the orientation of the anticyclone (to be discussed below) resulted in the re-establishment of the southern channel.

3. Effects of multiple interaction channels

By 00 UTC 16 September, Flo's maximum sustained winds had increased to 100 kt, which indicates that the intensification rate had increased to 15 kt per 6 h. It is hypothesized that the addition of the vacuum mechanism to the outflow regime played a major role in effecting this further increase in the intensification rate despite the slightly decreased total outflow at 200 mb shown in Fig. 3a. As shown

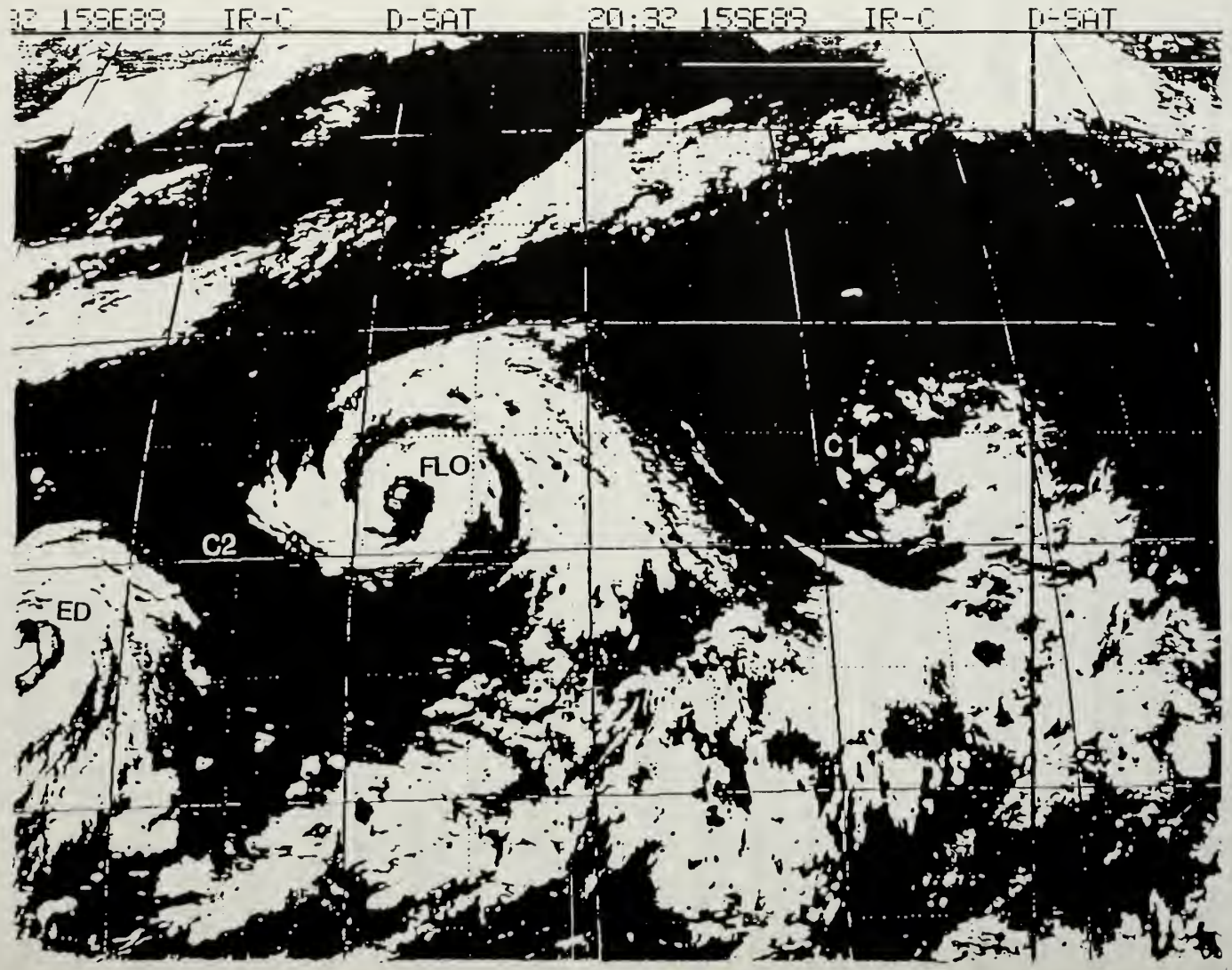

Fig. 26. As in Fig. 13, except for 2032 UTC 15 September.

in Figs. 4a and 5a respectively, increasing EFC and decreasing bulk vertical shear were initiated concurrently with the development of the vacuum mechanism. Both of these factors were therefore favorable for continued intensification. Had not the loss of the southern outflow channel been balanced by these factors as well as by the existence of dual outflow channels to the north, the intensification of Flo during this period may have been considerably slower.

Upper-level support for continued intensification therefore consisted of: (i) the increasingly important vacuum mechanism; (ii) the maintenance of the flywheel mechanism provided by TUTT cell C1, which also continued to provide a strong reservoir function; and (iii) the slowly weakening reservoir function of C2. Each of these mass/heat export mechanisms is depicted in Fig. 26. Although just developing, the vacuum mechanism is revealed in this imagery when contrasted with the imagery from 12 UTC 14 September (Fig. 20). For example, the curvature of the cloud streaks was flattened on the northern periphery of Flo, which indicates that some of the outflow was being directed over the subtropical ridge and into the subtropical jet. The jet streak that formed from the merging of this northern outflow jet and the subtropical jet (Fig. 27) is marked on the imagery by a cloud pattern characteristic of the upper-level divergence associated with the right-rear entrance region of the jet streak. The establishment of such a jet streak is an important

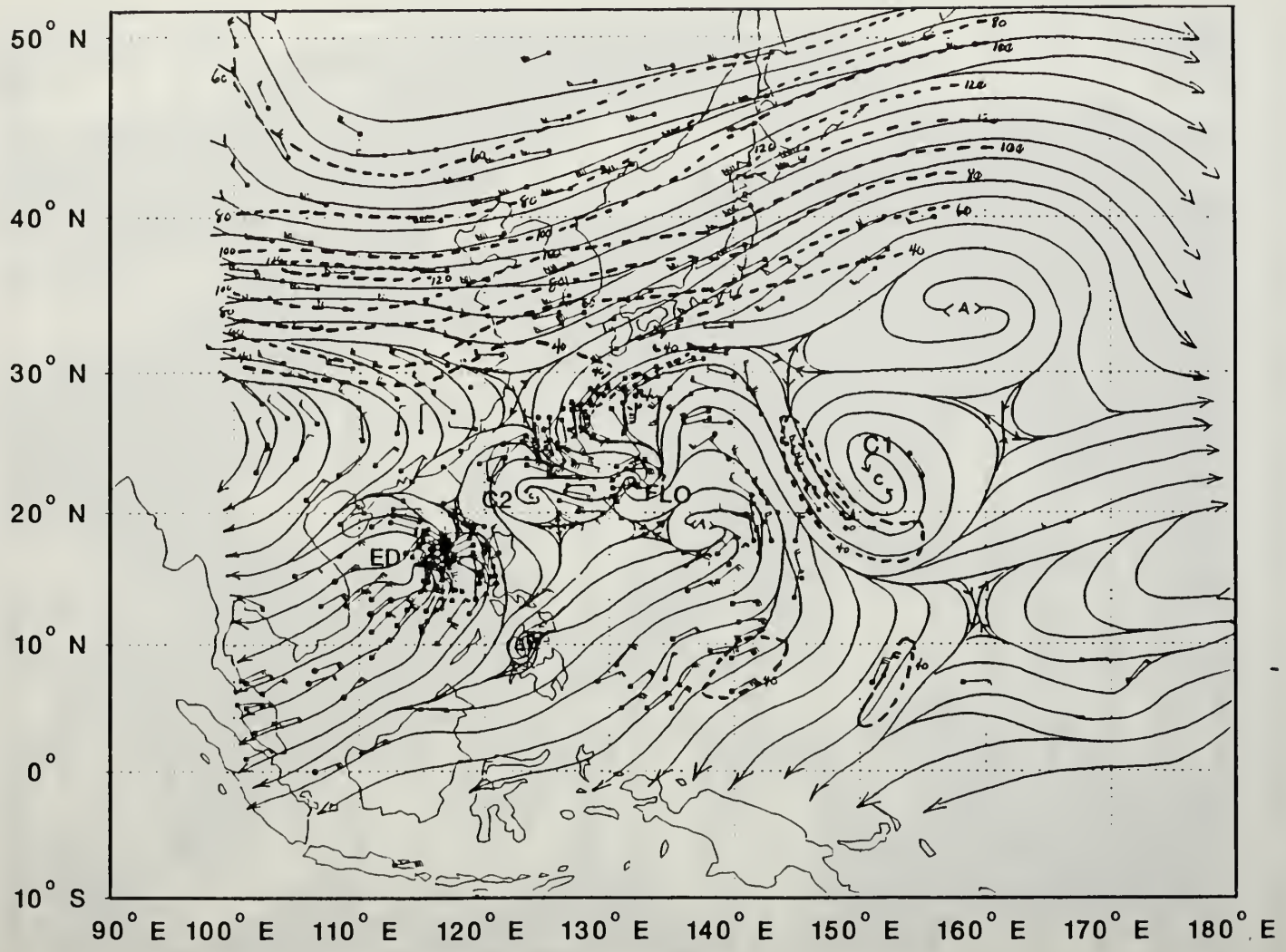

Fig. 27. As in Fig. 9, except for 00 UTC 16 September.

characteristic of the vacuum export mechanism, as is the change in the orientation of the cirrus blow-off that marks the tropical cyclone outflow pattern.

Further development of TUTT cell C1's flywheel mechanism is also evident on the satellite imagery in Fig. 26. An increasingly broad and intense region of cloudiness was noted on the southeastern periphery of the cell, which signified increased upper-level divergence and subsequent low-level convergence and convection. The flywheel mechanism appeared to have sufficiently expanded such that a significant proportion of the outflow from Flo did not converge into TUTT cell C1. As a result, the reservoir function of C1 became secondary, and thus C1 was unlikely to quickly fill and weaken. The vertical structure and extent of C1 (Fig. 28) had changed little since 06 UTC 14 September (Fig. 7b), and the apparently stronger cold-core signature (vertical extent down to 600 mb) may have been due to a more opportune cross-section orientation. Analysis of a time series of rawinsonde profiles from Marcus Island (24.0°N, 154.0°E) suggests that C1 maintained a vertical structure down to at least 500 mb (Fig. 8).

Finally, the continued presence of TUTT cell C2 is also evident on the imagery in Fig. 26 as a markedly cloud-free region directly between typhoons Flo and Ed. The northeastern quadrant of C2 is evident as a small, cloudless indentation on the southwestern periphery of Flo's cloud bank. The vertical

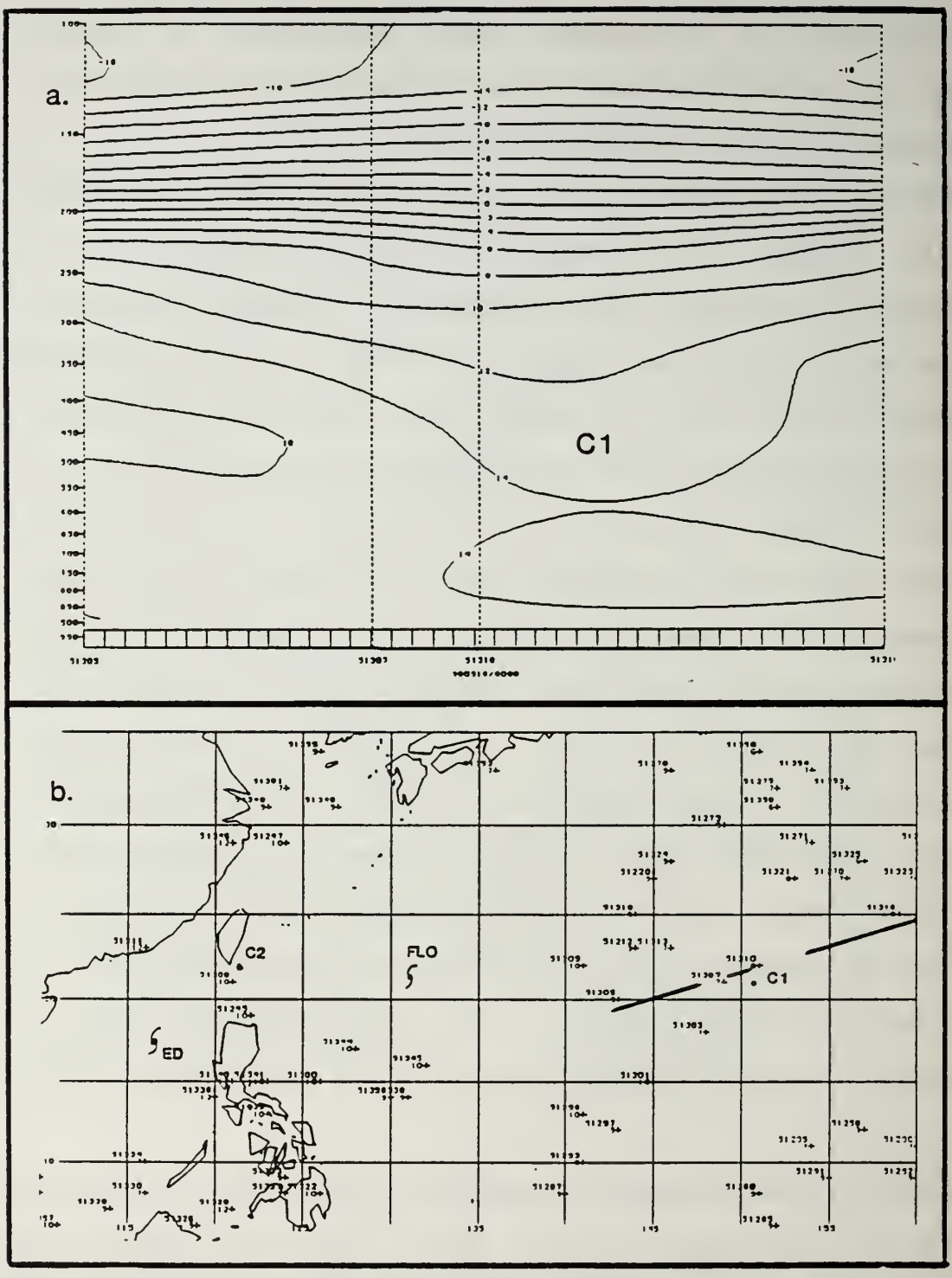

Fig. 28. (a) As in Fig. 7a, except for cold low C1 at 00 UTC 16 September. (b) As in Fig. 7b, except for cross-section in (a).

structure and extent of C2 as inferred from a time series of rawinsonde profiles (Fig. 29) from the Russian ship EREH (20.0°N, 126.0°E) had changed very little since 18 UTC 13 September (Fig. 16a). Both wind and temperature observations therefore indicated that C2 maintained a vertical structure down to approximately 300 mb. Evidently, the reservoir function had caused only minor filling of cell C2 because the associated subsidence was apparently spread to lower levels. Weakening of this cell appears to have been primarily in the form of a reduction in the horizontal extent. However, the lack of a vigorous signature for C2 on either the imagery or the analyses suggests that the reservoir function was at this point only marginally effective as a mass/heat export mechanism.

D. INTENSIFICATION TO MAXIMUM STRENGTH

Flo continued to intensify at an average rate of 15 kt per 6 hours for the 18 h period beginning 18 UTC 15 September and reached supertyphoon (130 kt) intensity at 12 UTC 16 September. This rapid intensification was supported by continued development of the vacuum mechanism to the north and by the strengthening of the flywheel function of C1 to the east.

1. Complex interaction with C1 and the subtropical ridge

The decrease in Flo's intensification rate to 5 kt per 6 h for the period 12 UTC 16 September through 00 UTC 17

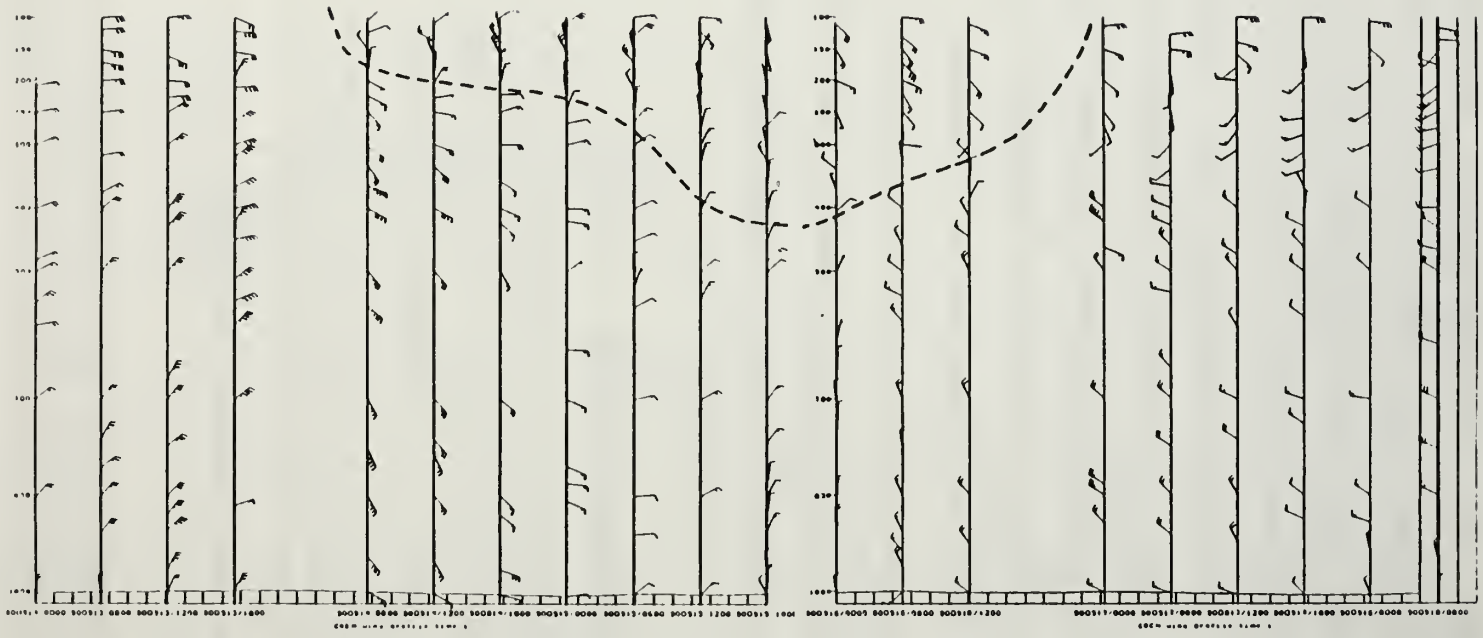

Fig. 29. As in Fig. 8, except for ship EREH (20.0°N, 126°E) from 00 UTC 13 September through 06 UTC 18 September. Cold low C2 tracked westward and passed over the ship around 12 UTC 15 September.

September does not appear to be easily explained by upper-level forcing. One explanation may be inadequate observations to support the intensity estimates provided by JTWC (Fig. 2). However, two more likely explanations are provided by subtle changes in the outflow pattern that occurred between 06 UTC and 12 UTC 16 September.

First, the development of an upper-level anticyclone northeast of Flo (Fig. 30) may have raised the geopotential heights northeast of Flo to the point that outflow into the C1 interaction channel may have temporarily decreased. Such a decrease would imply a corresponding decrease in the remote forcing provided by this export mechanism. While a continued decrease in the mass flux at 06 UTC 16 September is shown in Fig. 3a, a more important factor may have been a short-lived decrease in EFC that was also noted at this time (Fig. 4a). The approximate 600 n mi distance between Flo and this flow channel could translate into a time lag of approximately 12 to 18 h before a decrease in outflow of change in the EFC might have been reflected in a decrease in Flo's intensification rate. The fact that the intensification rate did not decrease until the 18 UTC 16 September observation (Fig. 2) appears to lend some credence to this supposition.

The second change in Flo's outflow pattern that may have contributed to the decreased intensification rate was the apparent weakening of the vacuum mechanism at 12 UTC 16 September. As shown in Fig. 31, Flo's northward track into the

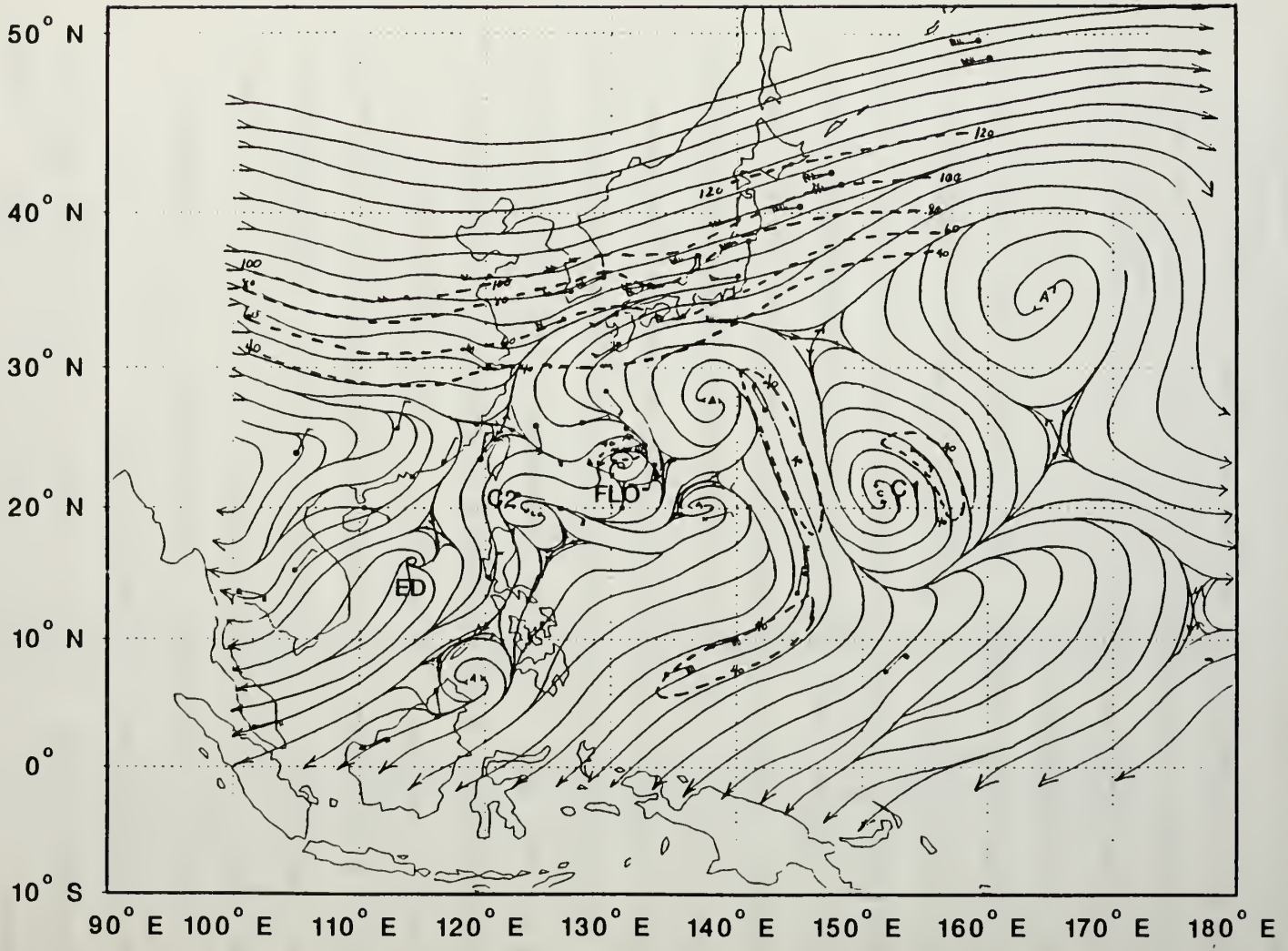

Fig. 30. As in Fig. 9, except for 06 UTC 16 September.

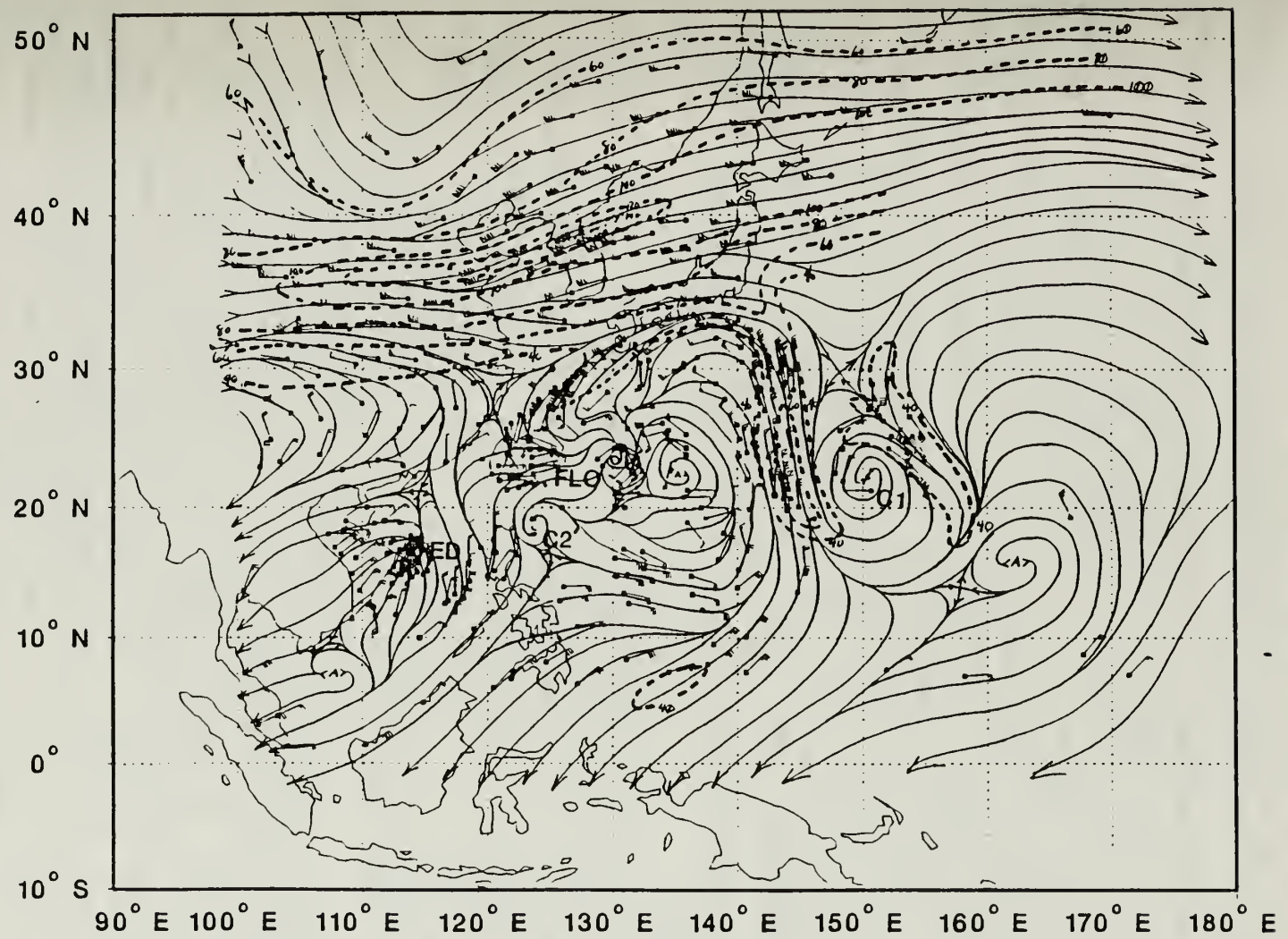

Fig. 31. As in Fig. 9, except for 12 UTC 16 September.

subtropical ridge had resulted in a tight anticyclonic turning of the northern outflow jets. This change in the upper-level circulation pattern is considered to be unfavorable for the development of the vacuum export mechanism. As a result, the outflow channel across the subtropical ridge appears to have weakened as the ridging northeast of Flo became less pronounced when compared to the prior 200 mb analysis (Fig. 30). The relative proximity of Flo to the subtropical ridge implies only a short time lag before an unfavorable change in the northern outflow channel might be reflected by a decreased intensification rate. Thus, it is possible that the weakened vacuum mechanism may have contributed to the slightly decreased intensification rate that became apparent at 18 UTC 16 September.

Counterbalancing the minor weakening of the vacuum mechanism at 12 UTC 16 September was an apparent strengthening of C1's flywheel function as determined by the much stronger jet streak (Fig. 31). Furthermore, the region of upper-level divergence that characterizes the flywheel function appears to have shifted to the cell's southwest and northeast quadrants. Consequently, the trajectory into C1 may have been slightly less favored, in which case the subsidence and filling associated with the reservoir function would have been reduced. Such an effect could prolong maintenance of the deep vertical structure of C1, and thereby allow the flywheel function to remain effective for a longer time. The

hypothesized 12 to 18 h lag time associated with the strengthened flywheel mechanism correlates well with the increased intensification rate that was reported at 06 UTC 17 September (Fig. 2).

Changes in the upper-level circulation at 00 UTC 17 September appeared to provide new support for an increase in Flo's intensification rate. As shown in Fig. 32, the deepening of the long-wave trough to the northwest of Flo appears to have increased the slope of the pressure surface on the northern side of the subtropical ridge. As a result, the tight anticyclonic turning northwest of Flo was somewhat reduced as compared to 12 UTC 16 September (Fig. 31). The northern outflow jets now had a more direct path across the break in the subtropical ridge, and thus the outflow parcels gained an increasing amount of kinetic energy as they descended the pressure surface slope on the poleward side of the subtropical ridge. The stronger upper-level jet (Fig. 32) is identified on the satellite imagery (Fig. 33) by the characteristic jet streak cloud pattern and cirrus blow-off.

Because Flo remained south of the subtropical ridge, much of the mass flow associated with these northern jets did not possess the northward velocity component required to cross the subtropical ridge. This mass flow favored the lower geopotential heights equatorward of the subtropical ridge, and thus a large region of upper-level divergence formed near 34°N, 135°E where this mass flow turned anticyclonically into

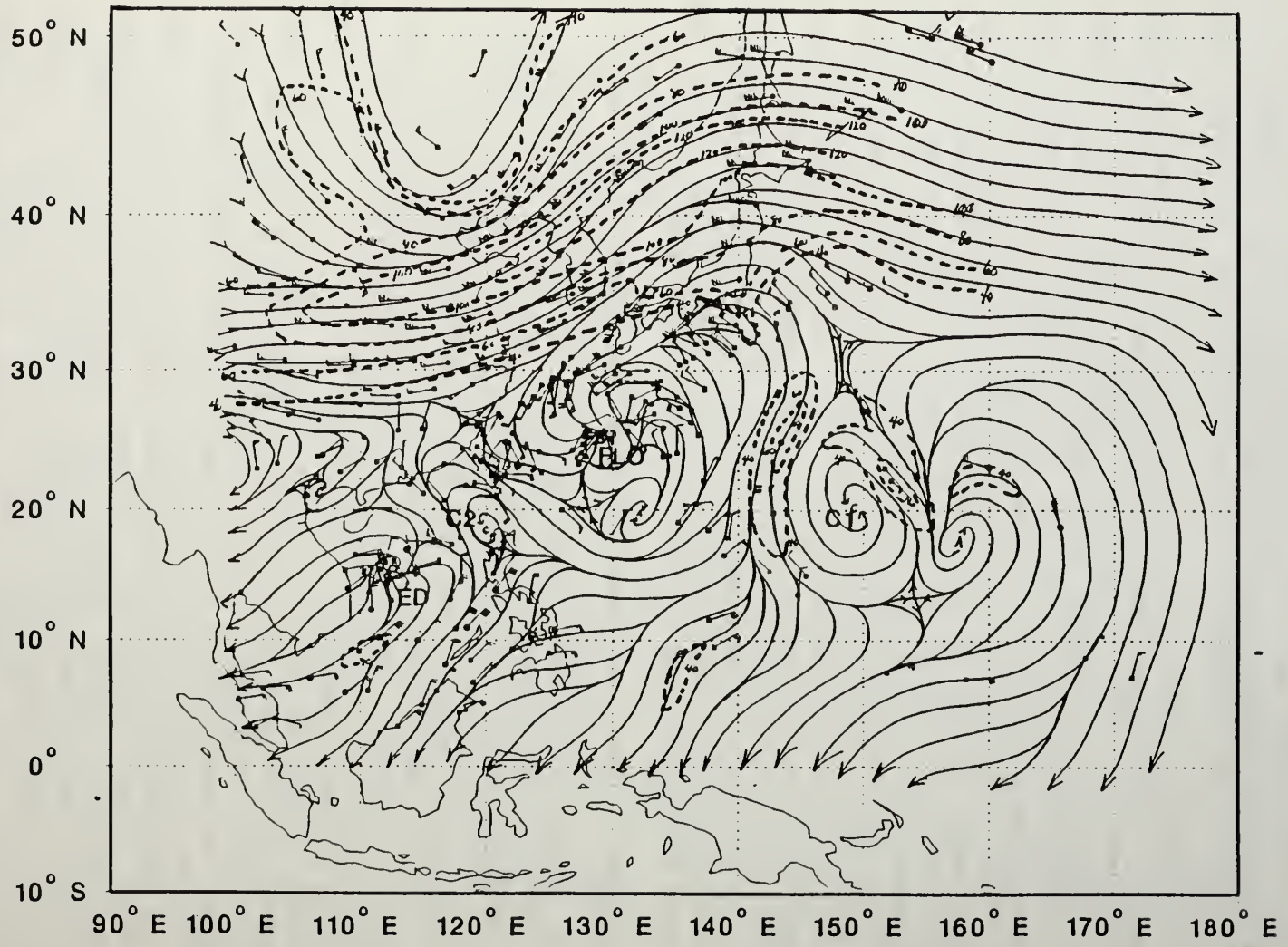

Fig. 32. As in Fig. 9, except for 00 UTC 17 September.

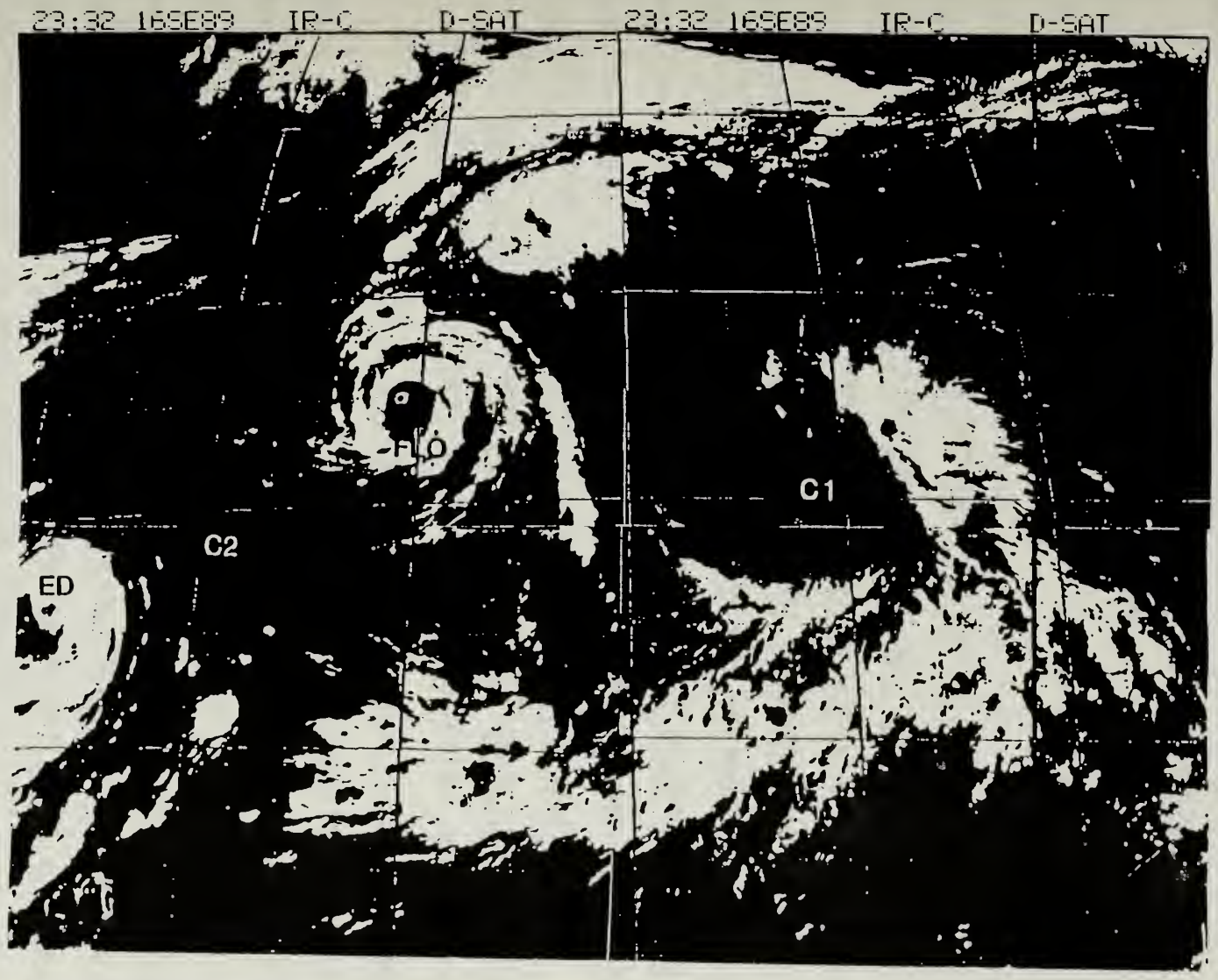

Fig. 33. As in Fig. 13, except for 2332 UTC 16 September.

the north-south flow channel separating C1 from Flo. This region of divergence is identified on the imagery by the convective cloudiness northeast of Flo. The increased flow into the north-south channel subsequently enhanced C1's flywheel mechanism, as is evident in the very broad region of upper-level divergence that extended south of C1 along 10°N (Fig. 32).

In summary, Flo's motion towards the subtropical ridge resulted in changes in the upper-level circulation that essentially reinvigorated both the flywheel mechanism of C1 and the vacuum mechanism of the subtropical jet. Consistent with this hypothesis, the mass flux at 200 mb was enhanced beginning around 00 UTC 17 September (Fig. 3a).

2. TUTT cell interaction effects

Coincident with the strengthening of the north-south channel to the east of Flo was the decay of the convective activity associated with the upper-level anticyclone east-southeast of Flo (also shown in Fig. 31). The combination of the strong northerly flow, which was no longer deflected by this anticyclone, and the anticyclonic turning associated with the outflow regime resulted in the development of a transient circulation feature southeast of Flo. It is hypothesized that this indraft anticyclone was essentially the remains of the anticyclone that had been positioned southeast of Flo since the inception of the flywheel mechanism. The key point here is

that the anticyclone had shifted from an outdraft orientation to an indraft orientation. As shown in Fig. 32, this indraft upper-level anticyclone appeared to have assumed the role of a mass/heat reservoir. More importantly, the change in the orientation of this anticyclone resulted in the redevelopment of a weak southern outflow channel, which contributed to the increased mass flux indicated in Fig. 3a. The reservoir function signatures of cells C1 and C2, as well as for this indraft anticyclone, are identified in the imagery (Fig. 33) as distinctly cloud-free regions characteristic of large-scale subsidence. It is hypothesized that the reinvigoration of C1's flywheel mechanism, combined with the addition of the southern outflow channel provided by the parasitic indraft anticyclone and the continued reservoir functions of C1 and C2, contributed to an increase in Flo's intensification rate.

3. Emergence of vacuum effect as dominant export mechanism

As analyzed in the ATCR (1991), the intensification rate did increase during the 12 h following 18 UTC 16 September (Fig. 2), and Flo reached maximum intensity of 145 kt sustained winds at 06 UTC 17 September. Although it is generally difficult to assess the accuracy of the intensity estimates, these analyses indicate that changes in the upper-level circulation may be identified that are consistent with the published intensification rates. It is important to note

that, while these upper-level circulations provide supporting evidence for the intensification rates, other physical mechanisms (not discussed here) also may have assisted Flo in first attaining and then maintaining its supertyphoon intensity.

The major changes in the upper-level circulation pattern at 06 UTC 17 September appear to have been associated with the movement of Flo into the subtropical ridge. As shown in Fig. 34, a break in the subtropical ridge appeared to develop as a result of both the nearly stationary long-wave trough to the northwest and Flo's continued track to the north. Consequently, Flo appeared to track through this break in the subtropical ridge. Without having to ascend the higher heights of the subtropical ridge, the air parcels in the northern outflow jets accelerated down the larger slope in the pressure surface associated with the more baroclinic midlatitude troposphere poleward of the ridge. As a result, the northern channel into the subtropical jet became the most favored outflow channel. Concurrent with this development was a large increase in the EFC (Fig. 4a) that provided further upper-level support for an increased intensification rate. Counter-balancing this effect was a similarly large increase in the bulk vertical shear (Fig. 5a) that occurred as Flo moved north of the subtropical ridge.

The dominance of the vacuum mechanism is evident in the imagery shown in Fig. 35, as the bulk of the outflow cirrus

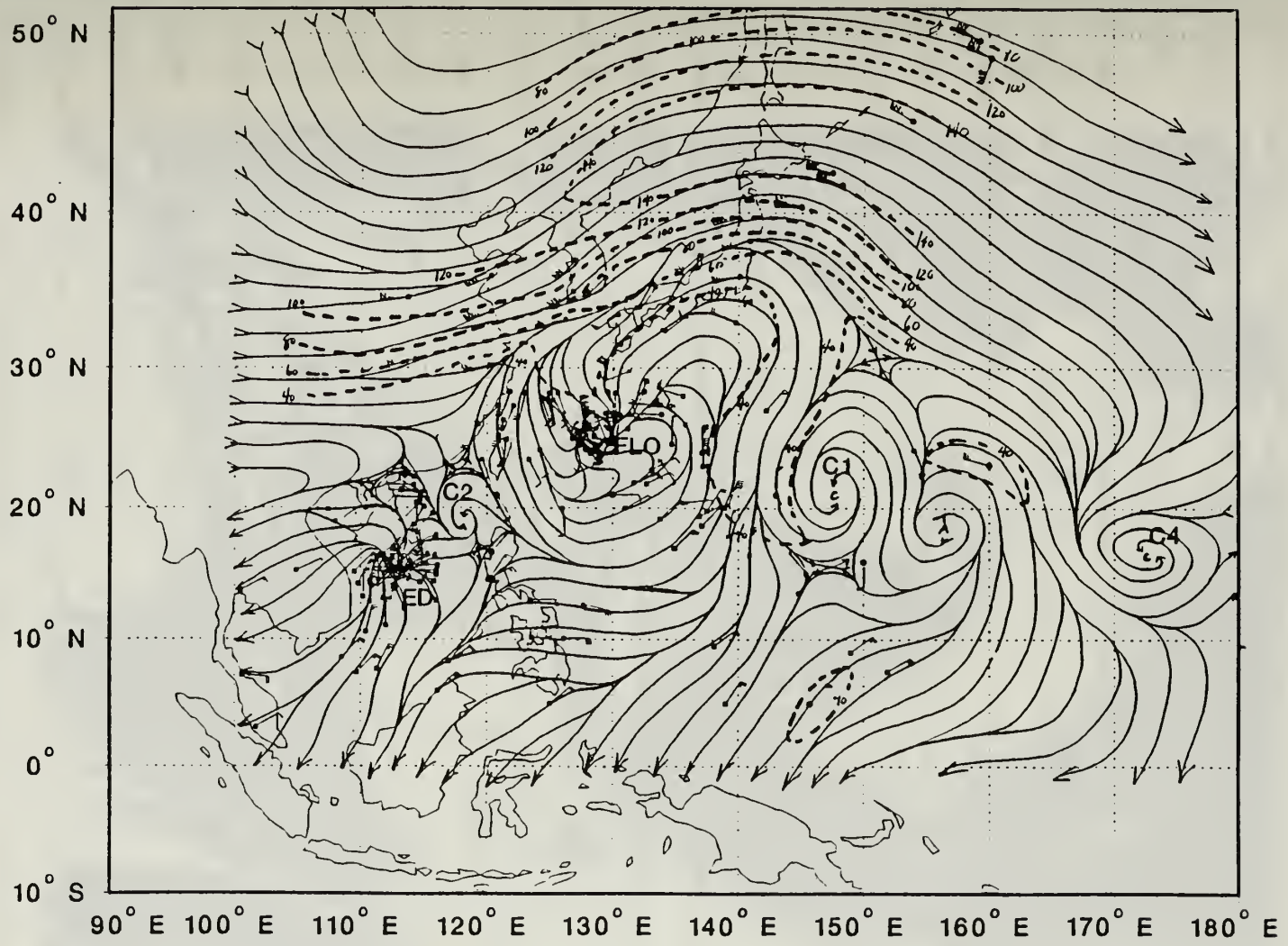

Fig. 34. As in Fig. 9, except for 06 UTC 17 September.

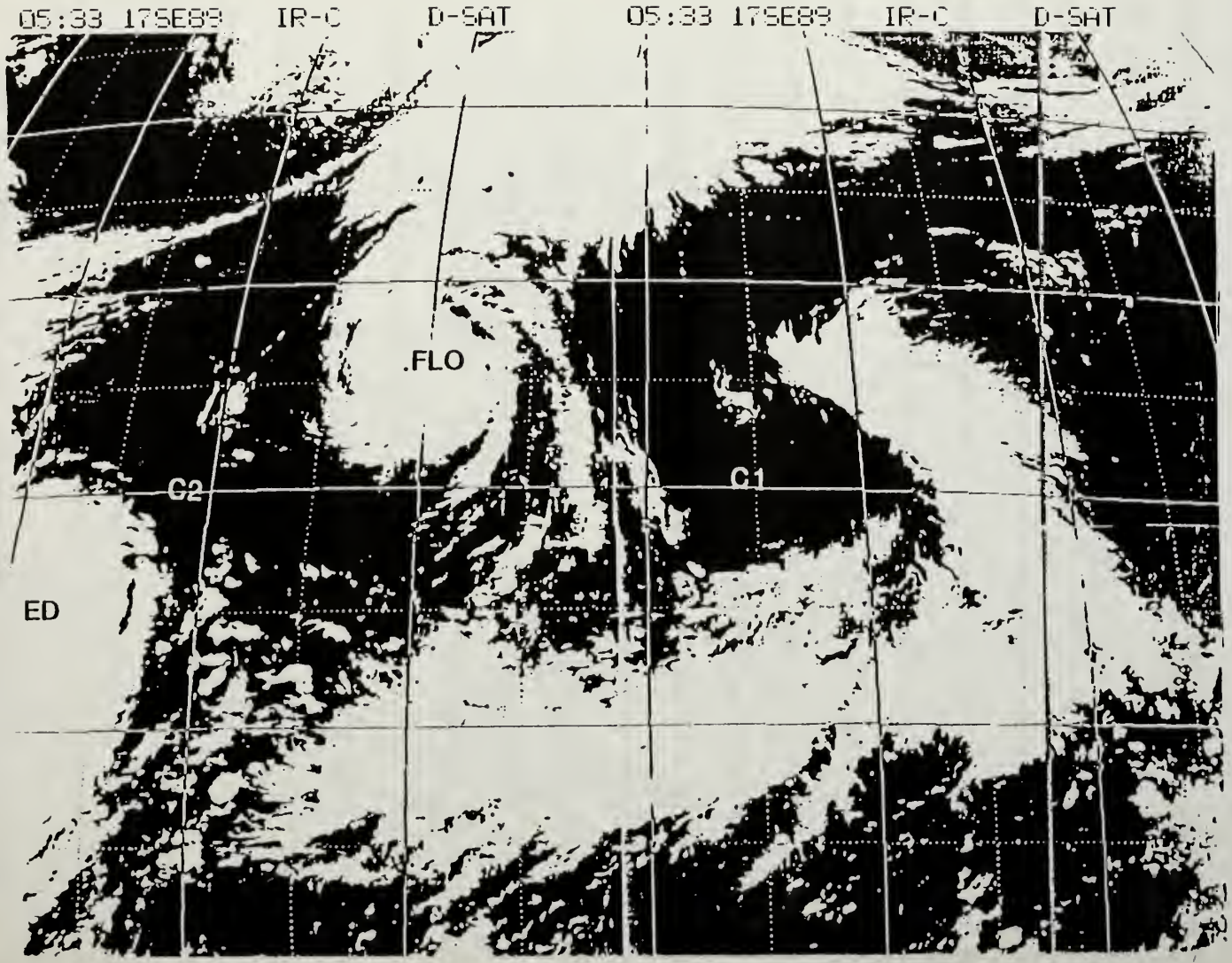

Fig. 35. As in Fig. 13, except for 0533 UTC 17 September.

blow-off had shifted from the northwest-southeast channel east of Flo to the northern channel into the subtropical jet. Although the upper-level divergence associated with the flywheel mechanism still appears to be strong on the imagery (Fig. 35), a marked decrease in the areal extent of this divergence region is depicted on the corresponding 200 mb analysis (Fig. 34). Much of the upper-level divergence along 10°N appears to have been the result of the outflow associated with the upper-level anticyclone that developed as a result of the convection southeast of C1. In addition, the areal extent of C1 decreased in comparison to the analysis shown in Fig. 32. These changes suggest that the reservoir function of C1 became relatively more important as the flywheel function weakened, and hence imply an increased likelihood that C1 would begin to fill. The slightly reduced vertical extent (only down to the 400-500 mb level) of C1 shown in Fig. 36 is consistent with this hypothesis. The end result of these changes appears to have been a net reduction in the efficiency of C1.

By 12 UTC 17 September, these changes in the upper-level circulation pattern were better defined. A major change in the upper-level forcing was the apparent absence of a direct interaction between Flo and C1 at 250 mb (not shown). The weakened outflow connection between Flo and C1 is further evident on the 200 mb analysis (Fig. 37) by a shift in the location of the major outflow jet from the east-southeast

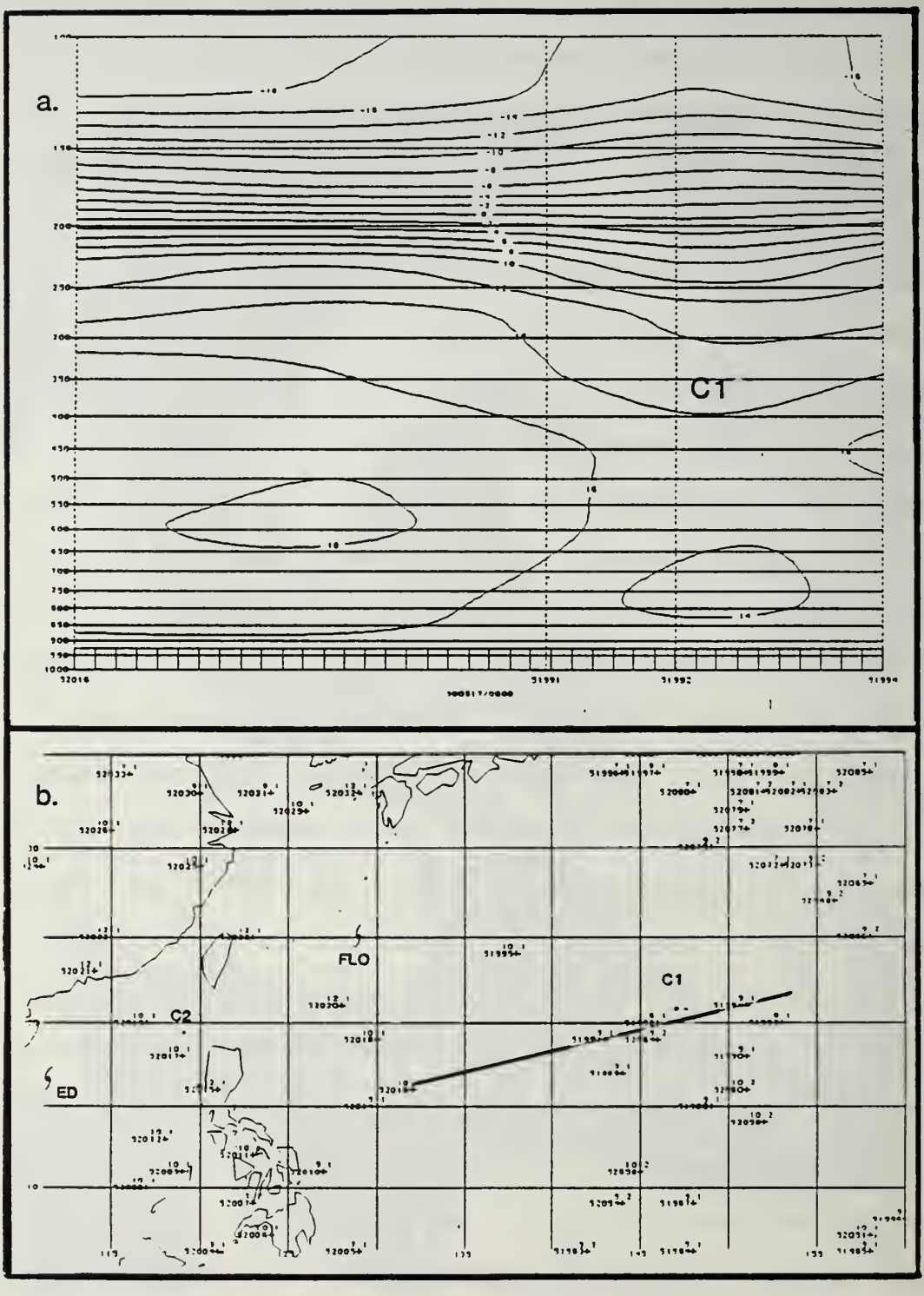

Fig. 36. (a) As in Fig. 7a, except for 06 UTC 17 September. (b) As in Fig. 7b, except for cross-section in (a).

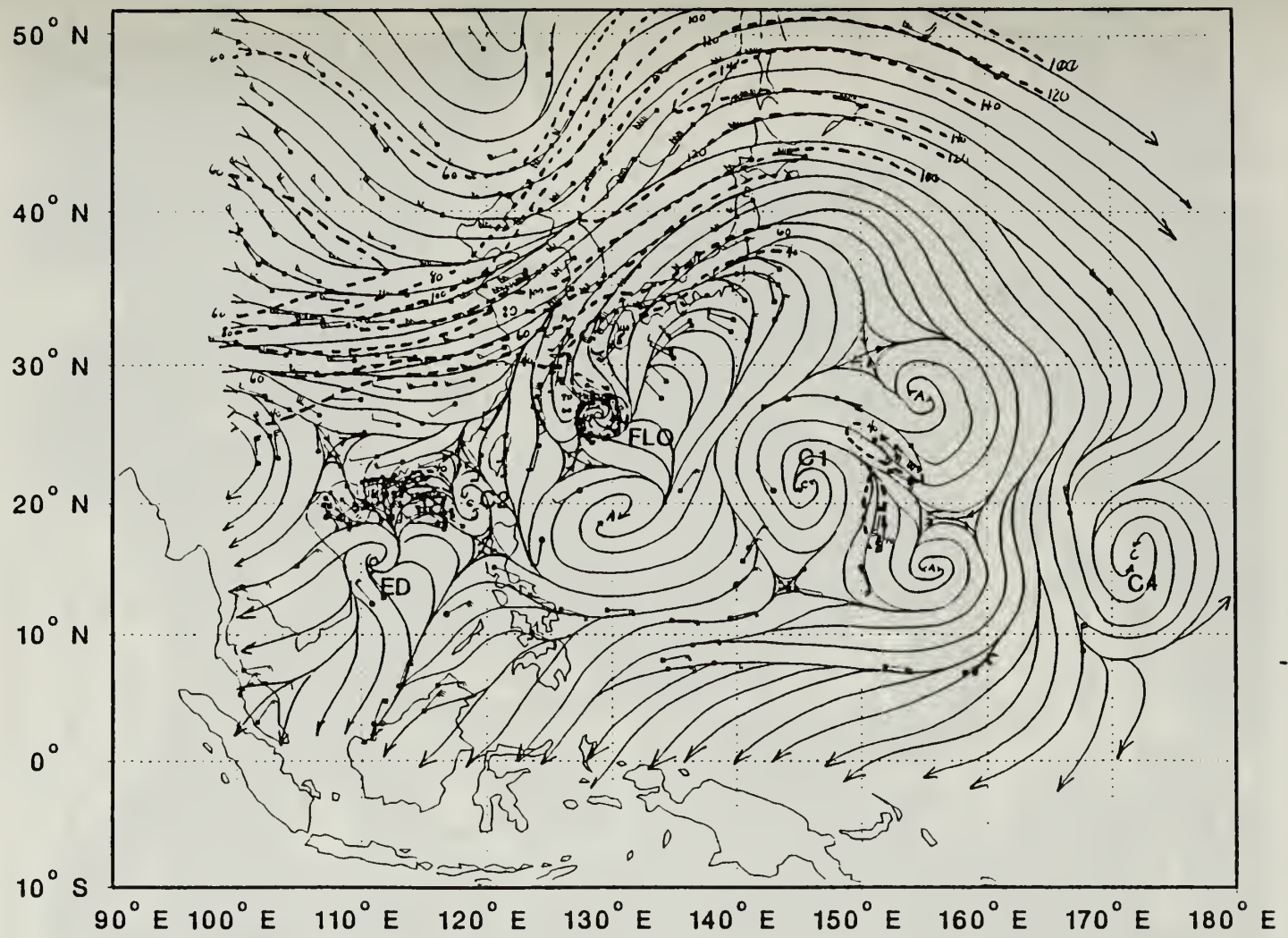

Fig. 37. As in Fig. 9, except for 12 UTC 17 September.

(into C1) to the north (into the subtropical jet). Flo crossed the subtropical ridge and ridging had redeveloped south and northeast of the storm. Little mass outflow is directed southeastward for subsequent interaction with C1. The weakening of the divergence region associated with C1's flywheel function is evident on the satellite imagery (Fig. 38) as a further decrease in the convective cloudiness along 10°N. In addition, the cirrus outflow appears to have been restricted to the northern channel, and thus it is associated with the dominant vacuum mechanism.

E. INITIAL WEAKENING

1. Loss of the flywheel mechanism

In the post-storm analysis by JTWC (ATCR 1991) shown in Fig. 2, Flo's intensity did not change between 06-12 UTC 17 September. Moreover, Flo began to recurve between 12-18 UTC 17 September along a track roughly following that of the Kuroshio current. While the warm air over the Kuroshio with this track would provide low-level support for continued intensification (Emanuel 1986), diminished upper-level support would seem to account for a decrease in intensity that began during this period.

As discussed above, this diminished upper-level support was primarily due to the decrease in the efficiency of the export mechanisms associated with C1 as a result of Flo's position north of the subtropical ridge. The northern outflow

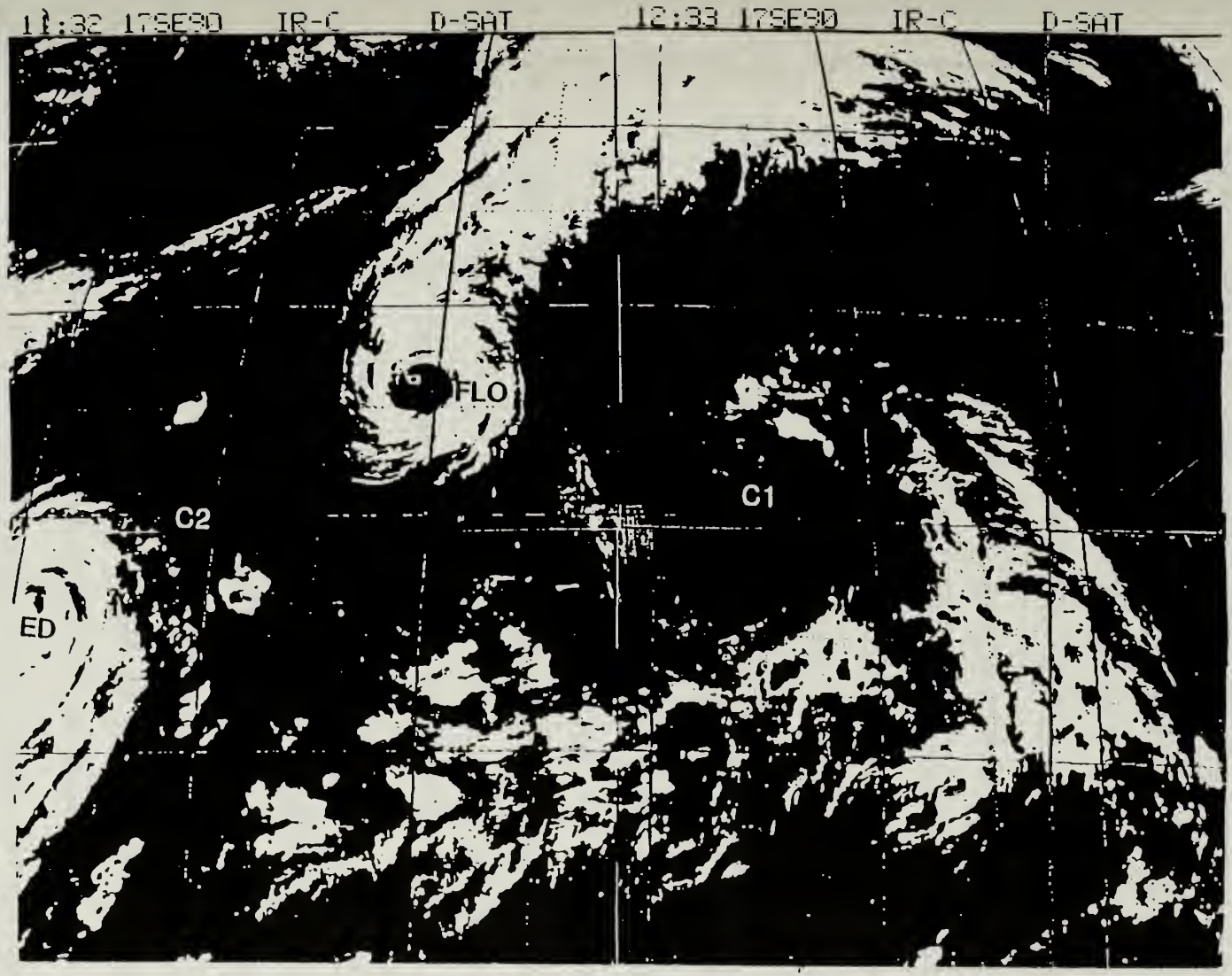

Fig. 38. As in Fig. 13, except for 1232 UTC 17 September.

jets now had to cross the subtropical ridge from north to south to interact with C1 (Fig. 37). As a result, the subtropical ridge acted essentially as a blocking mechanism, which reduced the mass outflow into the C1 flow channel. In addition, C2 had apparently weakened such that it no longer played a role in the upper-level forcing. A satellite temperature cross-section (not shown) through C2 indicated a nearly complete absence of any cold-core signature. TUTT cell C1, on the other hand, still maintained a significant vertical structure as well as a relatively large areal extent at 18 UTC 17 September (Fig. 39). Thus, despite the reduced efficiency of C1, it remained a significant upper-level circulation feature with a potential for additional interaction with Flo.

Flo's maximum sustained winds were estimated to have decreased to 135 kt by 18 UTC 17 September. While other physical mechanisms may have played a role in this weakening, the loss of C1's effective flywheel function was consistent with a reduction in intensity. Furthermore, the relatively short time lag of only 6 - 12 h between the loss of C1's flywheel mechanism and the decrease in Flo's intensity was consistent with the apparently abrupt decrease in mass flow into the C1 flow channel as Flo crossed the subtropical ridge.

Despite the decay of the flywheel function, the mass flux at 200 mb continued to increase during this period (Fig. 3a), although it did appear to level off beginning around 06 UTC 18 September. As shown in Fig. 40, two mass/heat export

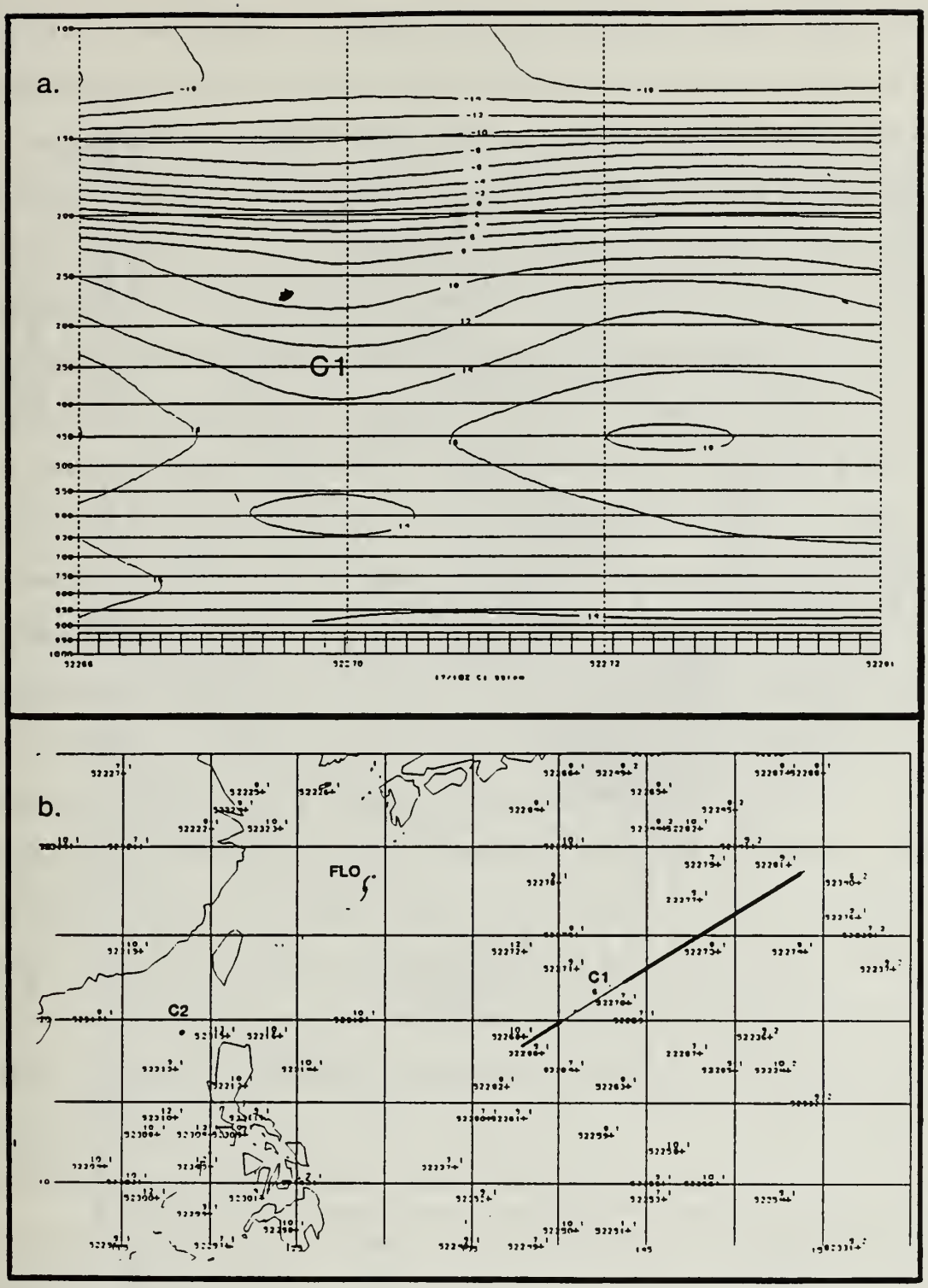

Fig. 39. (a) As in Fig. 7a, except for 18 UTC 17 September. (b) As in Fig. 7b, except for cross-section in (a).

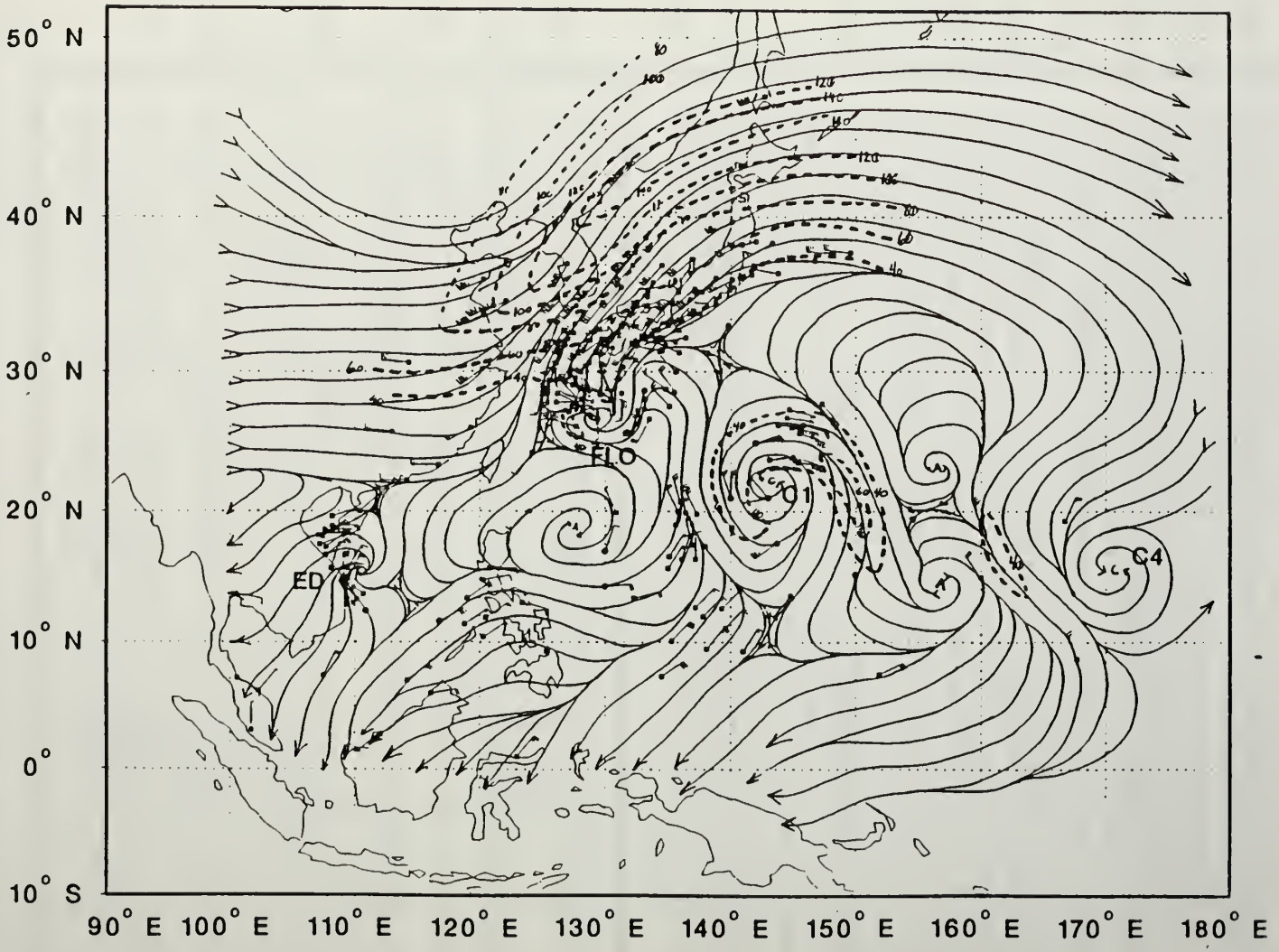

Fig. 40. As in Fig. 9, except for 18 UTC 17 September.

mechanisms remained: i) the northern channel and associated vacuum effect; and ii) the redeveloping reservoir function of C1. Apparently, only the vacuum effect remained as an efficient export mechanism, because a significant proportion of the inflow to C1 appears to have originated from the outflow associated with the convective activity to the east. It is hypothesized that much of the filling experienced by C1 during this period was a result of this eastern inflow, and thus the continued large increase in EFC (Fig. 4a) can also be attributed to the more dominant vacuum mechanism.

Two additional upper-level circulation features on the 200 mb analysis at 18 UTC 17 September (Fig. 40) must be considered. First, the parasitic indraft anticyclone south of Flo, although slowly weakening, continued to contribute to block development of a strong southward-directed outflow jet. Whereas an effective outflow channel enhances the export of mass and heat, any ridging adjacent to the cyclone such as the indraft anticyclone reduces the outward velocity. The kinetic energy of the outflow parcels decreases as they ascend the sloping pressure surface, converge into the center of the cell, and then subside. The characteristic cloud-free region associated with this subsidence is shown in Fig. 41 (note the 3 h time difference). Unless an alternate outflow mechanism exists to balance this decrease in upper-level forcing, the upper-level flow pattern cannot support the existing convection associated with the storm, and thus the storm will

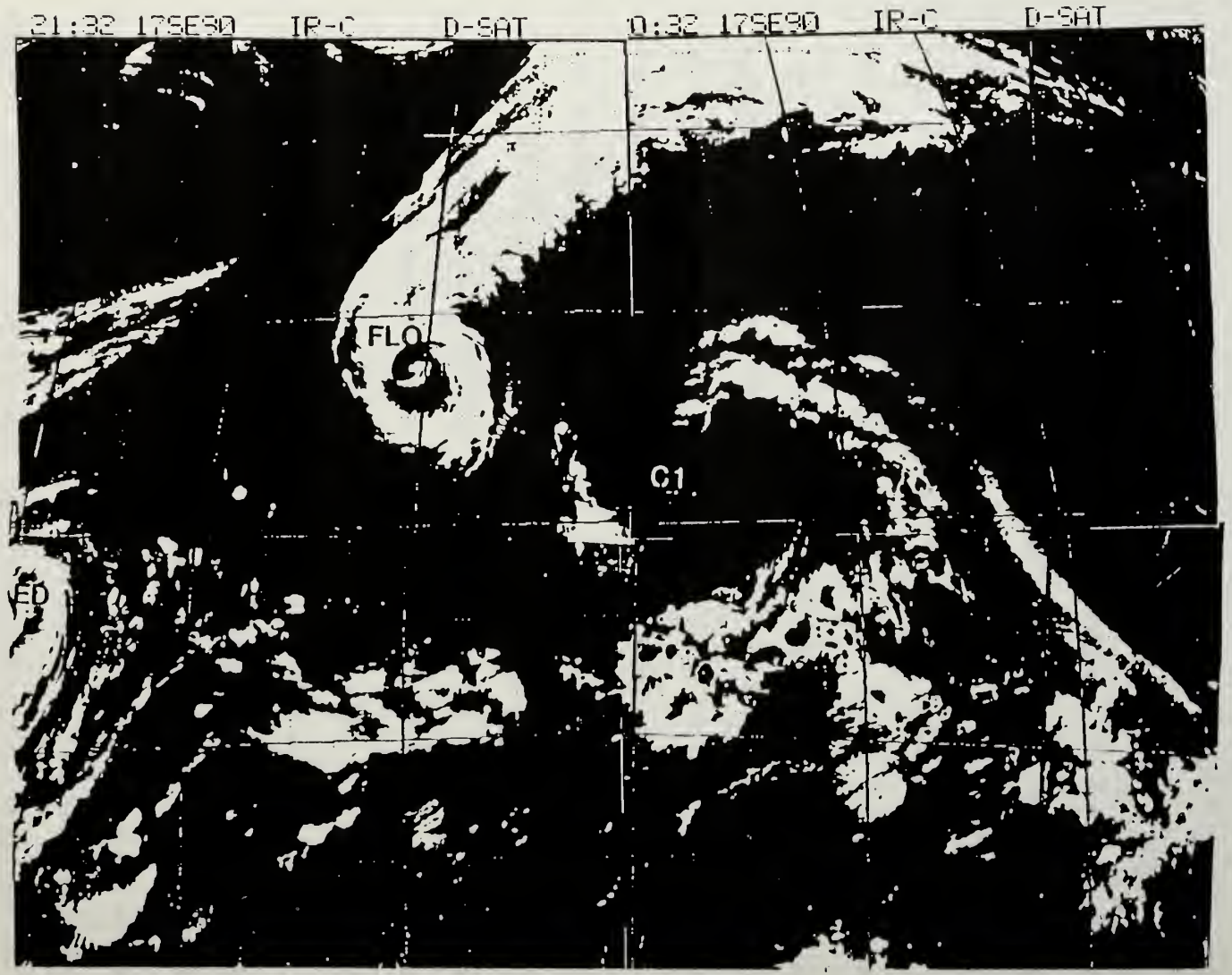

Fig. 41. As in Fig. 13, except for 2132 UTC 17 September.

weaken. It does not appear that such a counter-balancing mechanism existed at 18 UTC 17 September (Fig. 40), and thus it is likely that this effect contributed to the leveling-off of the mass outflow that occurred during the following 12 h (Fig. 3a).

The second prominent upper-level feature at 18 UTC 17 September was the TUTT cell C4 located near 10°N, 170°E. Although depicted on both the analysis and the corresponding satellite imagery (Fig. 41) as a region of upper-level divergence characteristic of the flywheel mechanism, this cell was too remote to provide any positive forcing on Flo.

By 00 UTC 18 September, Flo's maximum sustained winds had decreased to 125 kt. Favorable factors of strong mass flux (Fig. 3a) and EFC (Fig. 4a) associated with the relatively efficient mass/heat export mechanism were provided by the northward outflow channel. However, the increasing bulk vertical shear (Fig. 5a) was apparently the more dominant effect as Flo continued to track to the north. Moreover, the ridging south of Flo completely blocked the C1 flow channel at 200 mb (Fig. 42), although the reservoir function was evident at 250 mb (not shown). The dominance of the vacuum mechanism was evident on the imagery (Fig. 43) and was due in large part to the increase in the pressure surface slope caused by the approach of the long-wave trough from the west. Without the impediment to poleward flow, the outflowing air parcels accelerated down the pressure surface, merged with the

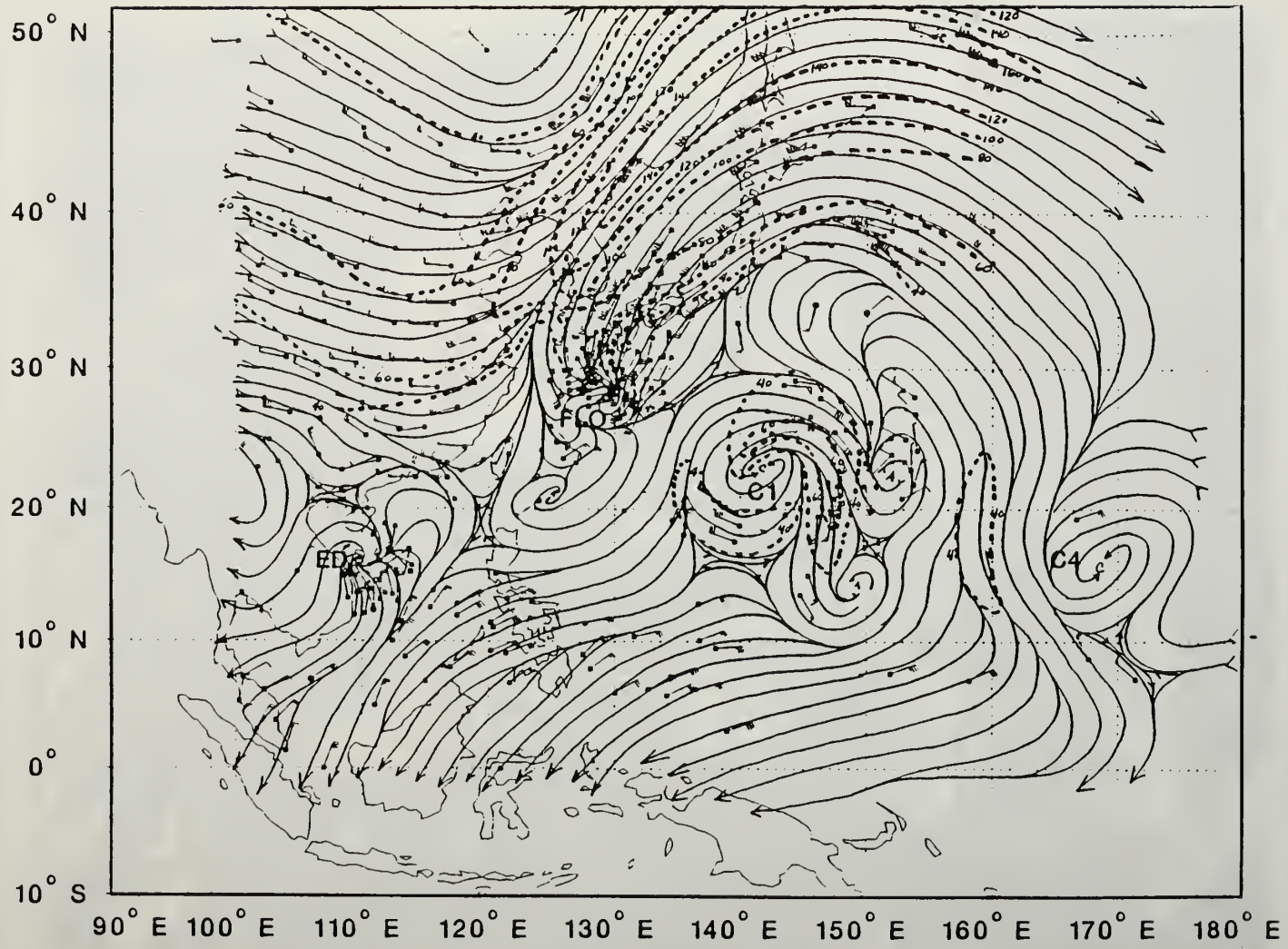

Fig. 42. As in Fig. 9, except for 00 UTC 18 September.

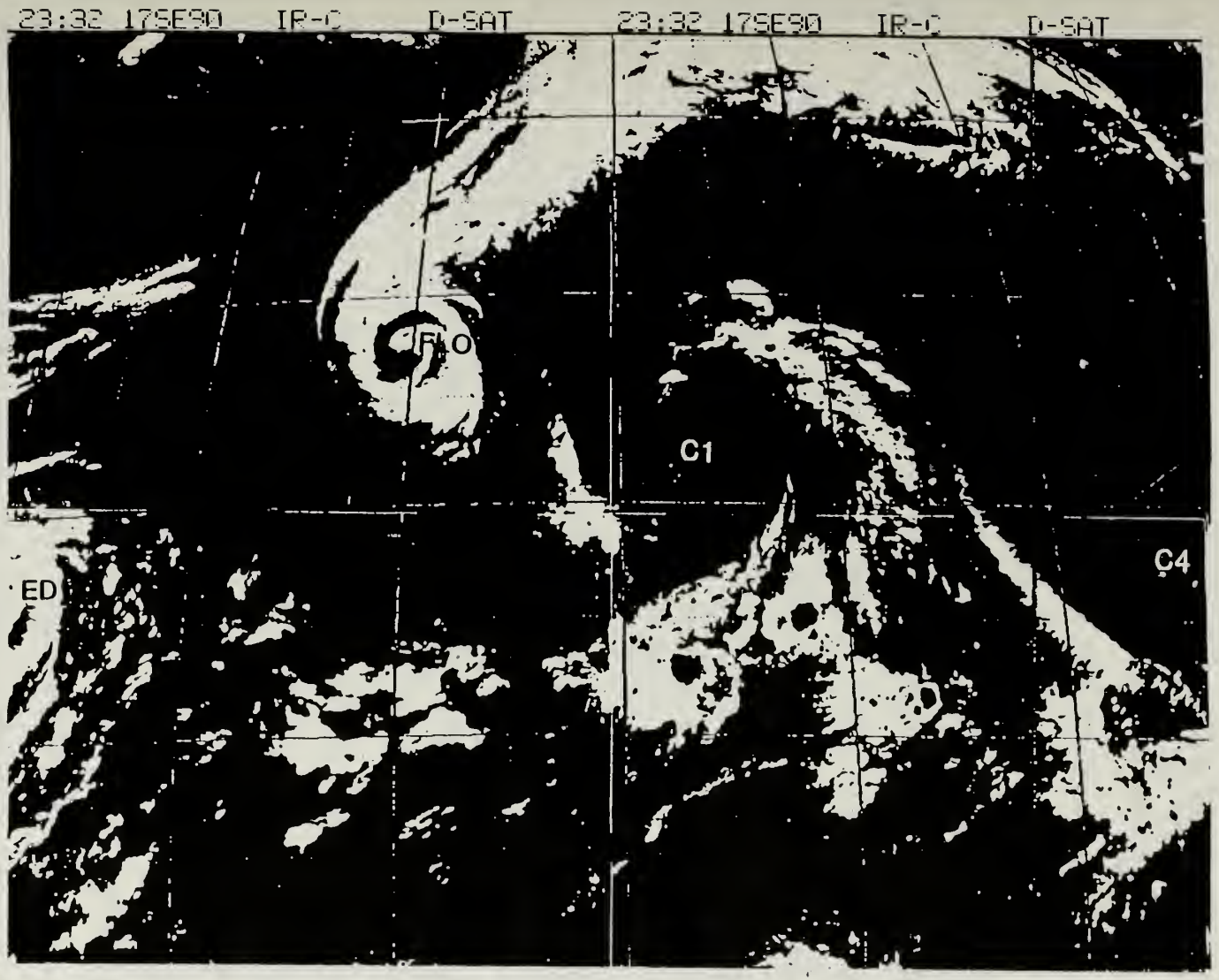

Fig. 43. As in Fig. 13, except for 2332 UTC 17 September.

subtropical jet, and created a strong jet streak connecting the tropical cyclone with the midlatitudes. The cloudiness that appeared along the southern side of the jet was enhanced in the right-rear entrance region of the jet streak and marked the preferred outflow channel for Flo (Fig. 43).

2. Resurgence of the reservoir function

Flo continued to steadily weaken, with maximum sustained winds decreasing to 115 kt by 06 UTC 18 September. The resurgence of the southern outflow channel into TUTT cell C1 marked a significant change in the upper-level circulation pattern (Fig. 44). Two primary factors may have contributed to the resurgence of this mass/heat export mechanism. First, the geopotential heights south of Flo appear to have decreased relative to earlier analyses as the approaching long-wave trough dug southward and as Flo continued to move to the north. With the introduction of these slightly lower heights, the outflowing air parcels did not lose as much kinetic energy in ascending the potential energy "hill" associated with the moderate ridging south of Flo. Once across this ridge, the sloping pressure surface associated with TUTT cell C1 provided the most favorable channel for the equatorward-directed outflow. Second, because of the proximity of C1 to Flo, acceleration of the parcels down the pressure surface did not produce an increase in kinetic energy sufficient to reestablish a flywheel mechanism. Nevertheless, a time series

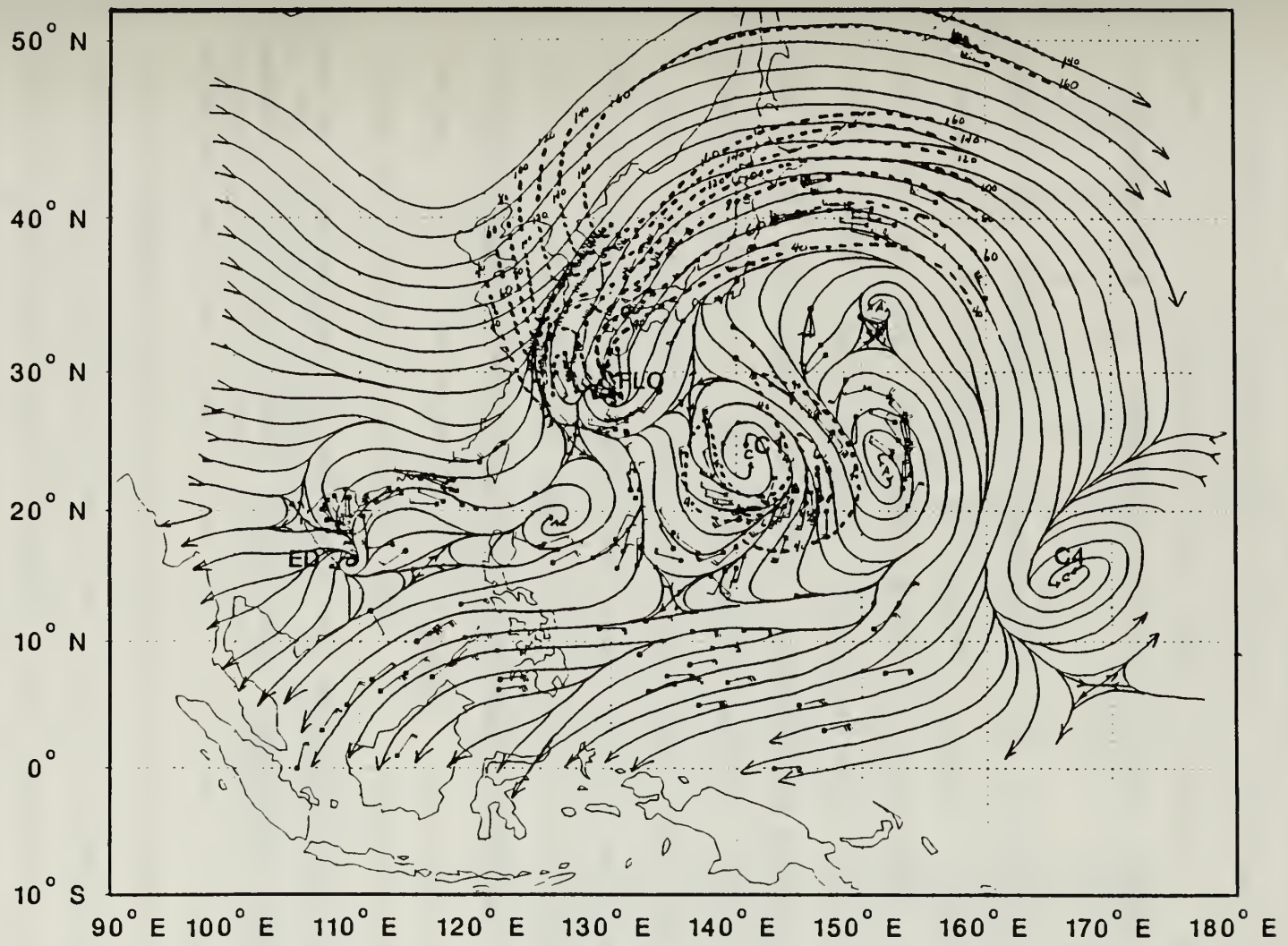

Fig. 44. As in Fig. 9, except for 06 UTC 18 September.

of rawinsonde profiles between 00 UTC 16 September and 12 UTC 18 September as C1 passed south and west of Chi Chi Jima (27.0°N, 142.0°E) suggests that C1 still maintained a significant vertical structure with potential for positive forcing on Flo (Fig. 45). Thus, the resurgence of the southern outflow channel marked the redevelopment of the reservoir function.

Flo's weakening rate decreased to an average of 5 kt per 6 h for the 12 hour period ending at 18 UTC 18 September. While the resurgence of C1's reservoir function may have contributed to the enhanced outflow that slowed Flo's weakening during this period, a much more important factor was the maintenance of the extremely efficient outflow channel towards the north and into the midlatitude westerlies. A slight decrease in bulk vertical shear (Fig. 5a) was also noted during this period. As shown in Fig. 46, both the northern outflow channel and the equatorward outflow associated with C1 appeared to provide efficient export mechanisms. However, the much stronger jet to the north indicates the dominance of this export mechanism. In an environment otherwise favorable for tropical cyclone intensification (Holland 1987) such dual outflow channels would be expected to contribute to a rapid intensification rate. Environmental factors such as increasing vertical wind shear over the storm (Fig. 5a) most likely accounted for much of the steady weakening as Flo continued to track into the

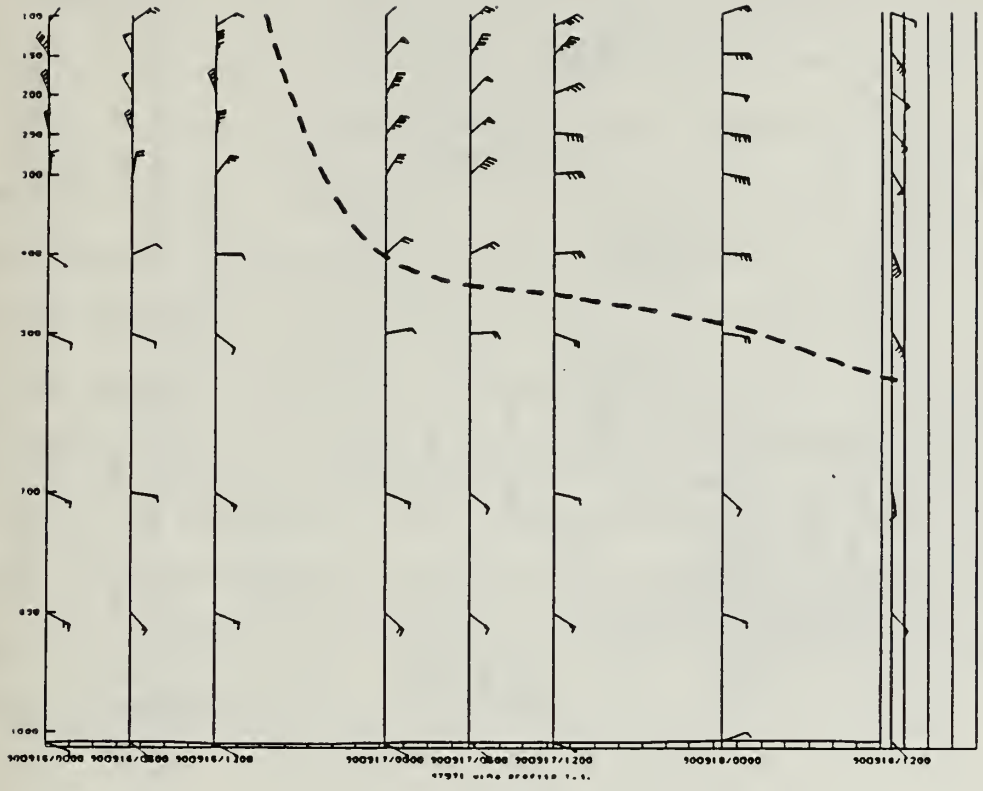

Fig. 45. As in Fig. 8, except for Chi Chi Jima (27.0°N, 142.0°E; WMO station number 47971) from 00 UTC 16 September through 12 UTC 18 September. Cold low C1 passed south and west of the station on an increasingly west to northwesterly track.

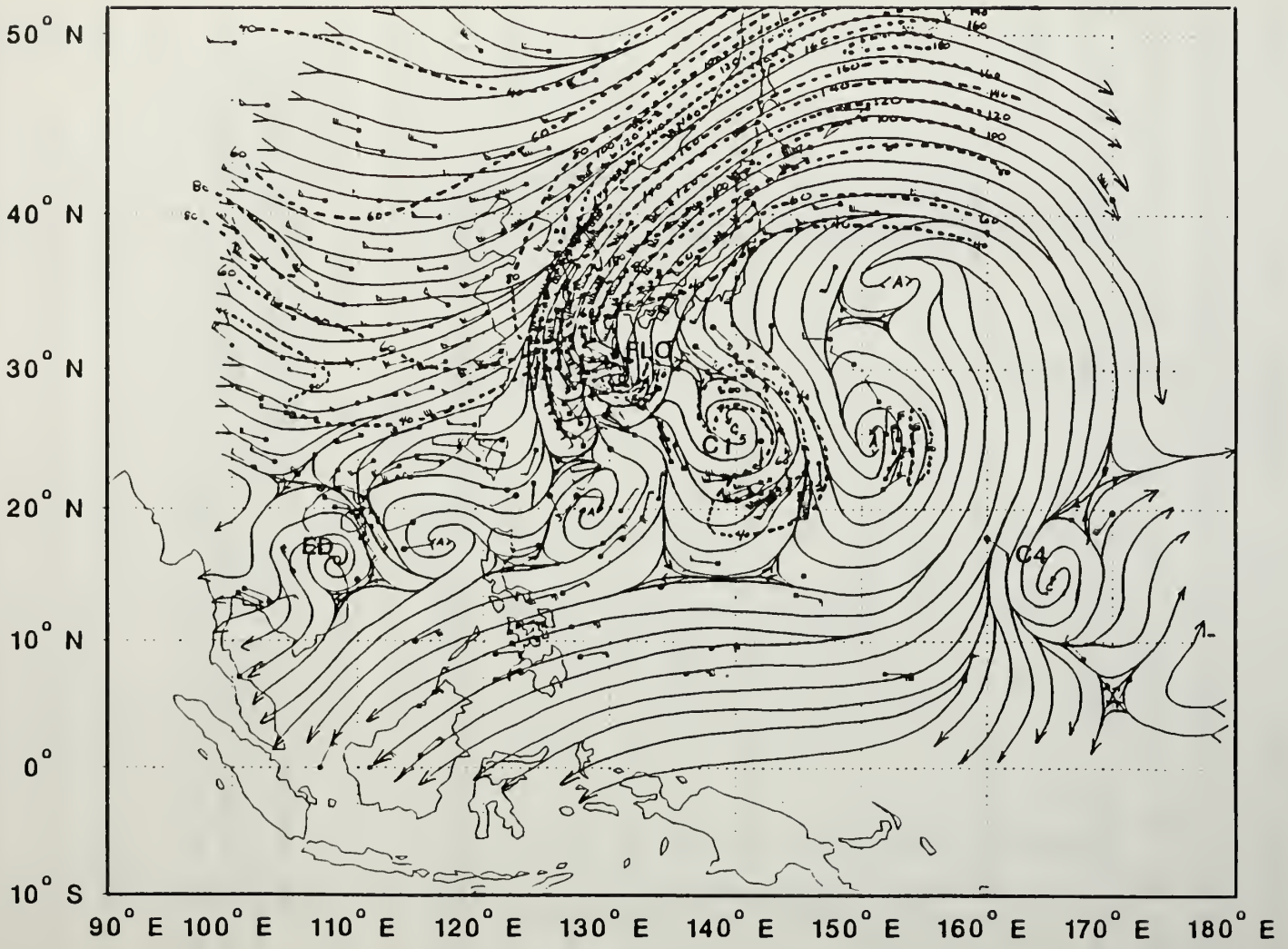

Fig. 46. As in Fig. 9, except for 12 UTC 18 September.

midlatitudes. The existence of two efficient mass/heat export mechanisms may have served only to retard this weakening.

As shown in Fig. 47, only one export mechanism remained after 18 UTC 18 September. The inflow to C1 from the south and east essentially fills this TUTT cell such that its vertical and horizontal extent were significantly reduced (Fig. 48). The loss of this export mechanism, combined with Flo's poleward motion, allowed a portion of the midlatitude westerlies to flow south of Flo. As a result, the southern outflow channel was blocked, while at the same time the vertical shear increased over Flo (Fig. 5a). While it appears that the northern outflow channel remained effective (Fig. 49) and both the mass flux (Fig. 3a) and EFC (Fig. 4a) remained strong, the midlatitude environment surrounding Flo could not support the existing convection, and thus Flo continued to steadily weaken.

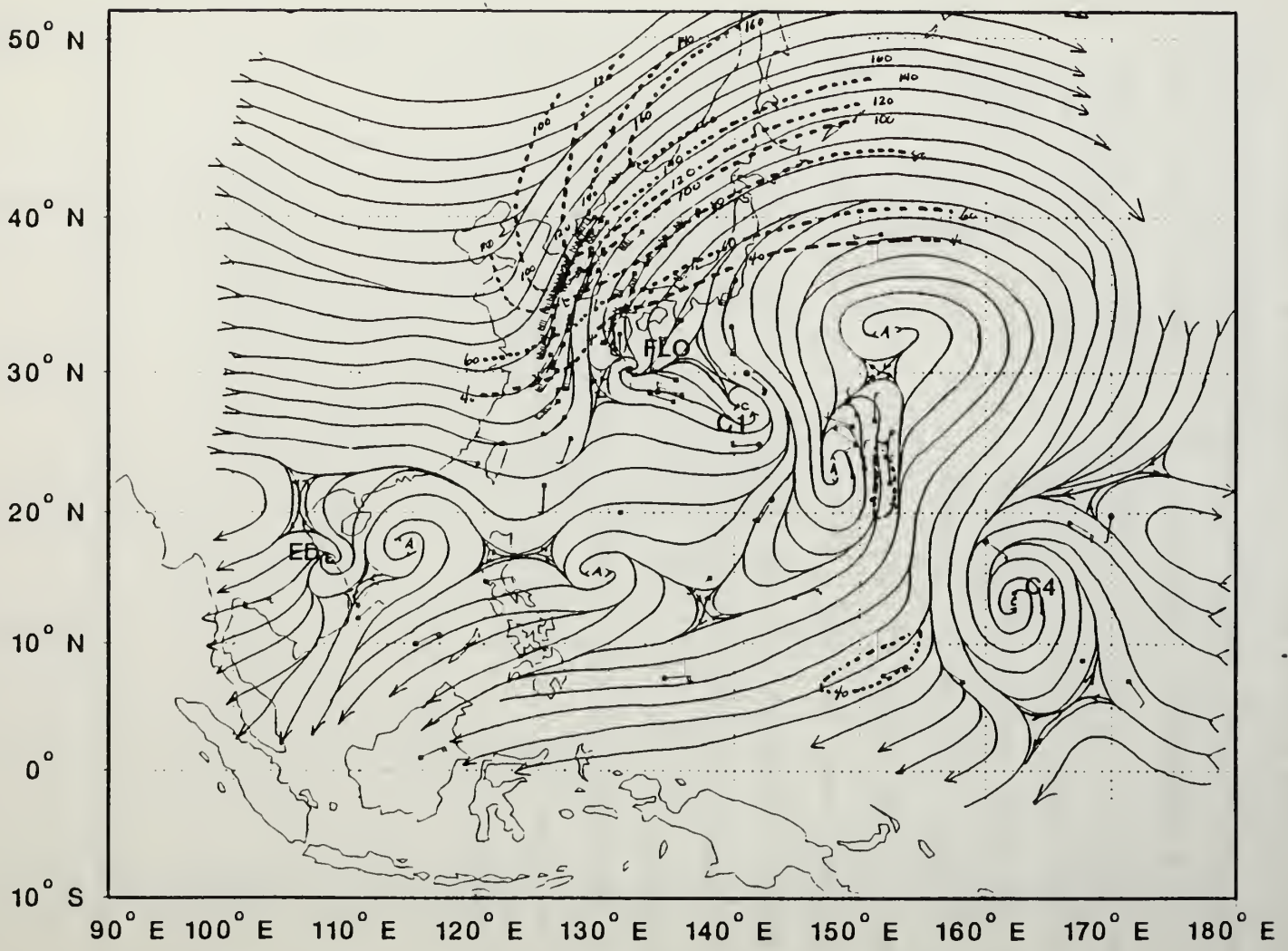

Fig. 47. As in Fig. 9, except for 18 UTC 18 September.

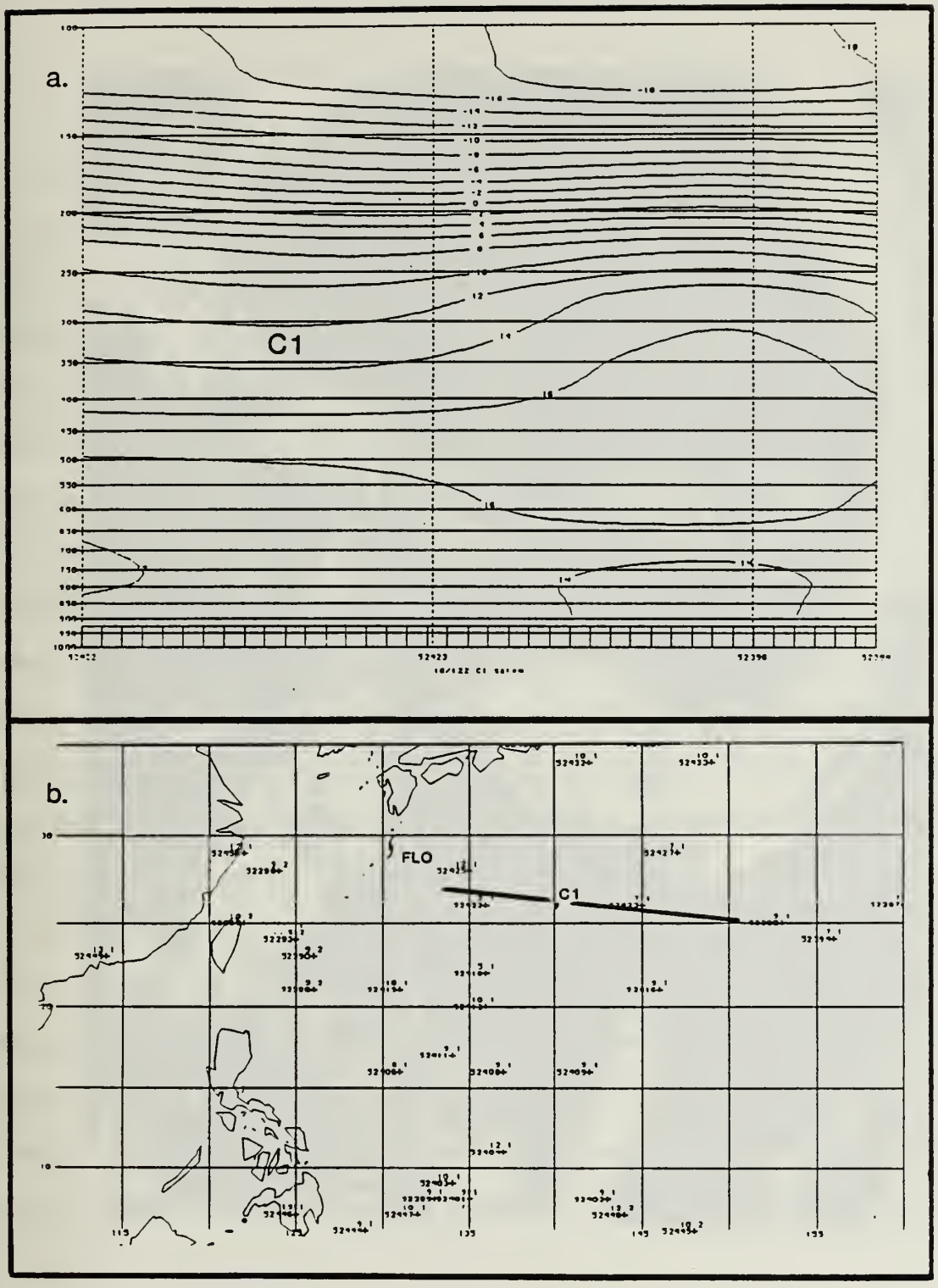

Fig. 48. (a) As in Fig. 7a, except for 12 UTC 18 September. (b) As in Fig. 7b, except for cross-section in (a).

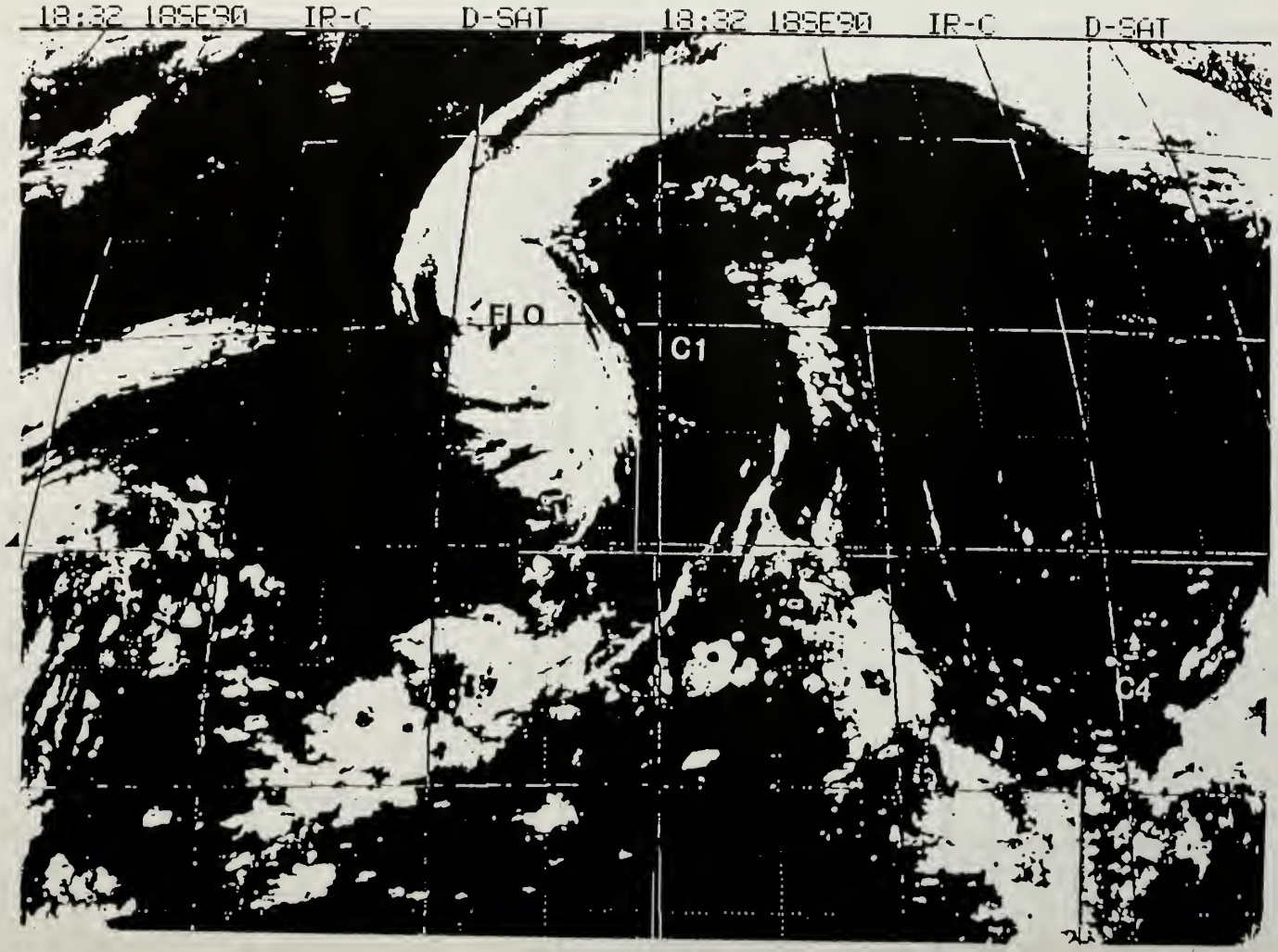

Fig. 49. As in Fig. 13, except for 1832 UTC 18 September.

IV. TYPHOON ED

A. DEVELOPMENT TO TYPHOON

As previously, the hypothesis of this section is that the position of the tropical cyclone relative to the upper-level circulations primarily determines when favorable conditions exist for the development of an interaction mechanism that may produce or sustain increased intensification rates. A similar analysis of typhoon Ed provides an opportunity to compare and contrast the possible contributions of upper-tropospheric forcing to the intensification rate. It will be shown that Ed developed amidst a less favorable upper-tropospheric environment (as compared to Flo), and therefore achieved only slightly more than minimal typhoon strength. Since the track was westward across high sea-surface temperatures and a generally favorable low-level inflow pattern (not shown), the lower-tropospheric conditions appeared to support further development of this storm. The following sections will demonstrate that upper-tropospheric conditions were not particularly favorable for rapid intensification of Ed. The simultaneous, but different mode of, development of Ed and Flo within the same region thus supports the overall hypothesis.

1. Slow evolution period

Whereas Flo intensified at a nearly constant rate of 5 kt per 6 h during the tropical storm to typhoon stage, Ed developed much more slowly (Fig. 50). At 00 UTC 13 September (Fig. 12), none of the three mass/heat export mechanisms described above for the development of Flo were available to Ed. Instead, the flow pattern was dominated by outflow into the upper-level easterlies, which were generally associated with the eastern China extension of the subtropical ridge. Several adjacent circulation features added to the complexity of the flow pattern above Ed (Fig. 12). The anticyclone east of Ed appeared to promote an eastward outflow, and then a type of flywheel acceleration turned this flow towards the south in conjunction with cold low C2. This differs from the flywheel pattern in Flo because the region of enhanced pressure gradient between the anticyclone and C2 was small, and the flow did not continue around C2. The weak nature of this pseudo-flywheel mechanism east of Ed is evident by the lack of deep convection in the diffluent area that typically characterizes the flywheel function (Fig. 19).

The decaying cold-core low (C3) located north of Ed in Fig. 12 was evidently the remains of either a westward extension of the TUTT or resulted from a passage of a long-wave trough through the region. Whichever the origin, this cell might seem to have a potential reservoir function similar to the C2 and Flo relationship (see previous section).

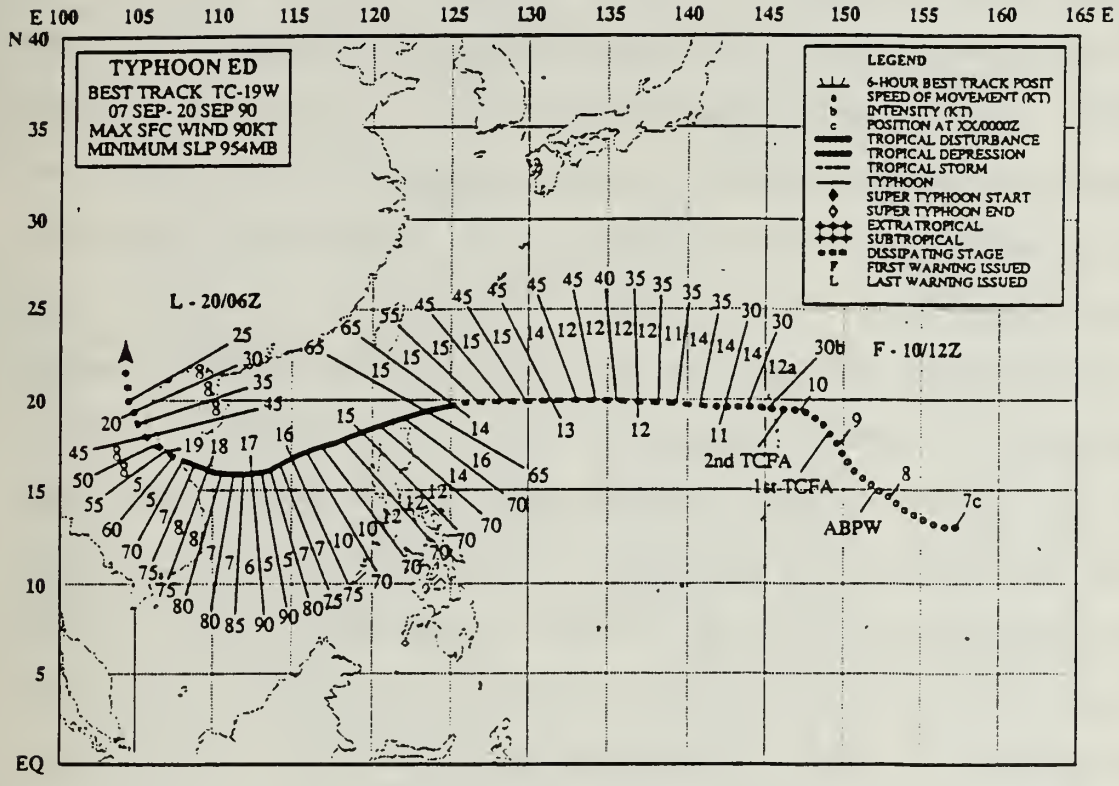

Fig. 50. Best track information for Typhoon Ed from ATCR (1990).

However, the outflow from Ed joined a west-southwestward channel and did not enter the circulation of C3.

Despite the complex circulation pattern, the southwest outflow channel was apparently favored due to the relatively higher geopotential heights surrounding Ed on the northern and eastern periphery (associated with the subtropical ridge and the upper-level anticyclone respectively) and lower heights to the south and west. Cirrus streamers associated with this outflow channel are apparent in Fig. 13, as are several convective clusters along 10°N that appear to be the result of speed divergence in this region at both 150 mb (not shown) and 200 mb (Fig. 12).

Significant changes in the circulation pattern become apparent at 06 UTC 13 September (Fig. 51) and appear to have been the result of the strengthening of the anticyclone east of Ed. Interestingly, this anticyclone closely resembles the anticyclone east of Flo at 12 UTC 14 September (Fig. 17). As is the case with Flo, the ridging associated with the development of the anticyclone dominated the interaction between this circulation feature and Ed.

The first consequence of this ridging is that the outflow of the anticyclone apparently caused an eastward displacement of the northeasterly flow channel that was crossing the subtropical ridge and flowing north of Ed at 00 UTC 13 September (Fig. 12). The associated ridging north and east of Ed at 06 UTC 13 September led to higher geopotential heights

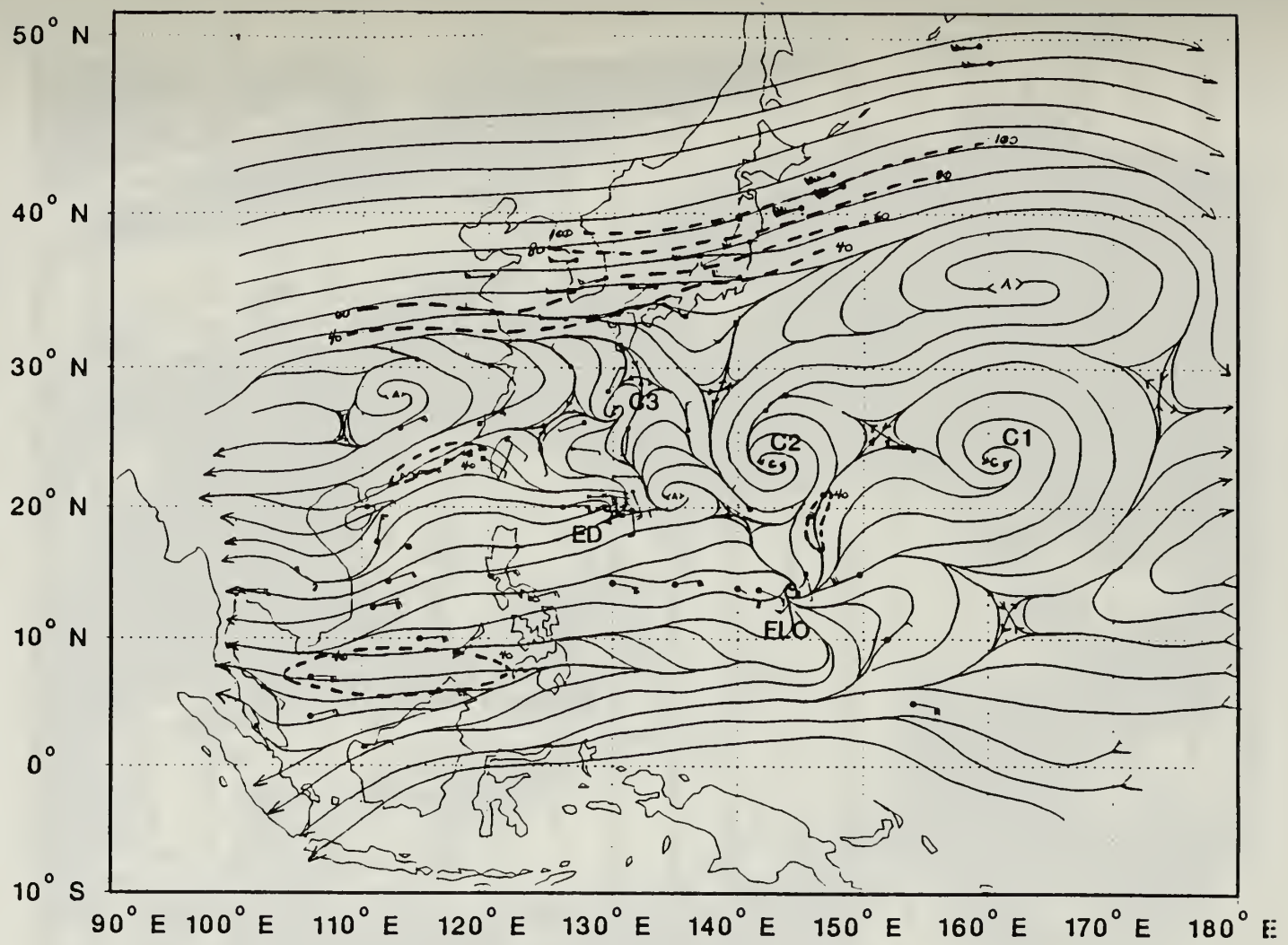

Fig. 51. As in Fig. 9, except for 06 UTC 13 September.

to the west and relatively lower geopotential heights to the east of a newly developed channel into TUTT cell C2 (Fig. 51). As a result of the increased pressure surface slope and the superposition of the outflow from the anticyclone with the flow crossing the subtropical ridge, a type of flywheel acceleration developed on the southwestern periphery of C2. Although the velocities marking this channel were not as large as when the flywheel function was operating between Flo and C1, this was potentially a favorable channel for removing warm air from Ed and moving it toward cold air in C2. Unfortunately, the observations at 200 mb (Fig. 51) and the corresponding 150 and 250 mb observations (not shown) do not support an interaction channel between Ed and TUTT cell C2. Instead, the outflow into this channel at 06 UTC 13 September appears to have originated from the adjacent anticyclone. Nevertheless, the characteristic sharp-edged cirrus cloud pattern marking a relatively strong flywheel-type flow channel is clearly evident on the southwestern periphery of C2 (Fig. 52), and thus there may have been some outflow from Ed that initially flowed northward and then turned anticyclonically into the C2 channel. If such a flow path did exist, it is not reflected in the analyses at other levels due to the paucity of data in this region.

The second consequence of the ridging northeast and east of Ed was an apparent blocking action that inhibited outflow to the east. Outflow from Ed was clearly limited to the

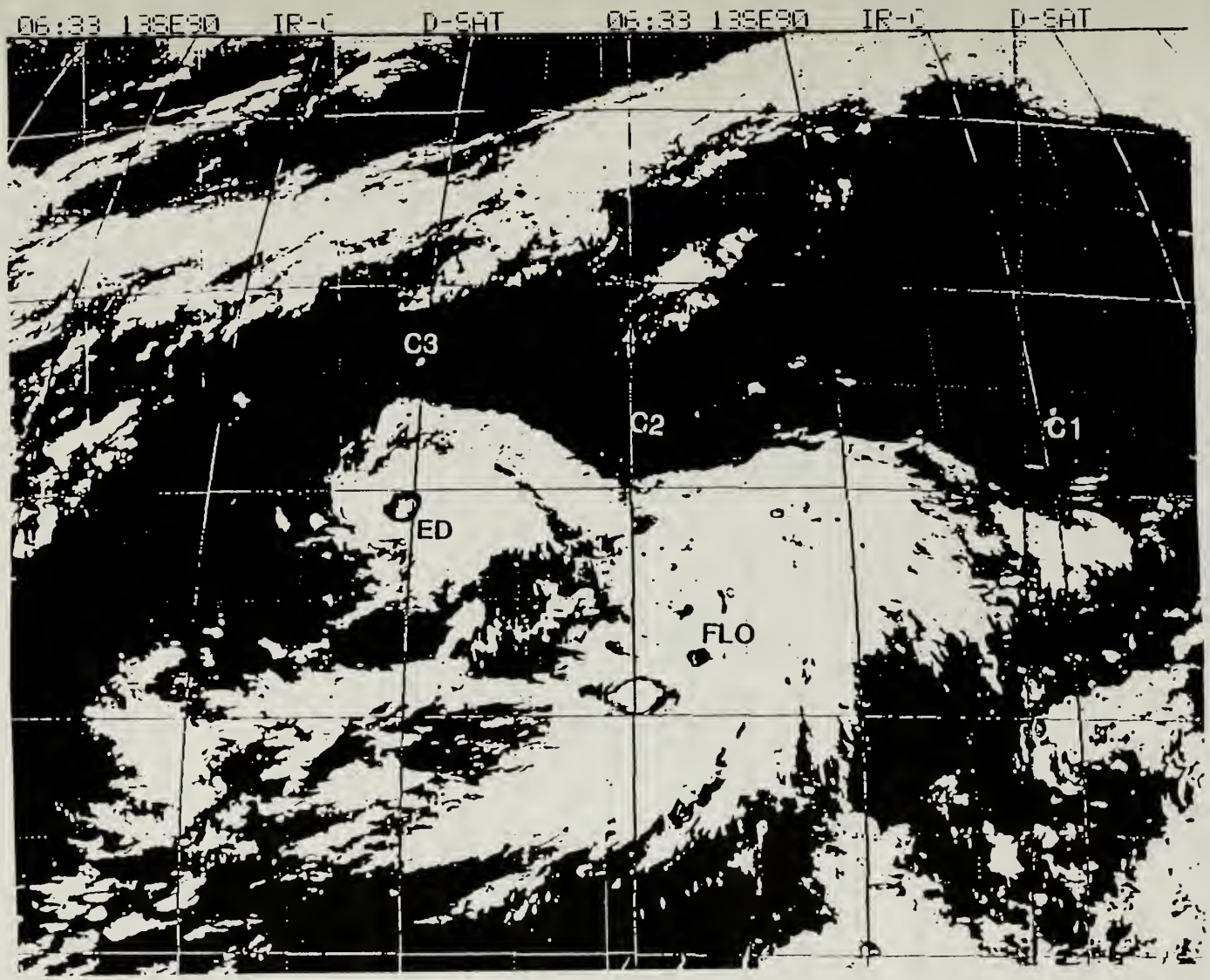

Fig. 52. As in Fig. 13, except for 0633 UTC 13 September.

western and southwestern channels as depicted on both the 150 mb and 250 mb analyses (not shown) and the 200 mb analysis (Fig. 51). As described below, a weak northern channel also developed. This scenario closely matched that at 12 UTC 14 September (Fig. 18) when the blocking mechanism provided by the anticyclone located southeast of Flo appeared to inhibit outflow to the south and east. While such a blocking action would seem to limit the number of outflow channels available (and hence limit the intensification), the associated ridging in this case apparently resulted in the development of a weak, northward flow channel into C3 (Fig. 51). In summary, a short-lived flow channel oriented NW - SE developed between Ed and C2 as a result of the eastward deflection of the flow crossing the subtropical ridge. The extent to which the associated modifications of the northward diffluent flow out of Ed contributed to its intensification is not clear.

Development of a weak outflow channel into C3 was evident by the relatively circular cloud-free region indicative of large-scale subsidence (Fig. 52). This cell now appeared to provide a reservoir-type export mechanism. The interaction between Ed and this cold-core cell was apparently of only a limited nature as no link occurred between these two features below 200 mb. Further evidence of the weak reservoir function is a minimal cold-core signature on the available satellite temperature sounding cross-sections (not shown) through this feature. The relatively large distance between this cell and

Ed suggests that the associated subsidence within the cell was not likely to hamper development. As ascertained from the review of the operational gradient-level analyses, the increase in Ed's intensification rate to 10 kt per 6 h that occurred between 12 - 18 UTC 13 September did not appear to be accounted for solely by significant changes in lower-tropospheric forcing. Thus, it seems likely that the weak reservoir function provided by this cold-core cell may have contributed to the increased intensification rate.

The effect of the northward diffluent flow channel out of Ed, which was comprised of the weak reservoir function of C3 and the short-lived flow channel into C2, apparently resulted in an increase in the mass flux at 200 mb (Fig. 3b) that began around 06 UTC 13 September. The time lag between initiation of these flow channels, the decrease in the mass inflow, and a corresponding increase in Ed's intensification rate was 6 - 12 h (ATCR 1990) and was consistent with the approximate 600 - 800 km distance between the TUTT cells and the tropical cyclone. However, the reservoir export mechanism rapidly weakened as is evident by the loss of the flow channel into C3 at 200 mb by 12 UTC 13 September (Fig. 53). While the loss of this link was apparently replaced by a flow channel between Ed and C3 at 150 mb through 00 UTC 14 September (Fig. 54), this new channel had wind observations of only 10 kt, and thus the export mechanism is considered to have remained very weak. Loss of the channel at 150 mb by 06 UTC 14 September (Fig. 55)

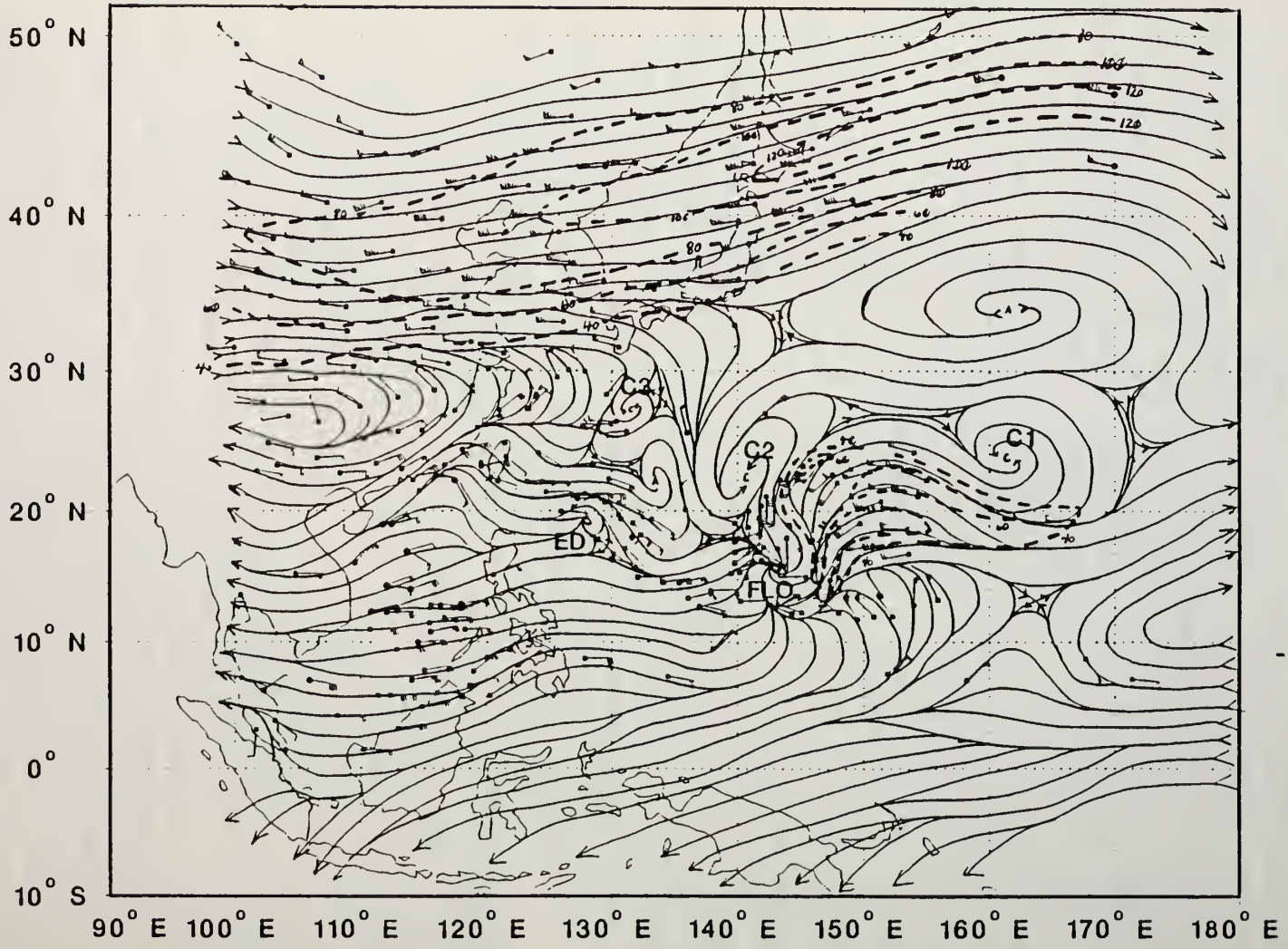

Fig. 53. As in Fig. 9, except for 12 UTC 13 September.

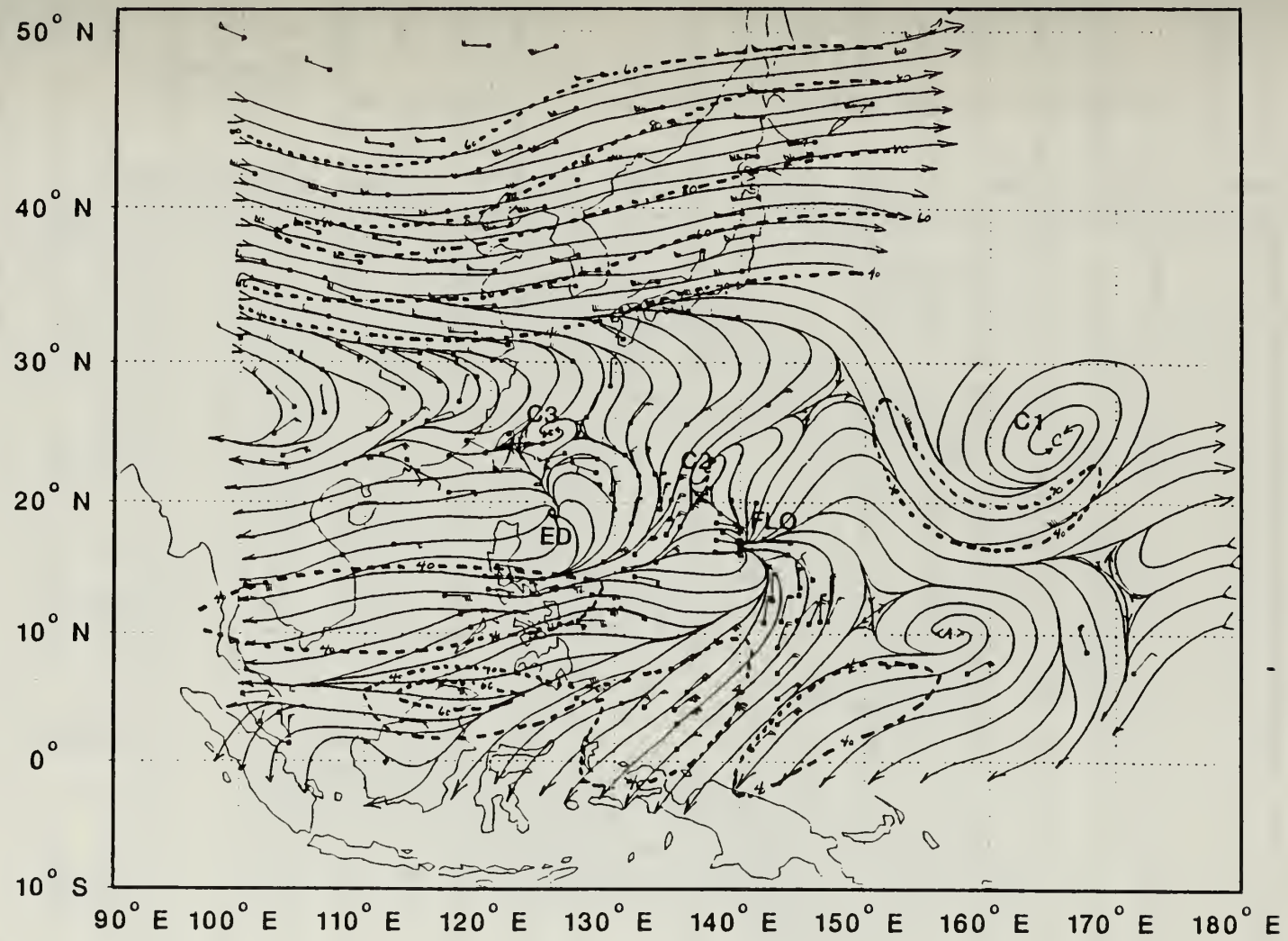

Fig. 54. As in Fig. 9, except for 150 mb at 00 UTC 14 September.

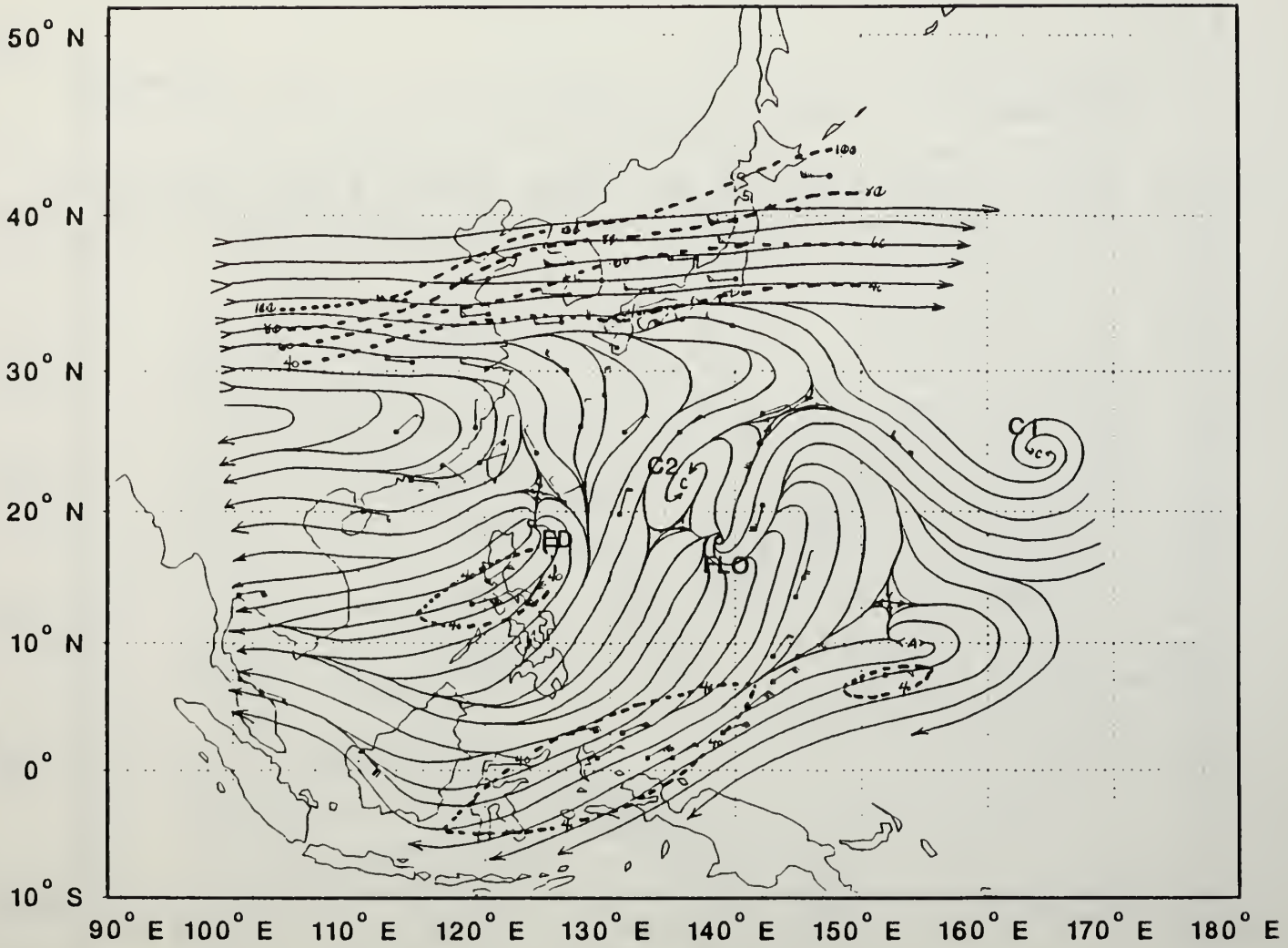

Fig. 55. As in Fig. 9, except for 150 mb at 06 UTC 14 September.

was consistent with the continued decrease in the mass flux that had begun around 18 UTC 13 September (Fig. 3b) and the decreased intensification rate that began at 12 UTC 14 September (Fig. 50).

The development and decay of this export mechanism and the corresponding changes in the intensification rates appear to lend some credence to the assertion that the decaying cold-core cell C3 produced some degree of positive forcing on Ed's intensity. Nevertheless, the forcing provided by this cell appears to have been significantly less than that provided by both TUTT cells C2 and C1 on Flo, and it does not appear to sufficiently account for Ed's rapid intensity increase that occurred between 12 UTC 13 September and 00 UTC 14 September.

2. Intensification period

A more important factor that may have contributed to the increase in Ed's intensity through 00 UTC 14 September was the further development of the flywheel-type mechanism that was comprised of primarily the outflow from the anticyclone adjacent to Ed at 06 UTC 13 September (Fig. 51). Development of this export mechanism does not appear to have continued at 200 mb as is evident by the lack of any northward or eastward-directed outflow at 12 UTC 13 September (Fig. 53). However, this flywheel-type mechanism was apparently effective at 150 mb as the analysis at this level (Fig. 56) clearly depicts northward and eastward outflow into a baroclinic flow channel.

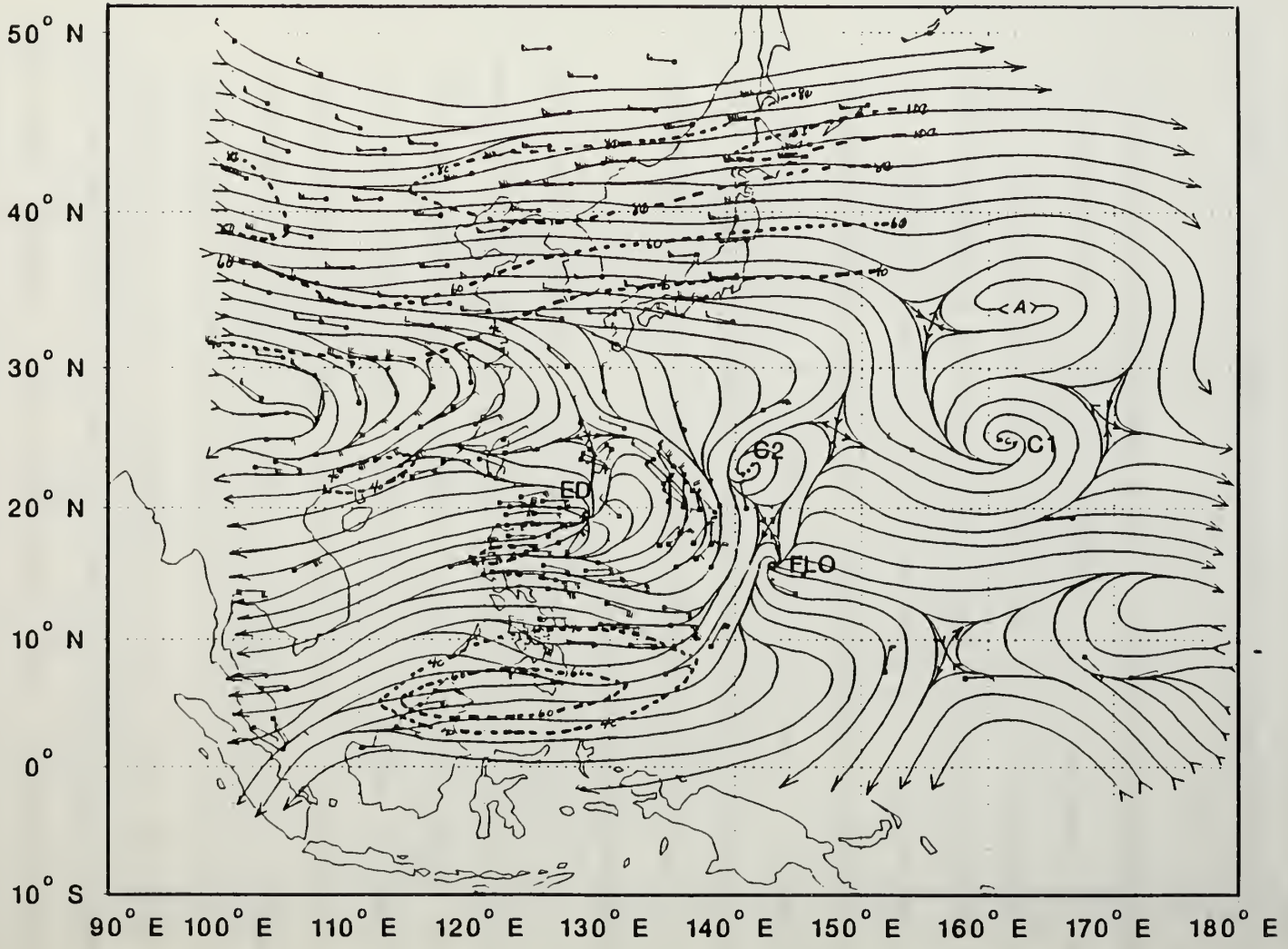

Fig. 56. As in Fig. 9, except for 150 mb at 12 UTC 13 September.

This channel had 15 - 25 kt wind observations flowing across a sloping pressure surface that was created by ridging on the west (the signature of the anticyclone at 150 mb) and cold-core low C2 to the east.

It is likely that as Ed intensified, the corresponding outflow level also increased. In this case, the ridging at 150 mb northeast of Ed helped to create a baroclinic flow channel with flywheel mechanism characteristics. Deep convection located at approximately 18°N, 134°E on the corresponding satellite imagery (Fig. 57) correlates well with the characteristic flywheel function diffluence that is evident at 150 mb (Fig. 56). In addition, the relatively sharp edge of the cirrus streamers that mark the southwestern periphery of C2 on this imagery correlates well with the flywheel-type flow channel depicted on the 200 mb analysis (Fig. 53). Unfortunately, the adjacent anticyclone continued to provide the outflow into this channel at levels below 150 mb, and thus the interaction channel between Ed and C2 was relatively shallow. Nevertheless, it is hypothesized that the existence of this channel at 150 mb through 00 UTC 14 September (Fig. 54; when Ed reached typhoon strength) contributed to the increased mass flux that occurred through 18 UTC 13 September (Fig. 3b). Thus, the short-lived flywheel function apparently played a significant role in the observed increase in the intensification rate.

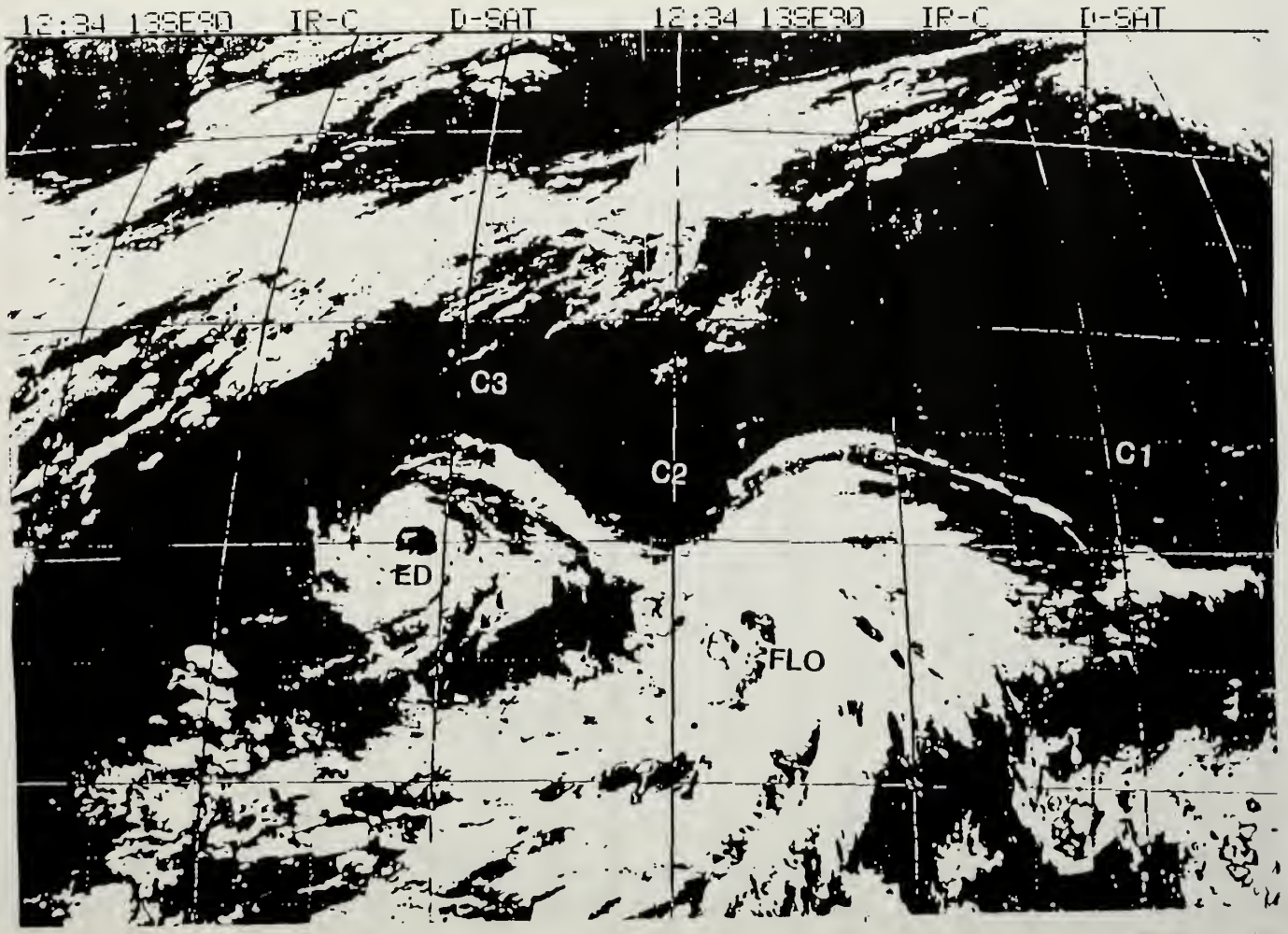

Fig. 57. As in Fig. 13, except for 1234 UTC 13 September.

This discussion relies heavily upon the assumption of accurate intensity estimates as provided by JTWC (ATCR 1990). The effects described above support a nominal increase in intensity for the period 12 UTC 13 September through 00 UTC 14 September as long as the general trend of the intensity estimates is correct.

The upper-level anticyclone at 200 mb northeast of Ed at 12 UTC 13 September decayed significantly by 18 UTC 13 September (not shown). Ridging associated with this anticyclone remained in place at 150 mb through 00 UTC 14 September (Fig. 54). However, the decreasing wind speeds (from 15 - 25 kt to 5 - 15 kt) that mark the flywheel-type flow channel at this level suggest that the slope of the pressure surface was decreasing as the anticyclone decayed. It is apparent that both the weakening of C2 and the elimination of the anticyclone by 06 UTC 14 September decoupled the eastward outflow of Ed at 150 mb into the adjacent cold pool (Fig. 55). The flywheel-type function was short-lived due to these changes. As shown in Fig. 14, the outflow was limited to the west and southwest by 00 UTC 14 September. The resulting decrease in the mass flux at 200 mb (Fig. 3b) was consistent with the loss of the northeastward flow channel at 150 mb (Fig. 55) and correlates well with the decrease in the intensification rate that occurred between 00 - 12 UTC 14 September (Fig. 50).

3. Mature stage

The separation of Ed from the decaying cold-core low C3 and the complete decay of the adjacent anticyclone allowed a strong north-south channel to develop between Ed and TUTT cell C2 (Fig. 14). The equatorward flow associated with this channel originated from the higher geopotential heights in the subtropical ridge, and slowly accelerated down a sloping pressure surface to generally lower geopotential heights to the south. Evidence of the strength of this channel is provided by a number of 30-40 kt wind observations surrounding Ed at 200 mb (Fig. 14). Although these observations suggest that significant vertical shear may have existed upstream of Ed, the westward outflow downstream of Ed was also enhanced. Such vertical shear, if over the central convective region of the storm, might have produced an absolute reduction in Ed's intensity. However, any negative tendency associated with vertical wind shear appears to have been counterbalanced by the favorable influence of increased outflow. The absence of any significant changes in the bulk vertical shear during the period 00 UTC 12 September to 12 UTC 15 September is consistent with this hypothesis (Fig. 5b).

The approximately constant intensity of Ed from 00 UTC 14 September through 18 UTC 15 September (Fig. 50) suggests that the strong north-south channel produced a more subtle effect on Ed's development. First, a distinct outflow pattern became evident at 150 mb (Fig. 54). This indicates a deep outflow

layer and continued vertical development of the tropical cyclone, and thus the equatorward flow channel apparently did not ventilate Ed's central convective region. Evidently, ventilation of the central convective region did not occur because the vertical structure of the tropical cyclone diverted the flow associated with the north-south channel around the storm. Convective activity was suppressed outside approximately 3 deg. lat. (Fig. 15). Thus, the relatively compact central convective region of Ed contrasts with the large and intense bands associated with Flo.

An additional consequence of the strong north-south flow channel is that it shielded the circulation of Ed from adjacent synoptic systems. Such synoptic systems are associated with interaction mechanisms that were hypothesized in the previous section to play an important role in producing increased intensification rates for Flo. Ed's position relative to TUTT cells C2 and C1 or to the subtropical ridge is therefore of secondary importance in comparison to its position within a strong equatorward upper-level flow channel.

Ed's proximity to the island of Luzon from 06 UTC 14 September through 06 UTC 15 September suggests the possibility that some disruption of low-level inflow may have contributed to the approximately constant intensity of Ed during this period. However, a review of the operational gradient-level analyses did not reveal any significant changes in the low-

level circulation pattern that may have slowed the intensification rate.

Another interesting development was a flow channel between Ed and an indraft anticyclone over eastern China that first became apparent at 250 mb on 06 UTC 14 September (not shown). This flow channel became distinct at 200 mb by 18 UTC 14 September (Fig. 58). The subsidence associated with the indraft anticyclone is marked by a relatively cloud-free region northwest of Ed at 22°N, 125°E (Fig. 59). As in the case of the interaction between Flo and the adjacent indraft anticyclone at 18 UTC 17 September (Fig. 40), the interaction between Ed and the indraft anticyclone did not appear to provide support for an increase in intensity. Although the indraft anticyclone would provide a basic mass reservoir function (i.e., a mass sink), outflow from a tropical cyclone would not be enhanced because the associated ridging results in a pressure surface slope unfavorable for increased outflow.

Development of the indraft anticyclone over eastern China appears to have been aided by a change in the orientation of the subtropical ridge. Comparison of Figs. 53 and 58 suggests that the subtropical ridge became more elongated with a reduced latitudinal extent through the period 12 UTC 13 September to 18 UTC 14 September. Both the northwestward track of Flo and the rotation of TUTT cell C2 around Flo to a position more directly between Ed and Flo played a role in modifying the orientation of the subtropical ridge. A distinct

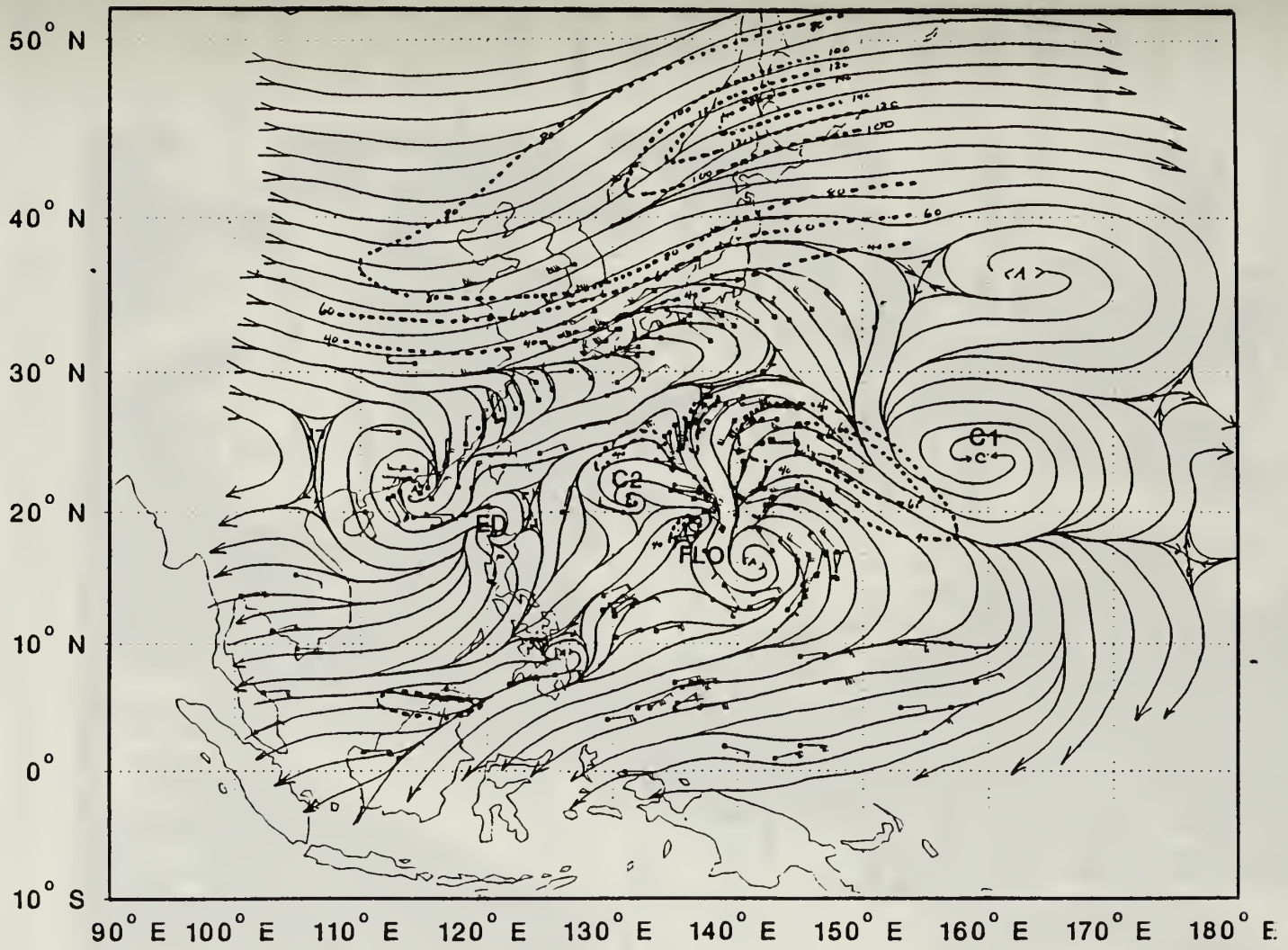

Fig. 58. As in Fig. 9, except for 18 UTC 14 September.

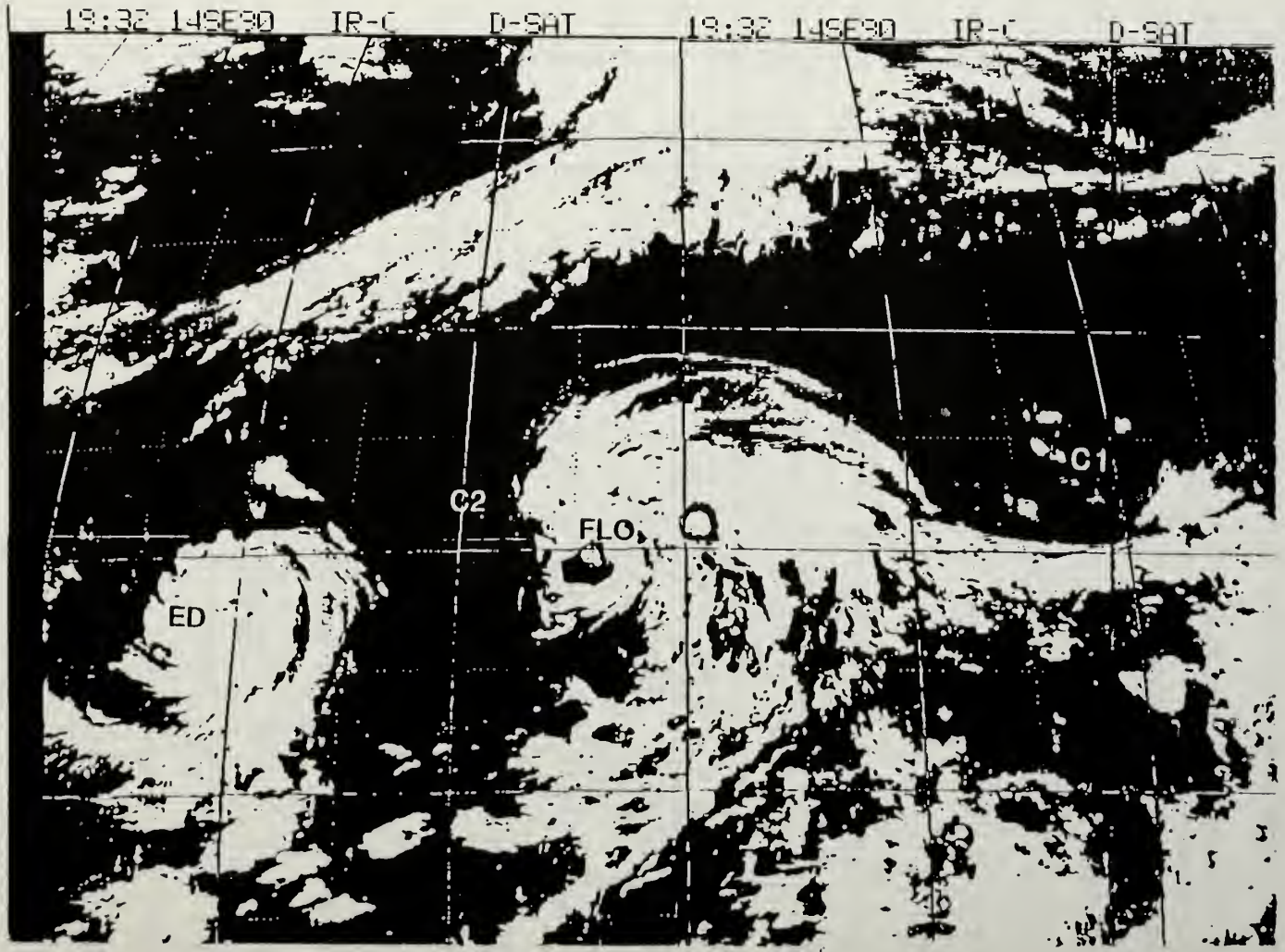

Fig. 59. As in Fig. 13, except for 1932 UTC 14 September.

split developed with a north-south channel between Ed and Flo (Fig. 58) and a more easterly component to the north of Ed, which also flowed into the indraft anticyclone. The north-south channel was especially well-defined at 150 mb (not shown) with several 20-30 kt wind observations.

In summary, the primary upper-level forcing on Ed's outflow regime during the period 06 UTC 14 September to 00 UTC 15 September was provided by the upper-level northeasterlies. Despite a generally decreasing trend in the mass flux during this period (Fig. 3b), Ed reached and then maintained typhoon intensity of 70 kt. Low values of the bulk vertical shear (Fig. 5b) and generally increasing values of EFC (Fig. 4b) were favorable for increased intensification, but the lack of a dual outflow pattern in the form of one or more of the interaction mechanisms described for Flo apparently prevented rapid intensification. The flow pattern of upper-level northeasterlies became progressively disrupted as Flo moved toward the subtropical ridge. A pattern of two flow channels around Ed was accompanied with convective activity in the spiral bands emanating southward and anticyclonically from Ed's center (Fig. 59).

B. INTENSIFICATION TO MAXIMUM STRENGTH

As the northern outflow jets of Flo penetrated through the break in the subtropical ridge, the subtropical ridge now extended only to the east China coast. As shown in Fig. 23,

retreat of this ridge was accompanied by significant weakening of the indraft anticyclone northwest of Ed. As evident by a comparison of Figs. 58 and 23, the decay of this circulation feature resulted in the redevelopment of an unimpeded flow channel from northeast to southwest on the northwestern periphery of Ed. Some of the mass comprising this flow channel appeared to originate from the northern and western outflow jets of Flo that did not converge into C2. Redevelopment of this channel therefore would suggest continued suppression of convective activity in this region due to both the increased vertical shear (Fig. 5b) and the subsidence associated with upper-level convergence.

An additional change in the upper-level flow pattern that first became evident at 12 UTC 15 September (Fig. 23) may have contributed to the increase in intensity that occurred between 18 UTC 15 September - 18 UTC 16 September (Fig. 50). Comparison of Figs. 58 and 23 reveals that C2 had moved westward relative to Ed and that the width of the flow channel separating Ed from C2 had decreased. Although the center position of C2 is poorly defined by the observations at 200 mb (Fig. 23), it is well-defined at 150 mb (not shown), which was apparently closer to the primary outflow level as determined by the number of cloud-track wind observations.

The juxtaposition of cold cell C2 near Ed led to the development of an interaction channel between these two features at 150, 200, and 250 mb on 18 UTC 15 September. The

resulting complex flow pattern in the region between Ed and Flo is best depicted on the 250 mb analysis (Fig. 60). Cold cell C2 appeared to be receiving outflow from both cyclones and thus provided a reservoir export mechanism. As shown in Fig. 26 (note the 2 h time difference), the characteristic cloud-free region resulted from the subsidence associated with the TUTT cell. Perhaps the most important aspect of the Ed and TUTT cell C2 juxtaposition was increased outflow toward the east (Fig. 60), which is consistent with the increased intensification rate during the following 12 to 18 h (Fig. 50).

Development of this eastward interaction channel with C2, although both weak and short-lived, is hypothesized to have been a key component of the upper-tropospheric forcing on Ed's intensification rate. Heretofore, Ed's position within an upper-level background of equatorward flow had limited the outflow jets to a single, generally southward-directed, outflow channel. As described by Holland (1987) and Guard (1980), a tropical cyclone outflow pattern that includes only one outflow channel will likely provide the upper-tropospheric forcing necessary to produce and sustain a typhoon of only minimal intensity. Existence of dual outflow channels, as was the case with Flo, increases the likelihood that the tropical cyclone will develop to supertyphoon intensity (Sadler 1978; Guard 1980). The development of a second mass/heat export channel in Ed's outflow pattern at 18 UTC 15 September was

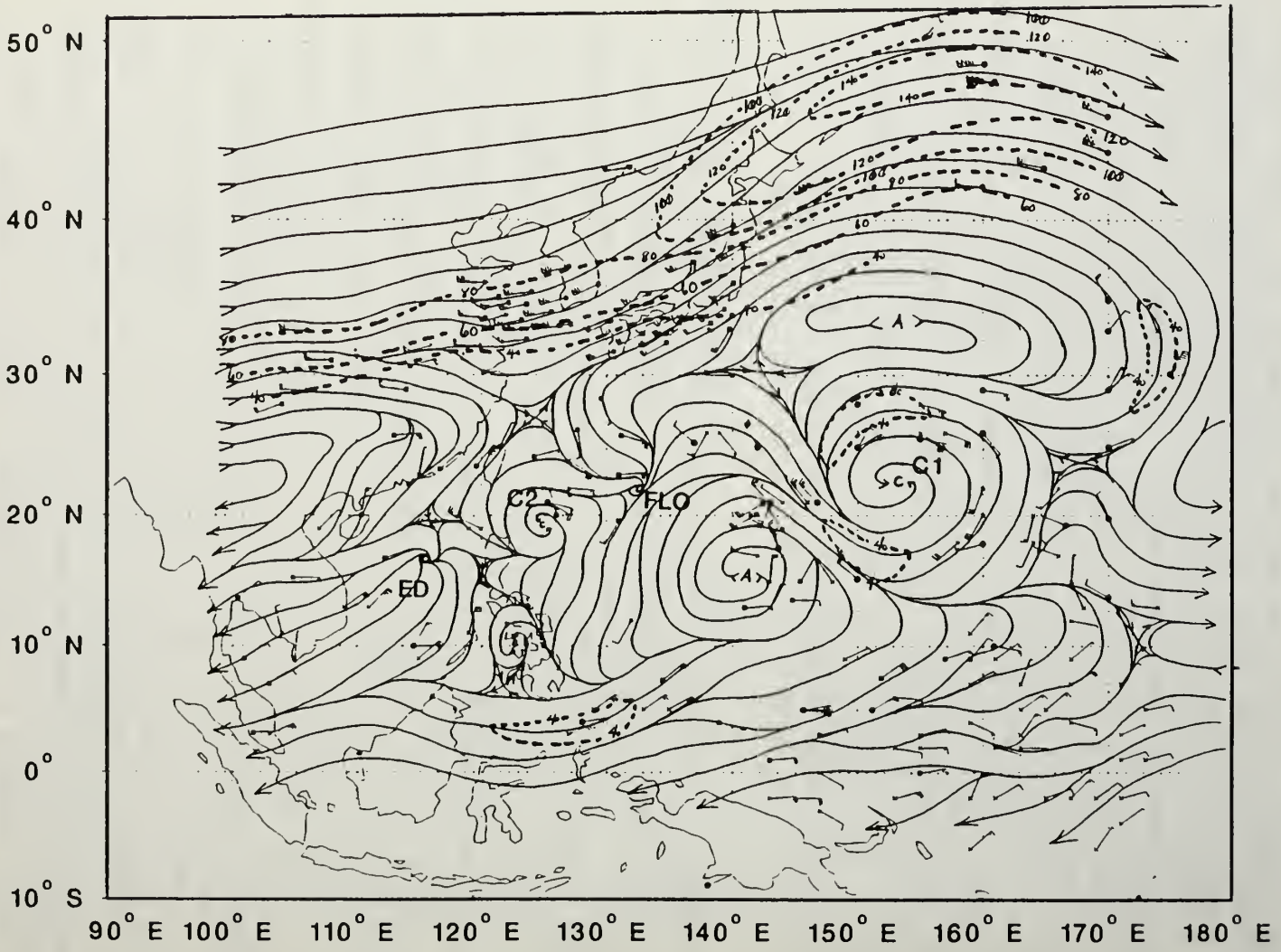

Fig. 60. As in Fig. 9, except for 250 mb at 18 UTC 15 September.

therefore of particular significance because it marked the first time that the upper troposphere appeared to support intensification beyond the minimal typhoon intensity of 70 kt.

Two primary factors combined to limit the effectiveness of this eastward interaction channel. First, Ed's position relative to the northerly flow associated with the eastern China anticyclone appeared to prevent development of a strong northward or northeastward-directed outflow jet. Moreover, the higher geopotential heights associated with this anticyclone acted as a potential energy barrier that was of sufficient magnitude to prevent development of a vacuum mechanism through interaction with the subtropical jet. Second, the relatively shallow C2 (not shown) did not provide a pressure surface slope of sufficient magnitude and extent that could greatly enhance the mass/heat export needed to produce the observed increase in Ed's intensity. Furthermore, significant inflow to C2 from the western outflow jets of Flo would suggest that this TUTT cell had only limited potential for producing a large change in Ed's intensity. In summary, both the position of C2 relative to Ed and the apparent weakness of this cold-core cell appeared to limit the effectiveness of the newly developed mass/heat export mechanism. Although the decrease in the outflow (Fig. 3b) does appear to have leveled-off in conjunction with the development of this reservoir mechanism, the lack of a large increase in the mass flux was consistent

with the hypothesis that this export mechanism provided only minimal upper-level support for intensification.

During the 12 h preceding maximum intensity, Ed's outflow pattern appeared to have a single outflow channel toward the southwest (Fig. 31). Northerly flow was found just to the east of Ed. However, these winds were only 5 - 10 kt at 12 UTC 16 September. Although weaker flow to northeast of Ed may have been more conducive to convective activity as a result of relatively low values of vertical shear (Fig. 5b) and upper-level diffluence, the second outflow channel to the east in conjunction with C2 had been removed. It is difficult to determine from the available imagery (Fig. 33) whether convective activity, especially in the cloud band that extends east and southeast of Ed, had been increased. An increased northern outflow jet is shown on the 200 mb analysis (Fig. 31) compared to the outflow jets at 12 UTC 15 September (Fig. 23). However, the loss of the direct outflow into C2 would seem to have been more detrimental. As shown in Fig. 3b, the outflow continued to slowly increase despite the loss of the C2 reservoir function, and thus the southern outflow channel and the increased northern outflow jet were apparently sufficient to support continued intensification.

Ed reached maximum intensity of 90 kt at 18 UTC 16 September (Fig. 50). Although upper-level effects likely played a large role in the increase in Ed's intensification rate, further study may identify other physical mechanisms,

perhaps at lower levels, that contributed to the intensification process.

C. INITIAL WEAKENING

As analyzed in the ATCR (1990), Ed began to weaken after 00 UTC 17 September (Fig. 50). Available observations and analyses do not reveal any changes in the upper-level forcing that support this decrease. It is hypothesized, therefore, that other environmental interactions associated with landfall may have induced this intensity decrease.

1. Approach of landfall

As described by Holland (1987), tropical cyclones begin to weaken as they approach steep mountainous terrain along a coast. Ed attained maximum intensity at a distance of approximately 300 n mi. seaward of the mountainous coast of eastern Vietnam. According to the intensity estimates provided by JTWC (ATCR 1990), Ed weakened at a rate of less than 5 kt per 6 h for the period 18 UTC 16 September through 06 UTC 18 September. The slow weakening in Ed was notably less than that in Holland (1987) because Ed moved parallel to the mountains and thus maintained a moisture source on one side.

2. Resurgence of a dual outflow channel pattern

Changes in the upper-level circulation pattern around 06 UTC 17 September may have also contributed to a slower weakening rate than might normally have been expected. In particular, an outflow channel between Ed and TUTT cell C2 was

reestablished (Fig. 34). Inflow to C2 was analyzed at 150, 200, and 250 mb, and the distinctly cloud-free region (Fig. 35) was consistent with subsidence and a weak reservoir function for C2 during this period. A significant cold-core signature associated with C2 is not detected on the available satellite temperature cross-sections (not shown). Nevertheless, the resulting dual outflow pattern may have improved evacuation of mass from Ed and thus may have counteracted the tendency to weaken as Ed approached landfall. The continued slow increase in the mass flux at 200 mb during this period was consistent with this hypothesis (Fig. 3b).

Another significant development at 12 UTC 17 September was the opening of a channel for the northern outflow jets of Ed into the midlatitudes as a result of the deepening of the long-wave trough situated roughly along 120°E (Fig. 37). As was the case with Flo, the geopotential heights were lowered north of Ed. The air parcels associated with the northern outflow jets could now break through the subtropical ridge and accelerate down the sloping pressure surface on the northern side of a narrow subtropical ridge. This situation was somewhat analogous to the development of a vacuum export mechanism (Fig. 25) in Flo. A greatly increased number of reprocessed cloud-track wind observations were now found around the northern periphery of Ed's outflow regime (Fig. 37). The newly developed flow channel across the break in the subtropical ridge contributed to an upper-tropospheric

circulation pattern that resulted in a continued increase in mass flux at 200 mb (Fig. 3b) that was favorable for increased mass evacuation from the central convective region of Ed. Unfortunately, the corresponding satellite imagery is poorly oriented relative to Ed, and thus only the southeastern outflow channel is apparent (Fig. 38).

By 18 UTC 17 September, all traces of TUTT cell C2 had disappeared, and Ed was less than 100 n miles off the coast of Vietnam (Fig. 40). Steady weakening consistent with the studies described above would normally be expected as the distance between Ed and the coast continued to decrease. However, the flow channel across the subtropical ridge is hypothesized to have maintained an environment favorable for mass/heat evacuation, and hence Ed's intensity remained at a relatively strong 80 kt (Fig. 50). While this interaction channel remained open through 00 UTC 19 September (not shown), it is likely that orographic effects dominated the forcing on Ed's intensification rate after 06 UTC 18 September, when Ed approached within 60 n mi. of the Vietnamese coast. The upper-troposphere appeared to have played little role in determining Ed's intensity once orographic effects became dominant.

V. SUMMARY AND CONCLUSIONS

A. GOALS AND METHOD

A case study of the upper-tropospheric forcing on the intensification rates of tropical cyclones Flo and Ed during TCM-90 has been accomplished. As a preliminary step, a review was made of the operational gradient-level and upper-level (200 mb) streamline analyses that were produced during IOP's 5, 6, and 7 of TCM-90 (00 UTC 13 September - 00 UTC 19 September 1990). These analyses were produced every 12 h using mostly routine observations combined with the available real-time TCM-90 observations. The charts were reviewed to determine whether the additional real-time data during TCM-90 were sufficient to describe the upper-level interactions that induced observed intensity changes in the tropical cyclones. Of specific interest was the role that upper-level cold lows, or TUTT cells, played in producing changes in the intensification rates. This review of the operational charts indicated that the spatial and temporal resolution afforded by the routine, real-time observations within the tropics is insufficient to fully describe upper-level forcing. Correlation between changes in the upper-level circulation pattern and corresponding changes in the intensities of Flo and Ed was difficult and inconclusive. This provided the

motivation for a more detailed analysis using the substantial number of non-real-time (delayed) TCM-90 observations, which includes reprocessed satellite cloud-drift winds, NASA DC8 observations, radar wind profiler data, satellite temperature soundings, and a few delayed upper-air soundings.

The hypothesis of the study is that the post-processed TCM-90 data set provides sufficient spatial and temporal resolution to depict upper-tropospheric forcing on tropical cyclones Flo and Ed, and that such forcing can be related to changes in the intensification rates of these storms. The goal of the study was to use this best-ever tropical region data set to: (i) identify specific interactions between the upper-level environment and the tropical cyclones; and (ii) subjectively correlate changes in these interactions with observed changes in the intensities of Flo and Ed.

The approach has been primarily a descriptive case study of the upper-level influences. Factors such as SST gradients and changes in the low-level circulation pattern that might have influenced the intensities of the tropical cyclones were checked, but were not thoroughly examined. In general, the significant changes in the intensification rates that occurred during the lifetimes of these two storms (Figs. 61 and 62) did not appear to have been supported by corresponding changes in these other factors. However, changes in intensification rate (relative to a steady intensification expected for an undisturbed environment; e.g., one Dvorak T number per day)

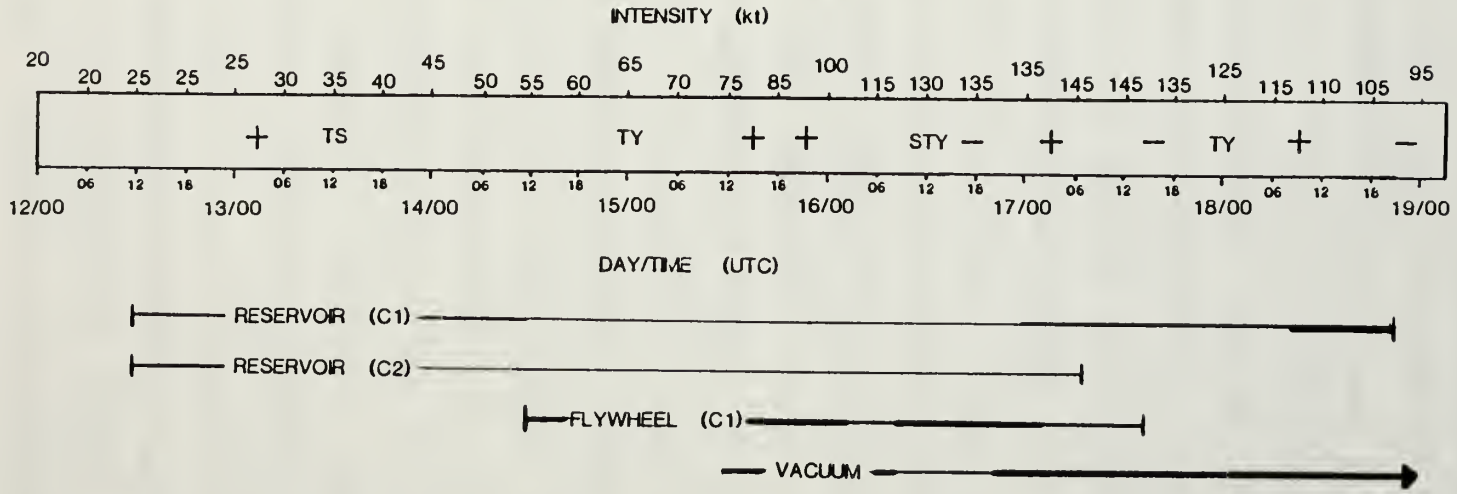

Fig. 61. Timeline of the intensification of Supertyphoon Flo. "+" ("-") within the timeline indicates times when the intensification rate increased (decreased), and "TS", "TY", "STY" indicate the times at which Flo attained tropical storm, typhoon, and supertyphoon intensity respectively. Lines below the timeline depict when each of the three interaction mechanisms was operating, with the thickness indicating the relative strength of the mechanism.

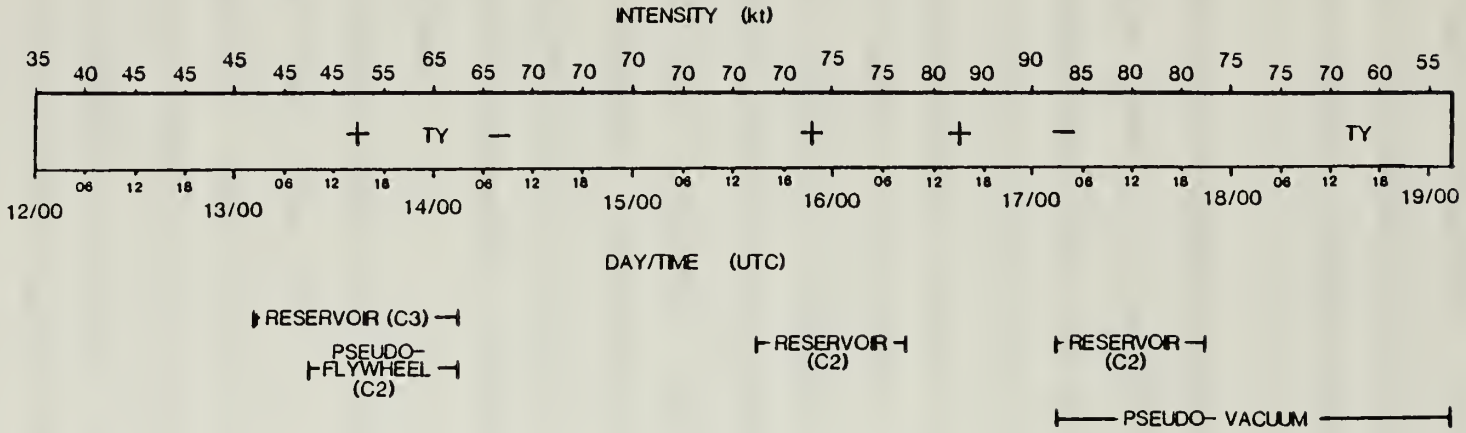

Fig. 62. As in Fig. 61, except for Typhoon Ed.

appeared to be associated in each case with an interaction between the tropical cyclone and an adjacent upper-level synoptic circulation. Thus, the case study has a somewhat biased upper-level perspective, because it has not been demonstrated that other physical mechanisms at lower levels did not have some role in the intensity changes of the two storms.

High resolution, hand-drawn streamline analyses of the 150, 200, 250 and 300 mb winds from the final TCM-90 observational data set (Harr et al. 1991) were constructed for 00, 06, 12 and 18 UTC during the period 00 UTC 12 September through 00 UTC 19 September. Partial isotach analyses of the highest wind regions in the tropical cyclone outflow and subtropical jets were also produced. Satellite imagery was used extensively in the construction of these analyses. The 6-h analyses improved the time continuity over that of the operational charts. Four levels were analyzed to achieve vertical consistency and to increase the horizontal resolution at adjacent levels in data-sparse regions. A careful post-analysis allowed for repositioning of upper-level systems to produce best tracks (see Fig. 1) that were much more smoothly varying than those deduced from the operational charts.

In general, the wind observations near the center of the tropical cyclone are a reflection of both the horizontal motion of the air parcels and of previous vertical motion. For example, if the observations nearest the tropical cyclone at

250 mb are located 100 km from the storm center and suggest anticyclonic outflow, then the air parcels that contributed to produce this wind vector may, in fact, have originated as outflow from a higher level within the storm. Thus, outflow at a certain level cannot necessarily be assumed based solely upon observations that are located 100 km from the center of the storm. Adhering to accepted guidelines, the streamlines were produced by "drawing to the observations." However, the subjective analyses reflect this outflow regime concept that accounts for previous vertical motion in the eyewall.

The objective of this multi-layer analysis approach was to describe the vertical structure of the upper-level flow pattern. For example, the vertical structure of adjacent synoptic features such as cold lows may play a role in upper-level forcing of the tropical cyclones and thus must be considered. Vertical cross-sections of polar-orbiting satellite temperature retrievals and time series of rawinsonde profiles were therefore used to define the vertical structure of these features.

A quantitative measure of the upper-level forcing was determined through the use of a radial-band averaging technique applied to the final set of 200 mb streamlines. The magnitude of the average radial wind component across a 6 deg. lat. circle surrounding the storm center at each map time was interpreted as a measure of the mass flux in the outflow layer. The radial and tangential wind components were

similarly used to calculate the eddy flux convergence (EFC) of relative angular momentum at 200 mb for both Flo and Ed. Finally, the mean wind speed and direction crossing the 6 deg. lat. circle at each map time were used to calculate a vector difference that was interpreted as a measure of the bulk vertical shear of the outflow layer relative to the lower troposphere winds advecting the storm. Changes in the mass flux, EFC, and magnitude of the bulk shear vector were subjectively correlated with both the development of the three interaction mechanisms that were identified and the intensity estimates provided by JTWC (ATCR 1990) to quantify the influence of the upper-level forcing.

B. SUMMARY OF INTERACTION MECHANISMS

Subjective interpretation of both the streamline and isotach analyses and the available satellite imagery led to the definition of three basic interaction mechanisms that appeared to have major roles in upper-tropospheric forcing on the intensification rates of Flo and Ed. Several characteristics appear to be common for all three of these mechanisms. First, each mechanism contributed to the efficient export of mass and heat from the developing storm such that further evacuation of mass within the eye, and hence intensification, was favored. Second, each of the mechanisms removed mass and heat sufficiently far from the storm environment such that the subsequent subsidence does not

impede intensification. Finally, the degree of forcing or influence that each of the mechanisms exerted on Flo and Ed appeared to have been modulated by: (i) the position of the tropical cyclone relative to the circulation feature(s) that produced the interaction mechanism; and (ii) the vertical structure of these circulation feature(s) and the topography of the pressure surfaces that comprise the flow channels associated with the interaction mechanisms.

1. The TUTT cell reservoir function

The first interaction mechanism to develop in the case of both Flo and Ed was that of a TUTT cell acting as a mass/heat reservoir. As depicted in Fig. 11a, a TUTT cell can function as a mass/heat reservoir when a significant fraction of its inflow converges towards the center of the cold-core cell. The reservoir function may enhance evacuation of mass from the center of the tropical cyclone because the TUTT cell acts as a more favorable mass sink for the outflow jets than does the more typically barotropic upper-level environment (Fig. 11c).

The TUTT cell reservoir function differs considerably from the tropical cyclone - TUTT cell interaction mechanism described by Sadler (1978), in which a region of upper-level divergence adjacent to the TUTT cell results in low-level convergence and convective activity. As shown for both TUTT cells labeled as C1 and C2 in Fig. 13, the TUTT cell

functioning as a mass reservoir is identified on satellite imagery as a markedly clear region occasionally surrounded on the periphery by cirrus streaks. The strong upper-level convergence of the northward-directed outflow jets of Flo into TUTT cells C1 and C2 that results in subsidence within these cold lows is depicted in the corresponding 200 mb streamline analysis (Fig. 12).

Temperature cross-sections and time series of rawinsondes indicated that the vertical structures of these cold-core cells were weakened only slowly by the steady inflow of warm tropical cyclone outflow air. This implies that: (i) there must be considerable low and/or middle-level divergence of the subsiding air within the cell for the cell to maintain its identity despite the constant filling resulting from the reservoir function; and (ii) since the cold-core structure was maintained, the reservoir function can play a role in the upper-level forcing for a long period of time.

2. The TUTT cell flywheel mechanism

The second interaction mechanism identified was that of a TUTT cell acting as a flywheel for the outflow jets of tropical cyclone Flo. Unlike the flow associated with a TUTT cell acting as a reservoir, a significant proportion of the flow is accelerated around the TUTT cell, which is interpreted here to function similar to a flywheel (Fig. 19). This flow does not converge into the cell's center. Instead, the

trajectories of the high velocity outflow parcels diverge on the southeastern periphery of the cell in response to the upward sloping pressure surface associated with the subequatorial ridge south of the cell. Existence of this divergence region is similar to that in the model of a tropical cyclone - TUTT cell interaction mechanism described by Sadler (1978). However, the divergence region in the flywheel case is more of a symptom that a strong outflow jet exists upstream, rather than being the upper-level divergence that triggers or sustains low-level convergence in a developing tropical storm as in the Sadler mechanism.

Satellite imagery (e.g., Fig. 20) depicts the flywheel mechanism by a characteristic signature of: (i) elongated cirrus streaks around the periphery of the TUTT cell that change from cyclonic curvature to anticyclonic curvature downstream; and (ii) towering cumulus and cumulonimbus clouds that mark the region of upper-level diffluence and the resulting deep convection. The strong cloud signature of the flywheel mechanism contrasts with the cloud-free signature of the reservoir function (e.g., Fig. 13) and offers two distinct advantages. First, the large number of clouds helps to locate the center of the cold low and hence to track its position relative to the tropical cyclone. Second, the increased number of clouds associated with the flywheel mechanism increases the number of available tracers and hence the number of satellite cloud-drift wind observations. As a result, the tropical

cyclone outflow jets are much better defined in the satellite imagery when the flywheel mechanism is present.

Analysis of the flywheel-type interaction mechanisms that developed (or did not develop) between Flo and C1, Flo and C2, and Ed and C2 suggest that the upper-level environment must satisfy two basic requirements if the flywheel mechanism is to develop. First, a sufficiently baroclinic flow channel must exist between the tropical cyclone and the cold-core low. The slope of the pressure surface must be of sufficient magnitude to provide a path along which the outflow parcels can accelerate to the velocities that will produce a region of diffluence in the southeastern periphery of the cell (Fig. 19a). Such velocities must be attained for the outflow parcels to develop a centrifugal force that exceeds the pressure gradient force associated with the pressure surface slope in the TUTT cell. Velocities of this magnitude can only be attained when the acceleration occurs over a path of sufficient length. Thus, the existence of an elongated flow channel is the second requirement that must be satisfied in order for the flywheel mechanism to develop.

A baroclinic flow channel of significant length developed early in the evolution of the interaction between cold-core low C1 and Flo. As shown in Fig. 17, the ridging associated with the anticyclones southeast of Flo raised the geopotential heights on the southwestern side of the flow channel and combined with the low heights in C1 to the east to create a

pressure surface slope of sufficient magnitude to develop the flywheel mechanism. Since C1 was approximately 20° long. east of Flo throughout this early interaction period, the position requirement was also satisfied.

3. The vacuum export mechanism

The third type of interaction mechanism that was identified forms as a result of the development of an efficient flow channel across the subtropical ridge and into the synoptic-scale jet (Fig. 25a). Outflow from the tropical cyclone is increased in association with the pressure surface slope on the northern side of the subtropical ridge (Fig. 25b). Once a northward flow channel across the subtropical ridge is initiated, a steeper pressure surface slope implies that the kinetic energy (velocity squared) of the outflow parcels increases as they merge into the subtropical jet. This creates a Bernoulli or "vacuum-type" effect that results in a highly efficient mass/heat export mechanism.

The development and influence of the vacuum mechanism is best illustrated by a description of the interactions between Flo and the subtropical ridge. The increased slope on the northern side of the ridge was produced by the approach of a long-wave trough from the west (Fig. 25c). The effective slope of the pressure surface increased, and thus the subtropical jet was intensified as the base of the trough moved into the region and lowered heights to the northwest of Flo. The

subtropical jet was therefore useful as a means of identifying a steeper north-south slope.

The northward flow channel across the subtropical ridge was initiated by the combination of Flo's continued motion towards the subtropical ridge in conjunction with the development of a weakness in the ridge. This weakness, which quickly transitioned into a clear break (Fig. 26), developed as result of the interaction of an approaching long-wave trough with a transient cold low northeast of Flo (Fig. 23) that lowered the geopotential heights north of Flo. Once the northward outflow jets were afforded this favorable path across the subtropical ridge, the increased pressure surface slopes on the northern side of the ridge accelerated the parcels, which enhanced the outflow and increased the evacuation of mass from the center of the storm.

As in the cases of the TUTT cell flywheel and reservoir functions, two major controlling factors appeared to determine whether the vacuum mechanism was likely to develop: (i) the position of the tropical cyclone relative to the subtropical jet; and (ii) the vertical structure, or topography, of the pressure surfaces and circulation features involved. For example, the vacuum mechanism did not develop until a weakness in the subtropical ridge lowered the geopotential heights such that flow across the ridge could be initiated. The position requirement is related to the distance between the tropical cyclone and the subtropical jet. If this distance is so large

that the Coriolis effect is dominant, then the outflow jets have the characteristic anticyclonic turning associated with the normal outflow regime. With only a slow descent along the pressure surface on the northern side of the subtropical ridge, less rapid increases in kinetic energy will occur at the expense of potential energy, and thus only a marginally efficient outflow channel can develop. In the case of Ed and Flo, this situation did not apply because the high geopotential heights of the subtropical ridge prevented development of the interaction mechanism during the period when the distance separating the two features was large. With the approach of the subtropical jet from one side and the tropical cyclone from the other side, a weakness developed in the subtropical ridge and the outflow crossed the ridge and accelerated down the steep pressure surfaces.

C. SUMMARY OF THE INTENSIFICATION PROCESSES

1. Supertyphoon Flo

As shown in the intensification timeline (Fig. 61), the reservoir functions of TUTT cells C1 and C2 were the first of the three interaction mechanisms to develop for Supertyphoon Flo. The upper-level forcing associated with the two reservoir functions was initiated around 12 UTC 12 September and was reflected by an increase in the mass flux at 200 mb (Fig. 3a). As a result of the increased outflow, the intensification rate increased between 00 UTC - 06 UTC 13

September. This time lag appeared to be commensurate with the distance between the tropical cyclone and the two cold lows. Thereafter, this function comprised the upper-level support for continued steady intensification of Flo through 12 UTC 14 September. The generally increasing trend in the mass flux during this period (Fig. 3a) was consistent with Flo's steadily increasing intensity. Additional upper-level support for the steadily increasing intensity was provided by an event of significantly enhanced eddy flux convergence (EFC) of relative angular momentum (Fig. 4a) that occurred during the period 00 UTC 13 September through 12 UTC 14 September.

As shown in Fig. 61, the reservoir export mechanism associated with TUTT cells C1 and C2 comprised a continual favorable upper-level forcing on Flo. Reinvigoration of the reservoir export mechanism between C1 and Flo at 06 UTC 18 September (Fig. 44) corresponded with a slowing of the weakening rate that occurred between 06 - 12 UTC 18 September (Fig. 61). This provides further evidence of the long-lasting potential for interaction that is characteristic of the properly positioned TUTT cell and suggests that the reservoir function can be considered to be the basic TUTT cell - tropical cyclone interaction mechanism. The potential for positive forcing on the intensification rate apparently always exists as a result of the favorable outflow pattern that can develop between the tropical cyclone and the adjacent upper-level cold pool.

Development of the flywheel export mechanism at 12 UTC 14 September resulted in a significant increase in the mass flux at 200 mb (Fig. 3a) and was followed by a large increase in the intensification rate 18 - 24 h later. The time lag here was consistent with the approximate 20° long. separating TUTT cell C1 and Flo. Concurrent with the increased mass flux was a significant decrease in the bulk vertical shear of the outflow layer (Fig. 5a). These two effects apparently dominated the upper-level forcing during the period 12 UTC 14 September through 12 UTC 15 September, because Flo continued to intensify despite the negative influence of decreased EFC (Fig. 4a).

The flywheel mechanism therefore played an important role in determining whether the upper-level flow pattern supported a rapid intensification rate and/or a high intensity storm. Development of the flywheel mechanism with cold low C1 played a major role in the continued rapid intensification of Flo at a time when other upper-level conditions unfavorable for further intensification had developed. It appeared that the flywheel mechanism sustained Flo's rapid intensification rate despite the temporary loss of the southern outflow channel due to ridging associated with the adjacent anticyclones (Fig. 18). As shown in Fig. 61, loss of the C1 flywheel interaction at 06 UTC 17 September resulted in a slowing of the intensification rate 12 h later, and contributed to an actual

decrease in the intensity of Flo beginning at 18 UTC 17 September.

Development of the vacuum mechanism between 06 UTC and 12 UTC 15 September was an additional contributing factor to the large increase in Flo's intensification rate that occurred during the following 12 h (Fig. 61). The initiation of this mechanism resulted in a second outflow channel to the north and was accompanied by the favorable influences of increased EFC (Fig. 4a) and a decreasing trend in the bulk vertical shear (Fig. 5a). The decrease in the mass flux that occurred between 12 UTC 15 September and 18 UTC 16 September is hypothesized to have been the result of the loss of the southern outflow channel into the upper-level easterlies. Flo continued to intensify despite the loss of the southern outflow channel as a result of the two highly efficient export mechanisms operating to the north combined with the positive influences of EFC and decreased bulk vertical shear.

Following the decay of the flywheel mechanism around 12 UTC 17 September, the reservoir function of C1 and the vacuum mechanism continued to provide upper-level support for further intensification. As shown in Fig. 3a, the mass flux steadily increased from 12 UTC 17 September through 00 UTC 19 September. Nevertheless, Flo began to weaken in conjunction with the increased vertical shear (Fig. 5a) that apparently dominated the upper-level forcing once Flo had crossed the

subtropical ridge and began to move northward into the midlatitude westerlies.

2. Typhoon Ed

As shown in Fig. 62, the upper-level forcing of Typhoon Ed was sporadic and short-lived and thus did not support rapid intensification or a high intensity storm. Nevertheless, the development and decay of the few interaction mechanisms that did occur correlated well with the calculated changes in the mass flux and the observed changes in intensity. This is best illustrated by the development of a weak reservoir function with TUTT cell C3 that preceded by 6 h the initiation of a short-lived flywheel interaction with cell C2.

The reservoir function that developed between Ed and TUTT cell C3 at 06 UTC 13 September (Fig. 51) was weak and short-lived as a result of the blocking action caused by the strong synoptic-scale flow. Nevertheless, this reservoir function marked the initiation of a dual-channel outflow pattern for Ed, which has been shown by Sadler (1976) and Guard (1980) to increase the likelihood for rapid tropical cyclone intensification. As shown in Fig. 3b, initiation of the reservoir function was reflected in an increase in the mass flux and was followed by an increase in the intensification rate between 12 UTC - 18 UTC 13 September.

The baroclinic, flywheel-type flow channel that developed between Ed and cold-low C2 around 12 UTC 13 September was a shallow feature that was mainly evident at 150 mb. Wind observations at 150 mb (Fig. 56) and satellite imagery (Fig. 57) suggested that the flywheel function did exist for the short period of time when the baroclinity requirement was satisfied. As shown in Fig. 3b, development of the flywheel function combined with the C3 reservoir to produce an increase in the mass flux that was followed by an increase in Ed's intensification rate (Fig. 62). This period of interaction was one of the few times when changes in the upper-level flow pattern around Ed appeared to support rapid intensification, but this was a transient feature.

Following a period of relatively benign upper-level forcing in which Ed's intensity remained constant at 70 kt (Fig. 62), a weak reservoir export mechanism developed with TUTT cell C2 around 18 UTC 15 September (Fig. 24). Throughout most of its existence, Ed was positioned within a strong northeasterly upper-level flow pattern that effectively blocked any interaction with the adjacent C2 (e.g., Fig. 14). Cell C2 appeared to maintain a vertical structure down to 300 mb (Fig. 29) that would have been sufficient for the development of a favorable outflow channel. When changes in the upper-level flow pattern did permit interaction between Ed and C2 (Fig. 62), the resulting reservoir function that developed at 18 UTC 13 September and then again at 06 UTC 17

September was weak because a large proportion of the inflow to the TUTT cell was from both the northeasterly flow channel and from Flo. The absence of significant changes in the mass flux (Fig. 3b) during the times when these mechanisms were operating was consistent with their weak nature. Nevertheless, the slight increase in the mass flux combined with the increasing trend in the EFC (Fig. 4b) apparently resulted in positive forcing that produced the intensity increase at 12 UTC 16 September. The reservoir function of C2 that was initiated at 06 UTC 17 September apparently helped to slow the weakening associated with Ed's interaction with the orography of Vietnam.

Development of a vacuum-type interaction between Ed and the subtropical jet occurred around 00 UTC 17 September (Fig. 62) and was reflected in the continued slow increase in the mass flux at 200 mb (Fig 3b). The opening of a channel into the midlatitudes for the northern outflow jets of Ed was a result of the deepening of a long-wave trough situated roughly along 120° E (Fig. 37). As was the case with Flo, the geopotential heights were lowered north of Ed. The air parcels associated with the northern outflow jets then broke through the subtropical ridge and accelerated down the sloping pressure surface on the northern side of the narrow subtropical ridge. Consequently, Ed acquired a dual outflow channel pattern that maintained an environment favorable for mass evacuation, which evidently temporarily offset the

expected weakening of the storm as orographic effects progressively began to dominate the environmental influences on Ed's intensification rate.

D. CONCLUSIONS

The three interaction mechanisms that were identified appeared to play a significant role in determining whether the upper troposphere supports sustained and/or rapid tropical cyclone intensification. Such interpretations could not be ascertained clearly from the TCM-90 operational streamline analyses because of deficiencies in both time continuity and data density. The streamline and isotach analyses for this study using the full TCM-90 data set have much improved temporal and spatial resolution of the upper-level circulation features. Careful attention to vertical consistency among the analyses at four pressure levels allowed identification of interaction channels, smaller-scale features, and other subtle changes in the flow patterns. This permitted a description of both the horizontal and vertical changes in the outflow regimes of Flo and Ed. For example, the level of maximum outflow (determined subjectively by the number and orientation of the cloud-drift winds) changed as the tropical cyclone developed. Analysis of only one or even two levels may have obscured such changes, and changes in the interaction mechanisms may also have been missed. The shallow flywheel-type interaction between Ed and cold low C2, which was clearly

evident at 150 mb but absent at 200 mb, is a prime example. Although the signature was shallow and short-lived, this interaction played a significant role in the upper-level forcing on Ed's intensification rate. Thus, continuity in both time and space, especially in the vertical, is important for identifying upper-level interactions that may play a large role in upper-level forcing on tropical cyclone intensity.

Remotely sensed data were invaluable for increasing both the horizontal and the vertical resolution of the analyses in the data-sparse tropics. Satellite temperature soundings were useful in identifying and assessing the vertical structure of strong upper-level features. The high density of these observations and the potential for constructing near real-time spatial cross-sections may compensate for the 1° -2° errors in the retrieval temperatures. Satellite imagery was especially useful in locating and orienting circulation features such as the TUTT cells. The satellite signature of the TUTT cell is helpful in inferring whether the cell is acting only as a mass/heat reservoir or has acquired a flywheel function (e.g., detecting the existence of deep convection marking upper-level divergence regions). Imagery was also invaluable for locating and verifying the existence of interaction channels associated with the vacuum mechanism. In summary, satellite imagery played a significant role in both the construction of the streamline analyses and in the subjective interpretation of the upper-level forcing.

The reprocessed satellite cloud-drift winds were invaluable for defining the tropical cyclone outflow jets as well as for identifying subtle changes in the interactions between various upper-level features. The baroclinic flow channels associated with the flywheel and vacuum mechanisms were best defined by these observations. Such channels were only poorly defined by the relatively sparse rawinsonde network. In general, the rawinsonde network could not resolve the complex upper-level flow pattern or the subtle changes in the upper-level forcing that appeared to determine whether conditions were favorable for intensification. Finally, the vertical resolution of the reprocessed cloud-drift winds on four pressure levels was invaluable for defining the changing vertical structure of both the circulation features and the interaction channels.

One advantage of the subjective (hand-analyzed) interpretation of the streamline and isotach analyses is that various levels could be combined to describe the vertical structure of significant upper-level circulation features. The interpretations here suggest that position and vertical structure considerations are most important for gaging the upper-level forcing on tropical cyclone intensification rates. A circulation feature such as a cold low that is typically favorable for developing an export mechanism must also be properly positioned relative to the tropical cyclone. Lack of a significant, long-lived interaction between Ed and TUTT cell

C2 clearly illustrates this idea. Vertical structure of these circulation features is similarly important and is best exemplified by the baroclinic considerations of the flywheel and vacuum mechanisms. Changes in the pressure surface slopes as a response to the motion, development, and decay of the various upper-level circulations played a significant role in determining whether an effective export mechanism developed or weakened.

Clearly, the outflow regimes of Flo and Ed were very complex in both time and space. Three interaction mechanisms were identified at different times and in different combinations. Other features such as the upper-level anticyclones also appeared to play a role in the upper-level forcing. Despite this complexity, a basic, nearly 1:1, qualitative relationship appeared to exist between the development of one or more of these interaction mechanisms and corresponding changes in the intensification rates (Figs. 61 and 62). In the case of both Flo and Ed, initiation (decay) of one or more of the interaction mechanisms described here resulted in either a corresponding increase (decrease) in the intensification rate or the sustaining of a rapid intensification (weakening).

Changes in the mass flux at 200 mb for both Flo and Ed were well correlated with both the evolution of the interaction mechanisms and the changes in the intensification rates. The mass flux calculations strongly suggest that

changes in the upper-level forcing preceded changes in the intensification rates for these two tropical cyclones. Strong evidence was therefore obtained for the view that environmental forcing leads the intensification process.

This study failed to find any similar correlation between changes in the upper-level forcing and corresponding changes in the motion of the tropical cyclones. It is possible that some indirect effects on motion may have occurred via vertical interactions between the outflow layer and the lower levels that advect the tropical cyclone. These effects are left for future studies.

The correlations between upper-level forcing (in terms of changes in the mass flux, EFC, and bulk vertical shear) and the intensification rates are considered to be significant. Unlike other studies that have had to rely on compositing techniques (Miller 1958) or objective analyses of widely-spaced observations (Molinari and Vollaro 1989), this study found significant evidence that changes in the upper-level forcing preceded changes in intensity using a careful, detailed hand-analysis of observations from the best-ever tropical cyclone region data set. Moreover, the considerable difference in the degree of upper-level forcing on Flo and Ed, and the similarly large difference in the ultimate intensities of these two storms, suggests that the presence of efficient mass/heat export mechanisms can play a major role in determining whether the upper troposphere supports the

development of an intense tropical cyclone.

VI. RECOMMENDATIONS

This study serves as a first step towards a complete description of the environmental forcing that contributed to the intensification of tropical cyclones Flo and Ed. Upper-level forcing was subjectively correlated with the intensity changes, and quantitative values for the mass divergence at a single outflow level were used to correlate with these intensity changes. Quantification of the mass fluxes associated with each of the interaction mechanisms that were identified is the next step towards an explanation of how such interactions can produce intensity changes. Two possible approaches to achieving such a quantitative description are: (i) a quantitative study of mass fluxes using a more rigorous treatment of the radial-band averaging technique applied to gridded fields from an objective analysis of the observations; and (ii) a modeling study to simulate outflow patterns and intensity changes for different relative positions and intensities of mass sources and sinks in the tropical cyclone environment.

Since gridded fields were not available for this study, the radial-band averaging technique applied here is subject to errors in the subjective determination of the mean wind in each radial sector. In addition, the results of the study were limited by the application of this technique to only one level

and at only one radius from the storms. By contrast, application of the technique to a four-dimensional gridded data field may provide a more quantitative description of the mass fluxes associated with each of the hypothesized interaction mechanisms. Since it was shown that the level of maximum outflow appeared to change during the development of the two storms, such an analysis should include a calculation of the mass divergence and eddy flux convergence (EFC) of relative angular momentum at several outflow levels. Perhaps the EFC associated with each of the three interaction mechanisms can provide an indication of the relative contribution to the intensity changes. Other factors such as vertical shear, which may have been induced by the same circulation features that combined to produce the interaction mechanisms, must be accounted for prior to correlating the interactions with intensity changes (DeMaria et al. 1991).

The primary advantage of the four-dimensional gridded data analysis approach is that observations, and not a simulation, are used to determine the effect of the interaction mechanisms. If enhanced EFC due to changes in the upper-level flow pattern can be positively correlated with intensity changes, then a more quantitative explanation for how these interaction mechanisms influence tropical cyclone intensification may be obtained.

A modeling study would provide an opportunity to explore the physics of simulated upper-level interactions in a more

benign environment. The interaction mechanisms described here can each be presumably modeled as a combination of mass sources and sinks. In the most simple experiment, a barotropic model (e.g., Ooyama 1989), in which the tropical cyclone is modeled as a fixed mass source and a TUTT cell is modeled as a mass sink, can be used to determine changes in the tropical cyclone outflow patterns and intensities for different positions and magnitudes of the mass sink. A more complete study would use a distribution of mass sinks and sources to better model both the cold lows and the upper-level anticyclones that appear to contribute to the development (or non-development) of the TUTT cell reservoir and flywheel interaction mechanisms. The orientation of the sources and sinks relative to the tropical cyclone should be varied to determine how the rotational wind pattern is modified such that one or both of the interaction mechanisms develops. Simulation of the vacuum mechanism as a mass source/sink problem may be more complex, as this mechanism may develop more as a result of a favorable pressure surface slope on the northern side of the subtropical ridge.

While these modeling studies may provide a means of isolating the interaction mechanisms, duplication of the baroclinic nature of the circulation patterns that were described in chapters III and IV would be very difficult. Moreover, since these mechanisms often acted in various combinations and at different stages in the development of Flo

and Ed, the models may not be able to simulate the subtle but important changes in the outflow patterns. Nevertheless, such studies would provide a necessary description of the physics and a quantification of the simulated interactions associated with the upper-level forcing and would complement the results of a quantitative mass flux study using a gridded analysis of observations.

LIST OF REFERENCES

ATCR, 1990: Annual tropical cyclone report. Joint Typhoon Warning Center, Guam, Mariana Islands.

Baker, N.L., 1991: Quality control of meteorological observations for the Fleet Numerical Oceanography Center Operational Atmospheric Database. Technical Note 124, Navy Oceanographic and Atmospheric Research Laboratory, Monterey, CA 93943-5001, 53 pp.

Chan, J.C.-L., and W.M. Gray, 1982: Tropical cyclone movement and surrounding flow relationships. *Mon. Wea. Rev.*, **110**, 1354-1374.

Demaria, M., J.J. Baik and J. Kaplan, 1991: Upper-level eddy angular momentum fluxes and tropical cyclone intensity change. submitted to *J. Atmos. Sci.*

Dvorak, V.F., 1984: Tropical cyclone intensity analysis using satellite data. NOAA Technical Report NESDIS 11, U.S. Dept. of Commerce, Washington, DC, 47 pp.

Elsberry, R.L., 1989: ONR Tropical Cyclone Motion Research Initiative: Field Experiment Planning Workshop. Technical Report NPS-63-89-002, Naval Postgraduate School, Monterey, CA 93943, 79 pp.

Elsberry, R.L., 1990: International experiments to study tropical cyclones in the western North Pacific. *Bull. Amer. Meteor. Soc.*, **71**, 1305-1316.

Elsberry, R.L., B.C. Diehl, J.C.-L. Chan, P.A. Harr, G.J. Holland, M. Lander, T. Neta and D. Thom, 1990: ONR Tropical Cyclone Motion Research Initiative: Field Experiment Summary. Technical Report NPS-MR-91-001, Naval Postgraduate School, Monterey CA 93943, 107 pp.

Emanuel, K.A., 1986: An air-sea interaction theory for tropical cyclones. Part I: Steady-state maintenance. *J. Atmos. Sci.*, **43**, 585-604.

Emanuel, K.A., 1988: The maximum intensity of hurricanes. *J. Atmos. Sci.*, **45**, 1143-1155.

Frank, W.M., 1987: Tropical cyclone formation. Chap. 3, *A Global View of Tropical Cyclones*, R.L. Elsberry, Ed., Office of Naval Research, 53-90.

Guard, C.P., 1980: A study of western North Pacific tropical storms and typhoons that intensify after recurvature. Technical Note, U.S. Air Force First Weather Wing, 22 pp.

Harr, P.A., T. Neta and R.L. Elsberry, 1991: ONR Tropical Cyclone Motion Research Initiative: Data users guide to observations. Technical Report NPS-MR-91-002, Naval Postgraduate School, Monterey CA 93943, 124 pp.

Holland, G.J., 1987: Mature structure and structure change. Chap. 2, *A Global View of Tropical Cyclones*, R.L. Elsberry, Ed., Office of Naval Research, 13-52.

Holland, G.J., and R.T. Merrill, 1984: On the dynamics of tropical cyclone structural changes. *Quart. J. Roy. Meteor. Soc.*, **110**, 187-210.

Kelly, G., E. Andersson, A. Hollingsworth, P. Lonnberg, J. Pailleux and Z. Zhang, 1991: Quality control of operational physical retrievals of satellite sounding data. *Mon. Wea. Rev.*, **119**, 1866-1880.

McBride, J.L., and R. Zehr, 1981: Observational analysis of tropical cyclone formation. Part II: Comparison of non-developing versus developing systems. *J. Atmos. Sci.*, **38**, 1132-1151.

Merrill, R.T., 1988: Environment influences on hurricane intensification. *J. Atmos. Sci.*, **45**, 1678-1687.

Miller, B.I., 1958: On the maximum intensity of hurricanes. *J. Meteor.*, **15**, 184-195.

Molinari, J., and D. Vollaro, 1989: External influences on hurricane intensity. Part I: Outflow layer eddy angular momentum fluxes. *J. Atmos. Sci.*, **46**, 1093-1105.

National Oceanic and Atmospheric Administration (NOAA), 1990: Oceanographic Monthly Summary, September. U.S. Department of Commerce, 23 pp.

Ooyama, K.V., 1982: Conceptual evolution of the theory and modeling of the tropical cyclone. *J. Meteor. Soc. Jpn.*, **60**, 369-379.

Ooyama, K.V., 1987: Numerical experiments of steady and transient jets with a simple model of the hurricane outflow layer. Preprints, *17th Conf. on Tropical Meteor.*, Miami, Amer. Meteor. Soc., 318-320.

Pfeffer, R.L., 1958: Concerning the mechanisms of hurricanes. *J. Meteor.*, **15**, 113-120.

Pfeffer, R.L., and M. Challa, 1981: A numerical study of the role of eddy fluxes of momentum in the development of Atlantic hurricanes. *J. Atmos. Sci.*, **38**, 2393-2398.

Riehl, H., 1950: A model of hurricane formation. *J. Appl. Phys.*, **21**, 917-925.

Sadler, J.C., 1976: A role of the tropical upper-tropospheric trough in early season typhoon development. *Mon. Wea. Rev.*, **104**, 1266-1278.

-----, 1978: Mid-season typhoon development and intensity changes and the tropical upper-tropospheric trough. *Mon. Wea. Rev.*, **106**, 1137-1152.

INITIAL DISTRIBUTION LIST

1.	Defense Technical Information Center Cameron Station Alexandria, VA 22304-6145	2
2.	Library, Code 52 Naval Postgraduate School Monterey, CA 93943-5000	2
3.	Director Naval Oceanography Division Naval Observatory 34th and Massachusetts Avenue NW Washington, DC 20390	1
4.	Commander Naval Oceanography Command Stennis Space Center MS 39529-5000	1
5.	Commanding Officer Fleet Numerical Oceanography Center Monterey, CA 93943-5005	1
6.	Director Naval Research Laboratory Monterey, CA 93943-5006	1
7.	Chief of Naval Research 800 N. Quincy Street Arlington, VA 22217	1
8.	JOINT TYPHOON WARNING CENTER COMNAVMARIANAS Box 17 FPO San Francisco, CA 96630-2926	1
9.	Chairman (Code MR/HY) Department of Meteorology Naval Postgraduate School Monterey, CA 93943-5000	1
10.	Professor Russell L. Elsberry (Code MR/ES) Department of Meteorology Naval Postgraduate School Monterey, CA 93943-5000	1

11. Lieutenant Commander L.E. Carr 1
Department of Meteorology
Naval Postgraduate School
Monterey, CA 93943-5000

12. Lieutenant Jeff H. Rucker 1
Naval Eastern Oceanography Center
Naval Air Station
Norfolk, VA 23511

13. Professor Bill Gray 1
Atmos. Science Department
Colorado State University
Ft. Collins, CO 80523

14. Dr. Greg Holland 1
Bureau Met. Res. Ctr.
P.O. Box 1289K
Melbourne, Victoria, 3001
Australia

15. Dr. Hugh Willoughby 1
Hurricane Research Division
AOML/NOAA
4301 Rickenbacker Causeway
Miami, FL 33149

16. Professor R.T. Williams (Code MR/WU) 1
Department of Meteorology
Naval Postgraduate School
Monterey, CA 93943-5000

84-217

NAVAL POSTGRADUATE SCHOOL
MONTEREY, CALIFORNIA 93943-5002

Thesis
R8332 Rucker
c.1 Upper-tropospheric forcing of the intensification rates of tropical cyclones Flo and Ed based on TCM-90 observations.

Thesis
R8332 Rucker
c.1 Upper-tropospheric forcing of the intensification rates of tropical cyclones Flo and Ed based on TCM-90 observations.

DOULEY KNOX LIBRARY
3 2768 00018329 7